FINAL REPORT

Improved Understanding of Permafrost Controls on Hydrology in Interior Alaska by Integration of Ground-Based Geophysical Permafrost Characterization and Numerical Modeling

SERDP Project RC-2111

MAY 2015

Michelle A. Walvoord
Frederick D. Day-Lewis
John W. Lane, Jr.
Robert G. Striegl
Clifford I. Voss
U.S. Geological Survey

Thomas A. Douglas
U.S. Army ERDC-CRREL

Distribution Statement A
This document has been cleared for public release

SERDP
DOD ▪ EPA ▪ DOE

This report was prepared under contract to the Department of Defense Strategic Environmental Research and Development Program (SERDP). The publication of this report does not indicate endorsement by the Department of Defense, nor should the contents be construed as reflecting the official policy or position of the Department of Defense. Reference herein to any specific commercial product, process, or service by trade name, trademark, manufacturer, or otherwise, does not necessarily constitute or imply its endorsement, recommendation, or favoring by the Department of Defense.

REPORT DOCUMENTATION PAGE

Form Approved
OMB No. 0704-0188

Public reporting burden for this collection of information is estimated to average 1 hour per response, including the time for reviewing instructions, searching existing data sources, gathering and maintaining the data needed, and completing and reviewing this collection of information. Send comments regarding this burden estimate or any other aspect of this collection of information, including suggestions for reducing this burden to Department of Defense, Washington Headquarters Services, Directorate for Information Operations and Reports (0704-0188), 1215 Jefferson Davis Highway, Suite 1204, Arlington, VA 22202-4302. Respondents should be aware that notwithstanding any other provision of law, no person shall be subject to any penalty for failing to comply with a collection of information if it does not display a currently valid OMB control number. **PLEASE DO NOT RETURN YOUR FORM TO THE ABOVE ADDRESS.**

1. REPORT DATE *(DD-MM-YYYY)*
17-04-2015

2. REPORT TYPE
final

3. DATES COVERED *(From - To)*
03-2010 to 04-2015

4. TITLE AND SUBTITLE
Improved Understanding of Permafrost Controls on Hydrology in Interior Alaska by Integration of Ground-based Geophysical Permafrost Characterization and Numerical Modeling

5a. CONTRACT NUMBER

5b. GRANT NUMBER

5c. PROGRAM ELEMENT NUMBER

6. AUTHOR(S)
Walvoord, Michelle A.; Day-Lewis, Frederick: Douglas, Thomas; Lane, John W. Jr.; Voss, Clifford I.

5d. PROJECT NUMBER
RC-2111

5e. TASK NUMBER

5f. WORK UNIT NUMBER

7. PERFORMING ORGANIZATION NAME(S) AND ADDRESS(ES)
(1) USGS National Research Program –Central Region, Denver Federal Center Box 25046, CO, 80225;
(2) USGS Branch of Geophysics 11 Sherman Place, Storrs, CT 06269;
(3) US Army, ERDC, CRREL, Box 35170, Fort Wainwright, AK, 99703;
(4) USGS National Research Program – Western Region, 345 Middlefield Rd, Menlo Park, CA 94025

8. PERFORMING ORGANIZATION REPORT NUMBER

9. SPONSORING / MONITORING AGENCY NAME(S) AND ADDRESS(ES)
Strategic Environmental Research and Development Program
4800 Mark Center Drive, Suite 17D08, Alexandria, VA 22350

10. SPONSOR/MONITOR'S ACRONYM(S)
SERDP

11. SPONSOR/MONITOR'S REPORT NUMBER(S)
RC-2111

12. DISTRIBUTION / AVAILABILITY STATEMENT

Public Release

13. SUPPLEMENTARY NOTES

14. ABSTRACT
Permafrost and seasonal ground ice are key factors that control the routing of water above and below the land surface in interior Alaska; hence frozen ground affects water resources, ecosystem state, landscape evolution, and soil stability. Despite its hydrologic, ecologic, and geotechnical importance, the spatial distribution of permafrost and its relation to subsurface water flow remains poorly understood for many areas of interior Alaska largely due to its remoteness and inaccessibility. This study was aimed at improving the knowledge base by (1) developing a new numerical modeling tool for simulation of groundwater/permafrost interaction; (2) demonstrating and evaluating geophysical methods for mapping of permafrost distribution at several test sites; and (3) elucidating permafrost-controlled surface-water/groundwater exchanges using physics-based modeling to evaluate local settings that were characterized by field efforts and by evaluating larger scale interactions based on generic understanding of permafrost patterns based on geophysical and other data. This research has resulted in both basic-science and methodological advances. The hydrologic modeling tools and approaches and the geophysical methods and evaluation approaches developed here are readily transferrable to a wide range of issues related to permafrost characterization and dynamics affecting cold-region DoD installations and operations.

15. SUBJECT TERMS
active layer, freeze/thaw dynamics, geophysics, ground ice, groundwater modeling, hydrologic impacts, interior Alaska, lakes, permafrost, sub-arctic, taliks, Yukon Flats

16. SECURITY CLASSIFICATION OF:			**17. LIMITATION OF ABSTRACT**	**18. NUMBER OF PAGES**	**19a. NAME OF RESPONSIBLE PERSON**
a. REPORT	**b. ABSTRACT**	**c. THIS PAGE**			Michelle Walvoord
U	U	U	U	118	**19b. TELEPHONE NUMBER** *(include area code)* 303-236-4998

Standard Form 298 (Rev. 8-98)
Prescribed by ANSI Std. Z39.18

Table of Contents

List of Tables iv
List of Figures v
List of Acronyms viii
Keywords ix
Acknowledgements ix
Abstract 1
1. Objectives 3
2. Background 4
2.1 General 4
2.2 Hydrologic Models for Simulating Frozen Ground Dynamics 4
2.3 Permafrost and Lithologic Characterization Using Geophysics 5
2.4 Integrated Hydrologic Analyses and Model Applications 5
3. Hydrologic Model Development 7
3.1. Materials and Methods 7
3.1.1 Freeze/Thaw Processes 7
3.1.2 Generalized Boundary Conditions 10
3.1.3 Lake Capability 11
3.2 Results and Discussion 13
3.2.1. Freeze/Thaw: The Frozen Wall 13
3.2.2. Generalized Boundary Conditions: Dam with Vertical Sides (Seepage Face) 15
3.2.3. Lake Capability: 3-Lake Example 17
4. Geophysical Investigations 20
4.1 Study Area 21
4.2 Materials and Methods 22
4.2.1 Resistivity 23
4.2.2 Electromagnetics 25
4.2.3 Time-domain electromagnetics 28

4.2.4 Ground Penetrating Radar 29
4.2.5 Passive Seismic 31
4.3 Results and Discussion 32
5. Hydrologic Analyses and Model Applications 34
5.1 Regional Groundwater Flow in the Yukon Flats Basin 34
5.1.1 Materials and Methods 34
5.1.2 Results and Discussion 36
5.2 Generalized Permafrost Thaw/ Groundwater Flow Interaction 45
5.2.1 Materials and Methods 45
5.2.2 Results and Discussion 47
5.3. Lake Mass Balance Analysis 51
5.3.1 Materials and Methods 54
5.3.2 Results and Discussion 55
5.4 Lake Talik Evolution 58
5.4.1 Materials and Methods 58
5.4.2 Results and Discussion 60
5.5 Sensitivity Analysis of Geophysical Data to Permafrost Conditions 66
5.5.1 Materials and Methods 66
5.6 Permafrost Response to Lake Recession 78
5.6.1 Materials and Methods 78
5.6.2 Results and Discussion 80
5.7 Regional Synthesis of Yukon Flats Lake Dynamics and Linkages to Permafrost Conditions 85
5.7.1 Materials and Methods 86
5.7.2 Results and Discussion 88
6. Conclusions and Implications for Future Research/Implementation 91
6.1. Synthesis of Results and Research 91
6.2 Implementation of Tools and Approaches Developed 92
6.2.1 SUTRA 92
6.2.2 Geophysical Methods for Cold Regions 94
6.2.3 Integrated Approach for Future Assessments 94

6.3 Ramifications for DoD Operations, Infrastructure, and Planning in Interior Alaska 96
6.4 Remaining Gaps in Knowledge..... 98
6.5 Recommendations for Long-Term Permafrost Monitoring Program 99
7. Literature Cited 101
APPENDIX A. LIST OF SCIENTIFIC/TECHNICAL PUBLICATIONS 107
A-1. Articles in Peer-Reviewed Journals 107
A-2. Technical Reports 107
A-3. Conference Proceedings..... 108
A-4. Conference Abstracts 108

List of Tables

Table 5.1.2.1 List of select model simulations and corresponding permafrost distribution..... 40
Table 5.1.2.2 Model results for a permafrost thaw sequence in the Yukon Flats Basin..... 40
Table 5.1.2.2 Model-predicted baseflow for select permafrost distributions. 44
Table 5.5.1 Description of geologic units and physical properties used in numerical simulations. 68

List of Figures

Figure 3.1.3.1 Example for nine potential lakes based on given surface topography. 12
Figure 3.1.3.2 Hierarchy of nine lakes identified in the example problem. 13
Figure 3.2.1.1 Model schematic for the frozen wall example problem. 14
Figure 3.2.1.2 Flow field and temperature distribution after 25 days..... 15
Figure 3.2.1.3 Ice-saturation distribution after approximately 25 days. 15
Figure 3.2.2.1 Boundary conditions and finite-element mesh for the dam (seepage face) example. 16
Figure 3.2.2.2 Near-steady-state SUTRA results for the seepage face example. 17
Figure 3.2.3.1 Boundary conditions and finite-element mesh for the 3-lake example. 18
Figure 3.2.3.2 Areas of the model surface covered by lake water (blue) in the lake example. 18
Figure 3.2.3.3 Lake-water concentration as a function of time in the lake example. 19
Figure 4.0.1 Schematic diagram illustrating setups and data products for geophysical methods used in this work 20
Figure 4.0.2 Schematic diagram illustrating the tradeoff in coverage and resolution for geophysical methods used in this work. 21
Figure 4.1.1 Location map of Beaver Meadow and Twelvemile study areas..... 22
Figure 4.2.1.1 Resistivity line 2 from Twelvemile Lake collected August 2011 23
Figure 4.2.2.1 Comparison of direct-current resistivity results (top) and multi-frequency electromagnetic data (bottom) for Line 1, Twelvemile Lake. 25
Figure 4.2.2.2 FEMIC inversion results of data from GEM2 transects for 1-m depth. 26
Figure 4.2.2.3 Interpolated GEM2 inversion results from FEMIC at the 1-m depth. 27
Figure 4.2.2.4 Raw GEM2 data indicates electrical conductivity of the subsurface in the 2014 flooded meadow area. 28
Figure 4.2.3.1 Time-domain electromagnetic sounding for site 29
Figure 4.2.4.1 Interpreted permafrost distribution based on ground-penetrating radar collected in 2011-2012, in the vicinity of Twelvemile Lake..... 31
Figure 4.2.5.1 Representative passive-seismic results overlayed on resistivity cross-sectional image..... 32
Figure 4.3.1 Summary of geophysical methods useful for characterizing cold region features of interest at variable scales and resolution..... 33
Figure 5.1.1.1 Location map of the Yukon Flats Basin (after Williams, 1962). 36
Figure 5.1.2.1 Steady-state head distribution for the supra-permafrost zone (for base case PDISC1) (a), and the sub-permafrost zone (b). 38
Figure 5.1.2.2 Steady-state zone water budget results (not drawn to scale) for the base case, PDISC1. 39
Figure 5.1.2.3 Model results for groundwater discharge patterns with varying permafrost distributions..... 42
Figure 5.1.2.4 Model-calculated baseflow for selected river reaches with a variety of permafrost distributions..... 43

Figure 5.1.2.5 Model-calculated percentage of supra-permafrost (or shallow aquifer in thawed cases) contribution to baseflow. 43
Figure 5.2.1 'Tothian Hills' model domain (no vertical exaggeration) for reference topographic shape with finite-element mesh (coarsest of several used for simulations) and boundary conditions. 46
Figure 5.2.2.1 Comparison of conduction-dominated (left) and advection-influenced (middle) permafrost thaw during climate warming. 48
Figure 5.2.2.2 Effect of heterogeneity in permeability on evolution of permafrost thaw patterns: high-permeability layers. 49
Figure 5.2.2.3 Effect of heterogeneity in permeability on evolution of permafrost thaw pattern: example with high- and low-permeability patches. 50
Figure 5.2.2.4 Effect of lakes on evolution of permafrost thaw patterns. 51
Figure 5.3.0.1 Study site location. 53
Figure 5.3.0.2 Images of Twelvemile and Buddy Lakes between 1952 and 2011 (a-c) and time series of lake surface elevation (d). 54
Figure 5.3.1.1 Conceptual model of water fluxes considered in this study. 55
Figure 5.3.2.1 Maps showing resistivity of subsurface (upper 10 m) from the AEM survey and depth to ice from ground-based observations 56
Figure 5.4.1 Cross-section of two-dimensional cylindrical model with boundary conditions of temperature, fluid pressure, and heat flux (a). 59
Figure 5.4.2.1 Temporal evolution of groundwater flow and ice volume for the case of a 12m lake that is losing (a), gaining (b), and hydrostatic (c) for the current climate. 62
Figure 5.4.2.2 Cross-sections of 2D cylindrical model (mirrored) showing states of lake-talik formation, ice saturation, and groundwater movement where a 12m lake forms over a continuous permafrost layer of about 90m in thickness. 63
Figure 5.4.2.3 Group averages of simulation results for three categories: climate regime, lake flow, and maximum lake depth. 65
Figure 5.5.1 Axis-symmetric model geometry indicating different lithologic units and simulated lake depths/extents. 67
Figure 5.5.2.1 SUTRA model outputs and geophysical transformations from the 6-m gaining lake simulation at 240 years. 70
Figure 5.5.2.2 Mean resistivity model extracted from McMC ensembles. 72
Figure 5.5.2.3 Performance of geophysical parameter estimation in recovering true parameter values. 73
Figure 5.5.2.4 McMC-estimated resistivity posterior distributions 74
Figure 5.5.2.5 Resistivity probability distributions for the hydrostatic 6-m-deep lake scenario at simulation times 75
Figure 5.5.2.6 Comparison of airborne and ground-based measurements for recovering shallow thaw features. 77

Figure 5.6.2.1 Three-year ice saturation time series for multiple depths in the open-meadow model..... 81
Figure 5.6.2.2 Ice saturation envelope encompassing annual frost variation (including 3 date-specific profiles) and aggraded permafrost ice saturation 83
Figure 5.6.2.3 Strong shrub effect model ice saturation (Sh2-0R) (a), and shrub effect reduced by climate change model ice saturation (Sh2-0R-CW). 84
Figure 5.7.0.1 Location of study area (a, c), and lake surface-area change by physiographic unit (b). 85
Figure 5.7.1.1 Examples of the four different gravel-silt thaw states (Types A-D) interpreted from electrical resistivity cross sections of the airborne electromagnetic survey. 87
Figure 5.7.2.1 Relationships between lake surface-area trends and sublacustrine thaw states (a, b, and f) and sublacustrine thaw states and location (c-e). 89
Figure 6.3.1 An elevation map of interior Alaska DoD training areas and cantonments. 96

List of Acronyms

AEM – Airborne ElectroMagnetic

CRREL – Cold Regions Research and Engineering Laboratory

DEM – Digital Elevation Map

DoD – Department of Defense

FDEM – Frequency Domain ElectroMagnetic

FEMIC - Frequency-domain ElectroMagnetic Inversion Code

FWS – (United States) Fish and Wildfire Service

GCM – Global Climate Model

GRP – Ground Penetrating Radar

GSSI – Geophysical Survey Systems Incorporated

HVSR – Horizontal-to-Vertical Seismic-noise Ratio

IPCC – Intergovernmental Panel on Climate Change

IRIS – Incorporated Research Institution for Seismology

LIDAR –LIght Detection And Ranging

MODFLOW – MODular finitie-difference FLOW

NRCS – National Resources Conservational Service

REV – Representative Elementary Volume

SERDP – Strategic Environmental Research and Development Program

SNAP – Scenarios for Alaska Planning

SNOTEL – SNOw TELemetry Station

SUTRA – Saturated-Unsaturated, variable-density ground-water flow with solute or energy TRAnsport

TDEM – Time Domain ElectroMagnetic

PRISM – Parameter-elevation Regressions on Independent Slopes Model

SWE – Snow Water Equivalent

USGS – United States Geological Survey

2DRes – Two-dimensional Resistivity

Keywords

active layer, freeze/thaw dynamics, geophysics, ground ice, groundwater modeling, hydrologic impacts, interior Alaska, lakes, permafrost, sub-arctic, taliks, Yukon Flats

Acknowledgements

We would like to acknowledge important contributions from the following scientists and staff: Beth Astley (Army Corp of Engineers), Nikki Guldager (FWS), Douglas Halm (USGS), Jay Nolan (Rutgers University), Joshua Rose (FWS), Stephanie Saari (CRREL), Lee Slater (Rutgers University), Emily Voytek (USGS; now at Colorado School of Mines), and Eric White (USGS). We are grateful for support from SERDP under award RC-2111 to pursue this multidisciplinary study.

Abstract

Objectives: Permafrost and seasonal ground ice are key factors that control the routing of water above and below the land surface in interior Alaska. Hence, frozen ground affects water resources, ecosystem state, landscape evolution, and soil stability. Despite its hydrologic, ecologic, and geotechnical importance, the spatial distribution of permafrost and its relation to subsurface water flow remains poorly understood for many areas of interior Alaska largely due to its remoteness and inaccessibility. This study was aimed at improving the knowledge base by addressing the following objectives: (1) developing a new numerical modeling tool for simulation of groundwater/permafrost interaction, (2) demonstrating and evaluating geophysical methods for mapping of permafrost distribution at several test sites, and (3) elucidating permafrost-controlled surface-water/groundwater exchanges. The last objective was accomplished using physics-based modeling to evaluate local settings that were characterized by field efforts and by evaluating larger scale interactions based on generic understanding of permafrost patterns based on geophysical and other data.

Technical Approach: (1) The pre-existing U.S. Geological Survey (USGS) computer simulation code SUTRA (Saturated-Unsaturated, variable-density ground-water flow with solute or energy TRAnsport) was enhanced to simulate freezing and thawing of groundwater in saturated media. An additional enhancement addressed development of model capability to simulate freezing and thawing of groundwater in variably saturated media. These developments provide a tool that enable improved understanding of the interplay between frozen ground and groundwater to be developed. (2) Complementary ground-based geophysical techniques were used to map, between 2011 and 2014, the details of fine-scale subsurface geology and permafrost distributions at several specific study sites (10s to 100s of meters) in the Yukon Flats of east-central Alaska. A supplemental effort provided airborne geophysical characterization of large-scale permafrost distribution in interior Alaska (10s to 100s of kilometers). Comparison of results from a variety of methods enabled multi-scale interpretation of subsurface cryologic and geologic features. (3) Results from the small- and large-scale geophysical mapping were then used as the basis for a series of hydrologic model evaluations (based on SUTRA and other methodologies) that addressed questions related to permafrost/groundwater interaction and predicted system response to past changes in climatic and hydrologic conditions and also to potential future changes in these surface conditions.

Results: Completed research has resulted in both basic science and methodological advances. A groundwater modeling study of the Yukon Flats Basin of Alaska demonstrated and quantified the increase in baseflow to major rivers expected to result from permafrost degradation along a thaw sequence. The analysis showed the transition from continuous (>90%) to discontinuous (50−90%) permafrost coverage to be a critical one in terms of hydrologic change. Fully coupled fluid flow and heat transport simulations using the enhanced SUTRA model quantified rates of sub-lake talik (i.e., zone of year-round unfrozen ground that occurs in permafrost areas) development for a variety of conditions representative of those in the Yukon Flats. Lake talik evolution and cross sectional landscape simulations using SUTRA demonstrated the importance of advective heat transport in accelerating permafrost degradation compared with heat

conduction alone. Simulations with an imposed surface warming trend illustrated that permafrost thaws more quickly in places where there is active groundwater flow, particularly in groundwater recharge areas. Rates of permafrost growth and thaw depend on causal and hydrologic factors. Field-based geophysical investigations and SUTRA modeling results shed new light on permafrost-lake dynamics, providing a physically based explanation for the development of new permafrost around receding lakes in the presence of climate warming. Observations of new permafrost in the margins of receding lakes were shown consistent with the insulating effects of ecological succession. SUTRA simulations indicated, however, that such permafrost will persist for no more than about 70 years, under current projections of climate warming. Field results also provided insight into the present-day distribution of permafrost within the Yukon Flats, forming a valuable baseline to which future studies can compare. Methodological advances include demonstration of a multi-scale approach to geophysical mapping of permafrost and an integrated assessment of the capabilities and limitations of various geophysical techniques in the absence of deep subsurface information for ground-truthing. Software tools developed under the project, including SUTRA with cold region capabilities and FEMIC (Frequency-domain ElectroMagnetic Inversion Code) for analysis of large electromagnetic data sets, represent research products that will enable application of the project's approach in other studies.

Dissemination of the research results of this project have been made widely available via numerous presentations at national/international conferences and publication of journal articles, and several additional journal articles are planned. Collectively, these results have wide-ranging transferability to the characterization and system behavior of other permafrost-impacted environments.

Benefits: Knowledge gained and products developed within this study provide a broad foundation for future efforts to evaluate, in detail, the potential consequences of human-induced and climate-change stresses in key areas of Alaska. Furthermore, the hydrologic modeling tools and approaches and the geophysical methods and evaluation approaches developed here are readily transferrable to a wide range of issues related to permafrost characterization and dynamics affecting cold-region Department of Defense installations and operations.

A geophysical workshop offered as part of this project presented complementary approaches for subsurface characterization and monitoring in cold regions and, as a result, provided direct technology transfer.

Software for the enhanced SUTRA model and manuals describing its development and implementation will be publically available. Efforts in transitioning SUTRA with its capabilities for cold regions to a broad user community will continue on well after the project ends, in the form of regular USGS training workshops and support provided by its USGS developers. Additionally, a software package was developed for modeling and inversion of frequency-domain electromagnetic data. This will be published to enable follow-on research and wide-scale application of electromagnetic mapping of permafrost features.

All software codes produced by this project and all data collected as part of this project are archived and publically available. This open access will promote usage of the field-derived information and of the software tools. The data sets will serve as an important baseline for subsequent studies.

1. Objectives

The overarching goals of the study were to improve understanding of climate-change mediated aggradation and degradation of ground-ice and permafrost distribution in Alaska on the groundwater systems that control ecosystems and their biodiversity and to develop integrated approaches for anticipating future consequences.

Our specific technical objectives addressed within this report:

1. Develop quantitative software for numerical modeling of groundwater flow in aquifers impacted by freeze/thaw processes to address the Department of Defense's (DoD's) need for enhanced predictive hydrologic modeling in regions impacted by permafrost and seasonal ice.

2. Develop and implement a multi-method approach for determining the permafrost distribution in specific areas of strong hydrologic interest via ground-based geophysics and auxiliary data. The approach is to be broadly applicable to discontinuous permafrost regions.

3. Create numerical simulation models guided and informed by the geophysical characterization results, in order to gain general insight into the interplay of groundwater flow, ground ice (permafrost and seasonal ice), and climate.

We hypothesized that permafrost distribution plays an important role in the patterns and magnitude of groundwater flow and the distribution of surface water bodies, and in turn that groundwater flow and surface water bodies influence permafrost patterns and evolution. An integrated approach of permafrost characterization and coupled flow and energy transport modeling was used to qualitatively and quantitatively examine this hypothesis.

We focused the field initiative in the Yukon Flats in interior Alaska due to (a) the outstanding potential to leverage resources and efforts from a large, multidisciplinary study supported by the U.S. Geological Survey (USGS), and (b) the relevance of this area to DoD infrastructure underlain by similar discontinuous permafrost in interior Alaska.

2. Background

2.1 General

Alaskan ecosystems are responding to climate warming that has persisted for several decades (Hinzman et al., 2005). Variations in wetland and lake areas, soil moisture, and stream discharge magnitude and seasonal patterns are hydrologic changes that directly influence vegetation, biogeochemical cycling, and habitat sustainability. Evidence of lake area changes in parts of Alaska has been documented by remote sensing (Riordan et al., 2006; Rover et al., 2012). Walvoord and Striegl (2007) report historical increases in baseflow throughout the Yukon River Basin. The above mentioned studies propose a relation between observed hydrologic change and permafrost thaw. Yet while other research has demonstrated that permafrost is warming and thawing in some areas of Alaska (Lachenbruch and Marshall, 1986; Osterkamp and Romanovsky, 1999; Osterkamp, 2005), the link between permafrost degradation and specific hydrologic changes remains largely speculative. The challenges in substantiating inferred linkages and quantitatively evaluating permafrost hydrology derive from: (1) the complex and coupled interplay of ground ice evolution and water flow, (2) general lack of detailed subsurface information about permafrost distribution at multiple scales, and (3) a non-stationary climate, thus yielding a non-stationary hydrogeologic framework.

2.2 Hydrologic Models for Simulating Frozen Ground Dynamics

Quantitative predictive tools are needed for understanding processes occurring in the present-day subsurface system, for predicting possible future changes, and for evaluating management options for mitigating undesired ecological changes. However, subsurface ice distribution depends in a complex manner on the subsurface geologic fabric, the ground surface energy budget, and the groundwater flow itself. Numerical modeling codes, available at the start of this project, did not function at the scale required for practical hydrologic study and prediction, thus, new hydrologic computer codes were needed to forecast the hydrologic consequences of permafrost degradation and the resulting impact to military and federal infrastructure and operations. To provide a tool with which to develop understanding of the groundwater-ground ice system and potential feedbacks, the U.S. Geological Survey's SUTRA (Saturated-Unsaturated, variable-density ground-water flow with solute or energy TRAnsport) simulator (Voss and Provost, 2002) coupling groundwater flow and heat transport, was modified to include the water freeze/thaw process. To meet the additional needs of cold region model applications, generalized boundary conditions were added and a lake growth/decline package was coupled to the modified version of SUTRA.

2.3 Permafrost and Lithologic Characterization Using Geophysics

At the onset of this project, the actual permafrost distribution in Alaska as a whole, including location of its top and bottom, was largely unknown, except for discrete locations of limited extent. A common but generally untested assumption (by field measurements) in Alaska is that permafrost does not exist below major water bodies such as rivers and large lakes (e.g. see Lachenbruch et al., 1962; Williams, 1970; Burn, 2002, 2005). The correctness of this assumption is vital to our understanding of the interplay between surface water bodies and groundwater, and its viability underpins any meaningful prediction of future changes. The coupled cryologic/hydrologic response of systems to changes in ground ice distribution/groundwater flow is key to assessing the impact of environmental change in Alaskan ecosystems. Geophysical methods provide valuable insight into the spatial and vertical distribution of permafrost and relation to surface water bodies.

Numerous geophysical techniques (ground-penetrating radar, electromagnetics, electrical resistivity, and seismic) have been used to characterize glaciers (see review by French et al., 2006) and the depth and extent of permafrost (e.g., Hoekstra and McNeill, 1973; Daniels et al., 1976). Compared to conventional measurements of hydraulic properties (e.g., slug tests, pumping tests, tracer experiments, and coring) which require boreholes, geophysical surveys provide several advantages: (1) expanded spatial coverage, (2) higher resolution, and (3) lower cost.

Permafrost distribution is a critical gap in our general knowledge of permafrost environments that limits the forecasting potential of hydrologic models. For example, the impact of permafrost thaw on DoD lands in Alaska cannot be adequately addressed without improved characterization of the current distribution of permafrost on these lands and cost-effective means of continued monitoring at critical locations. To meet these needs, a multi-method geophysical approach that has wide applicability in characterizing permafrost distribution in the subsurface was developed in this project.

2.4 Integrated Hydrologic Analyses and Model Applications

The integration of analytical and numerical hydrologic modeling approaches with subsurface lithologic and cryologic characterization enables better understanding of the influence of permafrost on groundwater flow and vice versa. Integrated modeling enables testing of possible explanations of increased baseflow and observed changes in lake areas in interior Alaska. Permafrost information obtained via geophysical methods helps constrain conceptual models for both analytical and numerical approaches, guides numerical model scenario testing, and provides a means of numerical model calibration. Simulations that incorporate surface temperature variability are utilized to address the effects of climate on permafrost distribution and hydrologic processes. To gain insight into the interplay of subsurface water flow, subsurface ice, and surface

water bodies, several modeling studies were conducted that utilized information derived from the permafrost geophysical characterization results.

3. Hydrologic Model Development

3.1. Materials and Methods

The USGS-SUTRA code (Voss and Provost, 2002) that simulates groundwater flow of variable density with either solute or energy transport, was originally released in 1984 via a project funded by the U.S. Air Force Engineering and Services Center, Tyndall, A.F.B., Florida, and has been continually updated since then. The latest public release of the SUTRA code was used a basis for incorporating additional capabilities, described below, that are necessary for simulating important subsurface processes in cold regions.

3.1.1 Freeze/Thaw Processes

SUTRA was extended to incorporate the phase change between ice and liquid water. The enhanced code simulates dynamic ice formation when subsurface temperatures fall below a specified maximum freezing temperature. This new capability takes into account the latent heat of freezing/thawing, changes in relative permeability and effective porosity, and saturated-unsaturated freezing. Volumetric changes in the porous medium sometimes associated with freezing, such as frost heave, are not represented.

Ice and liquid saturations are defined as the fraction of ice and liquid water volumes, respectively, in the total pore volume. Ice saturation varies over a specified temperature range from 0 (thus, liquid saturation = 1) at the maximum freezing temperature, to 1 minus a specified residual liquid saturation at the specified minimum freezing temperature. The liquid water saturation and the ice saturation sum to equal the total water saturation.

The development of the groundwater-flow and energy-transport equations is similar to that in previous versions of SUTRA but is extended to include phase change between liquid water and ice. Derivation of the groundwater-flow equation begins with a transient total-mass balance for pore water, both frozen and unfrozen, and the total-water saturation is partitioned into liquid-water and ice saturations. Expansion in terms of derivatives with respect to pressure and temperature and incorporation of Darcy's Law then lead to a groundwater-flow equation that accounts for changes in saturated and unsaturated storage of liquid water and ice, flow of liquid water, external sources of water, and apparent sources of water associated with volumetric expansion or contraction of liquid water and ice due to temperature changes. As mentioned earlier, volumetric changes associated with phase change are not included. Derivation of the energy-transport equation begins with a total thermal-energy balance that includes liquid water, ice, and the solid matrix. These three constituents are assumed to be in thermal equilibrium with each other at any given point in the model, the thermal energies of the constituents are expressed as linear functions of their common temperature. The latent heat associated with freeze-thaw is introduced as the difference between the thermal energies of liquid water and ice at the freezing point, and the conductive-dispersive heat flux is expressed using an effective, or "bulk," thermal conductivity and is proportional to the temperature gradient. The first part of the derivation

yields the "divergent" form of the energy balance. To obtain the "convective" form solved by SUTRA, the term involving the divergence of the advective heat flux is expanded, and the total-water mass balance and the assumption of an immobile solid matrix are used to simplify the equation. The result is a temperature-based thermal-energy transport equation that takes into account changes in storage of thermal energy in the liquid water, ice and solid matrix due to changes in temperature and the amounts of liquid water and ice; advection and diffusion-dispersion of heat; and external sources and internal production of heat.

The modified SUTRA code allows for definition of non-linear freezing and relative permeability relations. Often, due to the lack of established constitutive relationships, liquid water can, for simplicity, be assumed to freeze according to a linear function of temperature with liquid saturation decreasing across a defined range, say from $0^{o}C$ to $-1^{o}C$. Further, an increase in ice saturation can be assumed to reduce the effective permeability of the geologic medium as a linear function between ice saturation and permeability or the $\log_{10}$ transform of permeability. For example, when assuming the $\log_{10}$, the relative permeability can be specified to have decreased (log-linearly) by three orders of magnitude ($1x10^{-3}$) when ice saturation reaches 0.80, a functionality patterned after nuclear magnetic resonance measurements and ice-permeability analyses by Kleinberg and Griffin (2005). For higher ice saturation, the $\log_{10}$ of relative permeability can be decreased linearly along a secondary slope toward a fully-restricting condition ($1x10^{-30}$) when ice saturation reaches 0.99. This coupling of water movement with energy transfer enables the simulation of both conductive and advective heat transport processes in cold region environments.

The SUTRA model for saturated-unsaturated freezing is based on the following assumptions:

1) The effects of water vapor are negligible. Only ice and liquid water need be considered.
2) At a given temperature, the porous medium contains more liquid water when it is fully saturated than it does when it is partially saturated. In other words, partially desaturating the medium cannot increase the liquid water saturation if the temperature remains constant.
3) At a given temperature, the porous medium contains more ice when it is fully saturated than it does when it is partially saturated. In other words, partially desaturating the medium cannot increase the ice saturation if the temperature remains constant.
4) Some minimum amount of liquid water always remains, regardless of the temperature.
5) Given the preceding assumptions, as little water as possible freezes.
6) Total-water saturation is a function only of pressure (not temperature).
7) Ice saturation under fully saturated conditions is a function only of temperature (not pressure).
8) Relative permeability is a function only of liquid-water saturation.
9) The formation of ice does not deform the porous medium (i.e., no volume expansion of the matrix), nor is water attracted to the freezing front by decreased pressures (i.e., no cryosuction). Similarly, the transition from ice to water does not deform the porous

medium (i.e., no volume reduction of the matrix). These assumptions limit the model to hydrological calculations in the absence of geomechanical feedbacks.

The SUTRA saturated-unsaturated freezing model was derived from a set of assumptions regarding the behavior of functions that determine the total-water, liquid-water, and ice saturations and the relative permeability. The development took a macroscopic approach in that it made no reference to physical processes at the pore scale. It is possible, however, to arrive at the same model by proceeding from a set of assumptions regarding pore-scale processes:

1) The porous medium is treated as a continuum, and the liquid-water and ice saturations at any point are aggregates of the states of individual pores within a representative elementary volume (REV) at that point.
2) Each pore can be characterized as having a single effective radius that influences both its tendency to saturate with water and its tendency to freeze.
3) An individual pore is either completely saturated (filled) or completely desaturated (empty), depending only on pressure. The smaller the radius of a pore, the lower (more negative) the pressure at which it desaturates. So, at a given pressure, all pores above a certain radius are desaturated (empty), and all pores below that radius are saturated (filled).
4) An individual pore is either completely frozen or completely unfrozen, depending only on temperature, the pore radius, and whether the pore is filled or empty. The smaller the radius of a pore, the lower the temperature at which it freezes. So, at a given temperature, all filled pores above a certain radius are frozen, and all pores below that radius are unfrozen.
5) The configuration of liquid water in the pore space in the presence of ice is the same as it would be under ice-free conditions at the same liquid-water saturation.

In the modified SUTRA model, a number of unsaturated-flow and ice-saturation functions are preprogrammed, and their parameters can be specified through a SUTRA input dataset. The preprogrammed water-saturation functions are:

- van Genuchten (1980),
- Brooks and Corey (1964),
- power law, and
- piecewise-linear;

the preprogrammed relative-permeability functions are:

- van Genuchten (1980),
- Brooks and Corey (1964),
- power law, and
- piecewise-linear;

and, the preprogrammed ice-saturation functions are:

- exponential,
- power law, and
- piecewise-linear.

In addition, any user-defined model that can be programmed into the unsaturated conditions subroutine is recognized within the same framework, so users may program their own functions and specify function parameters. The different types of water-saturation, relative-permeability, and ice-saturation functions may be used in any combination.

3.1.2 Generalized Boundary Conditions

An additional accomplishment in model development, exceeding tasks outlined in the proposal, was the incorporation of generalized boundary conditions for SUTRA. Two new types of "generalized" boundary conditions were implemented that facilitate simulation of a wider range of hydrologic processes that interact with the groundwater model, such as rivers, drains, and evapotranspiration. For "generalized-flow" conditions, inflow or outflow of fluid mass varies linearly with pressure, subject to optional upper and lower limits on flow and/or pressure. For "generalized-transport" conditions, inflow or outflow of solute mass or energy varies linearly with concentration or temperature, respectively.

Prior to the generalized boundary condition implementation, SUTRA supported only the following four types of boundary conditions:

- sources and sinks of fluid mass,
- sources and sinks of solute mass or thermal energy,
- specified pressures, and
- specified concentrations or temperatures.

These four types, which are still supported in the current version of SUTRA, allow users to represent a variety of physical processes that interact with the groundwater model, such as pumping or injection of water, recharge, pressure due to surface water of known depth and density, addition of tracer, and variations in surface temperature.

To facilitate representation of a wider range of physical process, two additional types of boundary conditions have been added:

- generalized flow conditions – sources and sinks of fluid mass that depend on pressure, and
- generalized transport conditions – sources and sinks of solute mass or energy that depend on concentration or temperature, respectively.

The two new types of boundary condition are "generalized" in the sense that they include the four original types as special cases while offering additional capabilities. Like the four original types, the two new types can be made time-dependent using input files.

Like sources and sinks of fluid mass and specified pressures, generalized-flow conditions require specification of concentrations or temperatures associated with inflows to the model. In addition, generalized-flow conditions require specification of concentrations or temperatures associated with outflows from the model. The latter requirement enables simulation of processes such as evaporation, in which fluid may leave the model at a concentration or temperature different from that of the groundwater.

3.1.3 Lake Capability

The lake capability simulates the evolution of lakes as they exchange fluid mass and solute mass or thermal energy with each other and with groundwater. This capability was fully integrated with SUTRA, thereby allowing lakes to form, fill, coalesce, drain, empty and divide. Simulated lakes interact with the groundwater flow model through boundary conditions. Lakes increase boundary pressures and receive and supply water and solute or energy that would otherwise have entered or exited the groundwater-flow system directly through boundary-condition nodes. Lakes can also activate and deactivate boundary conditions, giving the user considerable flexibility in modeling the effects of lakes on the groundwater-flow system.

Given the topography of the top surface of the model, SUTRA identifies the lakes that can form by “ponding” of water on the top surface. Increases and decreases in lake stage can cause lakes to coalesce and divide, leading to a hierarchy of “parent” and “child” lakes that is automatically determined by SUTRA at the start of the simulation. On each time step, SUTRA solves the groundwater flow equation, computes rates of exchange of water between groundwater and lakes, updates lake stages and concentrations or temperatures, computes rates of exchange of solute mass or thermal energy between lakes and groundwater, and solves the groundwater transport equation. The calculations are performed such that water mass and solute mass or thermal energy are conserved. To illustrate how the new function determines the set of potential lakes, consider the example shown in Figure 3.3.1. For simplicity, the topography in this example varies along only one grid direction, effectively reducing the dimensionality of the problem.

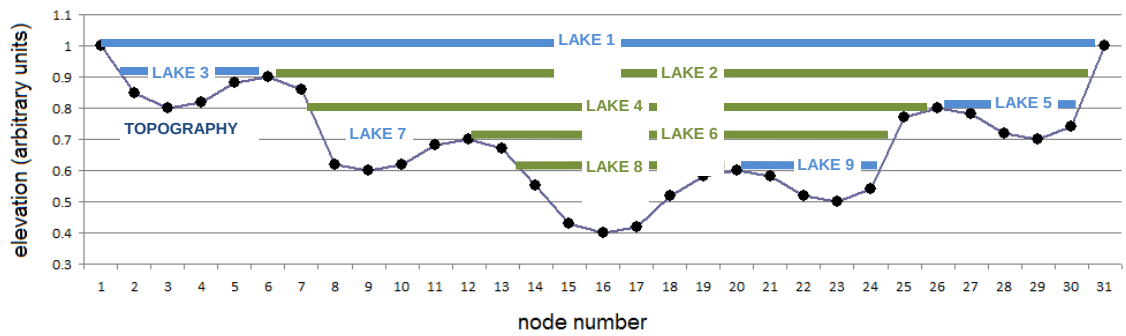

Figure 3.1.3.1 Example for nine potential lakes based on given surface topography. To simplify the explanation, the dimensionality of the problem has been reduced, and the node numbering includes only surface nodes. Black dots represent surface nodes. Blue and green horizontal lines show the stages at which the various lakes come into existence by splitting of larger lakes as the stage decreases. Two different colors are used to help differentiate adjacent ("sibling") lakes.

SUTRA identifies potential lakes by starting with the highest surface node and working its way down through surface nodes in order of decreasing elevation, finding the "sills" at which lakes divide. In this example, the search begins with the water stage set at 1.0 (the highest elevation, which is found at nodes 1 and 31). At this stage, all the lake water is coalesced in one lake, which we call lake 1.

When the stage drops below an elevation of 0.9 (node 6), lake 1 divides into two lakes: lake 2 on the right (nodes 7 – 31) and lake 3 on the left (nodes 1 – 5).

The next division occurs when the stage drops below 0.8 (node 26). Then lake 2 divides into lake 4 (nodes 8 – 25) and lake 5 (nodes 27 - 30). Similar divisions occur as the stage drop through elevations of 0.7 (node 12) and 0.6 (node 20).

In the end, SUTRA identifies the 9 potential lakes shown in Figure 3.3.1. The lakes form a hierarchy of "parents" and "children" that is mapped out as an inverted tree in Figure 3.3.2.

The potential lakes are conceptualized as distinct objects that can each hold a certain volume of water. Each surface node is assumed to be overlain by a "cell" that can collect water, and the capacity of a lake is the sum of the volumes of all the cells in that lake. The rate at which the lake stage rises as the volume of water in the lake increases is proportional to the surface area of the lake, which is the sum of the areas associated with all the submerged surface nodes in the lake. Thus, lake stage is a piecewise-linear function of volume, with an increase in slope occurring each time the lake stage rises high enough to submerge another node. If the volume of water in a lake is known, its stage can be computed using this function. Each lake has its own stage-volume function, which is computed automatically.

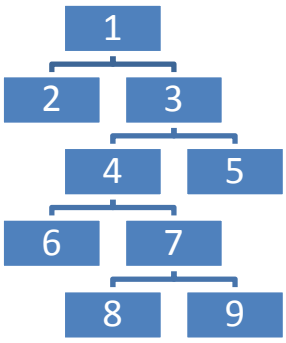

Figure 3.1.3.2 Hierarchy of nine lakes identified in the example problem.
Moving down the tree as stage decreases, lake 1 divides into lakes 2 and 3, lake 3 divides into lakes 4 and 5, etc. Moving up the tree as stage increases, lakes 8 and 9 coalesce into lake 7, lakes 6 and 7 coalesce into lake 4, etc. Lake 7 is the "parent" of lakes 8 and 9; lakes 8 and 9 are "siblings," as they are both "children" of lake 7.

The incorporation of the lake capability into the version of SUTRA with freezing capabilities was viewed as a critical model development aspect for simulating groundwater-surface water interaction among sets of cold region lakes that may be variably hydrologically connected in both time and space depending on permafrost configuration and interaction with climate.

3.2 Results and Discussion

The modified version of SUTRA with freeze/thaw capabilities has been compared with analytical solutions (Kurylyk et al., 2014a) and has been utilized by end users internal to (described in section 5) and external to (i.e., Ge et al., 2011; Kurylyk et al., 2014b) the SERDP-supported project. Version 3.0 incorporates the generalized boundary conditions and the lake evolution capability. Full documentation of the added capabilities and instruction on how to apply these capabilities with SUTRA simulations are provided in Provost and Voss (2014; USGS-approved and in final production). Version 4.0 incorporates the freeze/ thaw capability in addition to the added functions in Version 3.0. Full documentation and user instructions are provided in Voss et al. (in preparation). The SUTRA 3.0 and 4.0 software will be published concurrently with the reports and will be publicly available online.

Results of simulations using the modified SUTRA code are detailed in section 5 of this report. In addition, results of idealized test problems are discussed below.

3.2.1. Freeze/Thaw: The Frozen Wall

This example demonstrates the effect of freezing on the flow field in a groundwater system. The frozen wall is an engineered intervention that creates a region of low permeability that shields a contaminated portion of the aquifer from regional groundwater flow that would otherwise spread contaminants from the contaminated site to a larger area (i.e,. thermosyphoning technology and applications). A similar "frozen wall problem" was first proposed by McKenzie et al. (2007).

The area considered is a 25 m by 15 m area in which contaminant exists in a 4 m by 4 m square region centered along the south edge of the area (Figure 3.2.1.1). Regional groundwater flow in

this shallow, uniform aquifer occurs uniformly from west to east. An L-shaped frozen "wall" 0.5 m in width is emplaced by burying freezing coils through the entire thickness of the shallow aquifer. The wall is installed just upstream and along the lateral side of the contaminated area, at a distance of 0.5 m from the contaminated zone to avoid entraining contaminants during emplacement. The wall extends 5 m in the north-south and 5 m in the east-west directions.

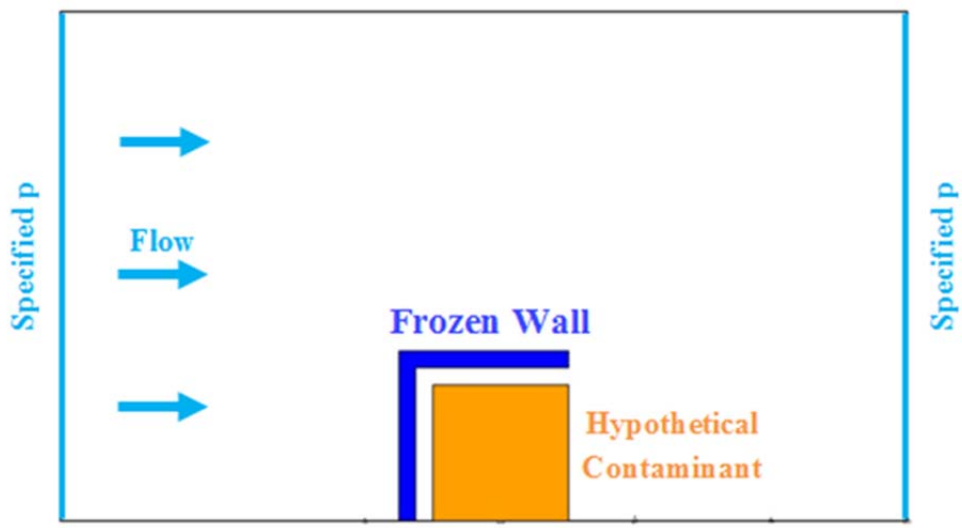

Figure 3.2.1.1 Model schematic for the frozen wall example problem.

The modeled area is initially at a temperature of 5 °C and water of the same temperature steadily recharges the area from one side. At the start of the simulation, a specified subfreezing temperature is set within the hypothetical wall, which is held at this temperature throughout the simulation. This may be considered as one half-section of a larger region containing a series of walls with uniform spacing that are perpendicular to the regional groundwater flow direction. Figure 3.2.1.2 illustrates the flow field and temperature distribution approximately 25 days after the wall freezing is initiated. Groundwater flows around the frozen wall, which forms a very low permeability barrier. Figure 3.2.1.3 shows the corresponding ice-saturation distribution.

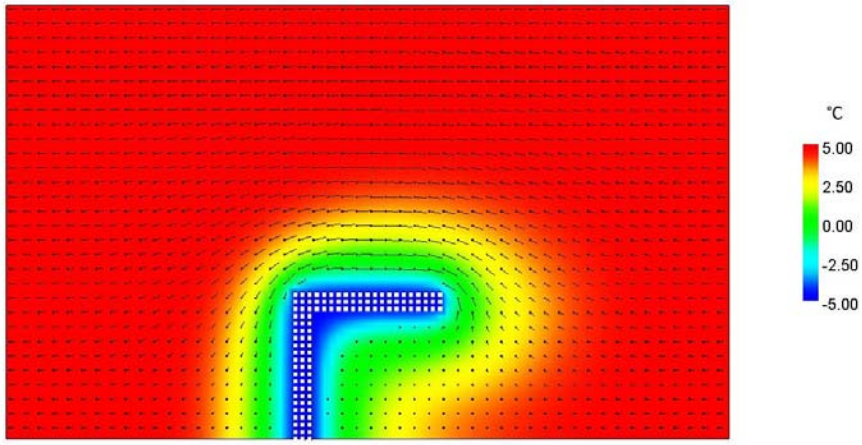

Figure 3.2.1.2 Flow field and temperature distribution after 25 days.
White squares denote model nodes that represent the frozen wall. Velocity vectors are drawn using a dot to show location and line segment to show direction and relative magnitude. Colored shading represents temperature in °C, as indicated in the legend.

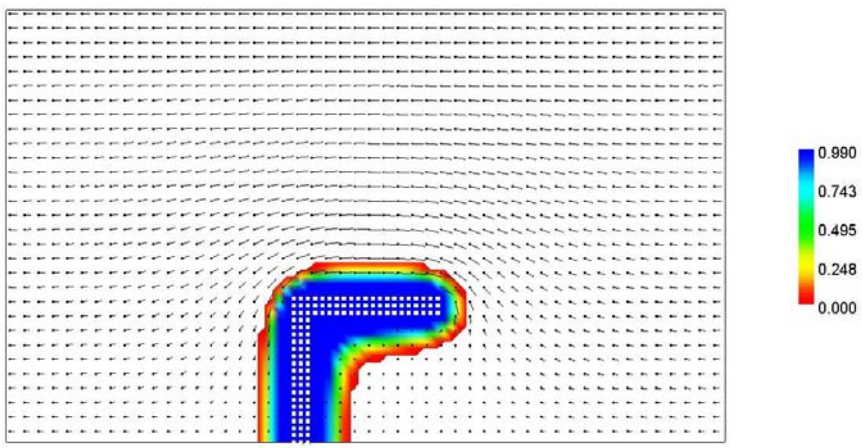

Figure 3.2.1.3 Ice-saturation distribution after approximately 25 days.
White squares denote model nodes that represent the frozen wall. Velocity vectors are drawn using a dot to show location and a line segment to show direction and relative magnitude. Colored shading represents ice saturation, as indicated in the legend. The area that is not colored is ice-free.

3.2.2. Generalized Boundary Conditions: Dam with Vertical Sides (Seepage Face)

This problem involves two-dimensional (2D), constant-density groundwater flow through a 10-meter-wide and 10-meter-high dam with vertical sides under steady-state conditions. The water level is held even with the top of the dam on the upstream side, where hydrostatic conditions prevail, and water does not accumulate on the downstream side, where water exits through a

seepage face (Figure 3.2.2.1). The seepage face boundary condition is implemented using a generalized flow condition.

Figure 3.2.2.2 shows the simulated, near-steady-state water table and flow field after approximately 82 hr of simulated time. Along the right vertical boundary, no flow crosses the boundary above the water table, and below the water table water discharges through the seepage face. The slight decrease in the slope of the water table as it nears the right vertical boundary is due to the fact that at that boundary the simulated water table must coincide exactly with a node at which $p = 0$ is specified; the water table cannot fall between two nodes at that boundary. The intersection of the water table with the right vertical boundary marks the top of the seepage face. The semi-analytical solution of Polubarinova-Kochina (1962), which does not account for flow through the unsaturated zone, predicts a slightly lower seepage face height (Figure 3.2.2.2, black circle). The Dupuit formula, which is exact if it is assumed that no flow occurs through the unsaturated zone, predicts discharge of 4.905×10^{-5} m^3/s per meter of dam thickness perpendicular to the cross section. This is 6 percent less than the discharge simulated by SUTRA, which is 5.228×10^{-5} m^3/s per meter of dam thickness.

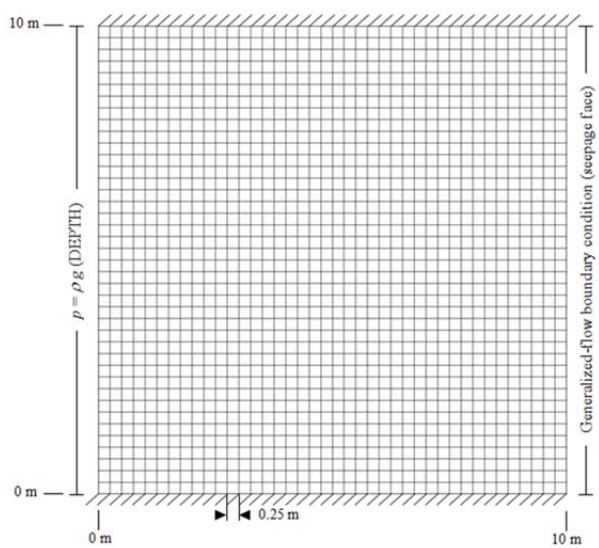

Figure 3.2.2.1 Boundary conditions and finite-element mesh for the dam (seepage face) example.

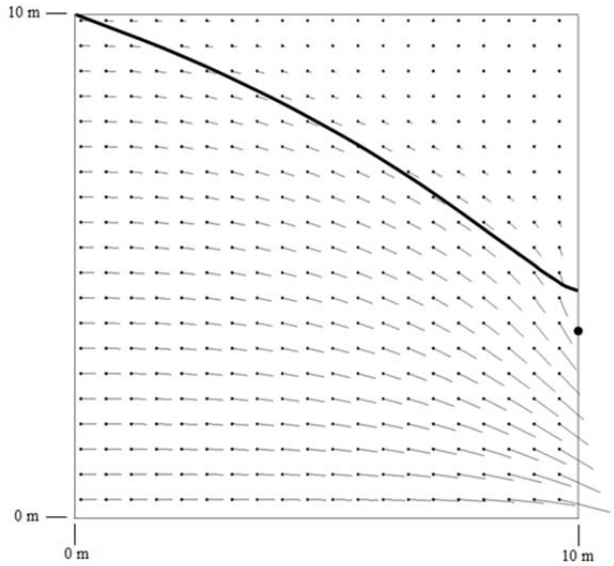

Figure 3.2.2.2 Near-steady-state SUTRA results for the seepage face example.
The thick line indicates the numerically simulated position of the water table (p = 0). The intersection of the thick line with the right vertical boundary indicates the numerically simulated top of the seepage face. The black circle indicates the top of the seepage face predicted by the semianalytical solution of Polubarinova-Kochina (1962). Dots indicate element centers from which flow-velocity vectors (thin line segments) emanate. Vector length is proportional to velocity magnitude. Vectors are plotted for every second element in each coordinate direction.

3.2.3. Lake Capability: 3-Lake Example

This problem involves interaction of 3D groundwater flow with lakes and transport of solute between groundwater and lakes. The model domain covers a 10-km-by-20-km rectangular area and is approximately 100 m deep, with a variable surface topography that includes three topographic depressions (Figure 3.2.3.1). Initially, no lake water is on the surface of the model. As topographically driven groundwater flow recharges at higher elevations and discharges at lower elevations, lakes form in the three topographic depressions. A source of solute at the model surface enters the groundwater and discharges into one of the lakes. As the lake stages rise, the lakes coalesce, and their waters mix. Eventually, one large lake forms. Subsequent withdrawal of lake water causes the lake stage to fall, and the large lake splits into the three original lakes. At the end of the simulation, the groundwater-lake flow system is near steady state.

Figure 3.2.3.2 shows areas of the model surface covered by lake water at a sequence of times during the simulation. Figure 3.2.3.3 illustrates how lake-water concentrations change with time.

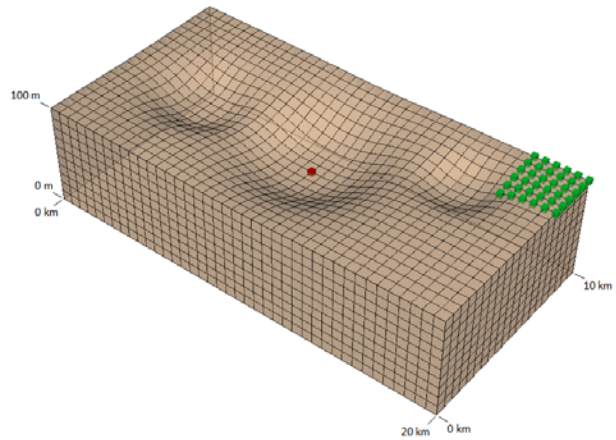

Figure 3.2.3.1 Boundary conditions and finite-element mesh for the 3-lake example. Green cubes denote specified-pressure nodes that act as solute sources. Red cube denotes a fluid sink node that withdraws lake water. (50X vertical exaggeration)

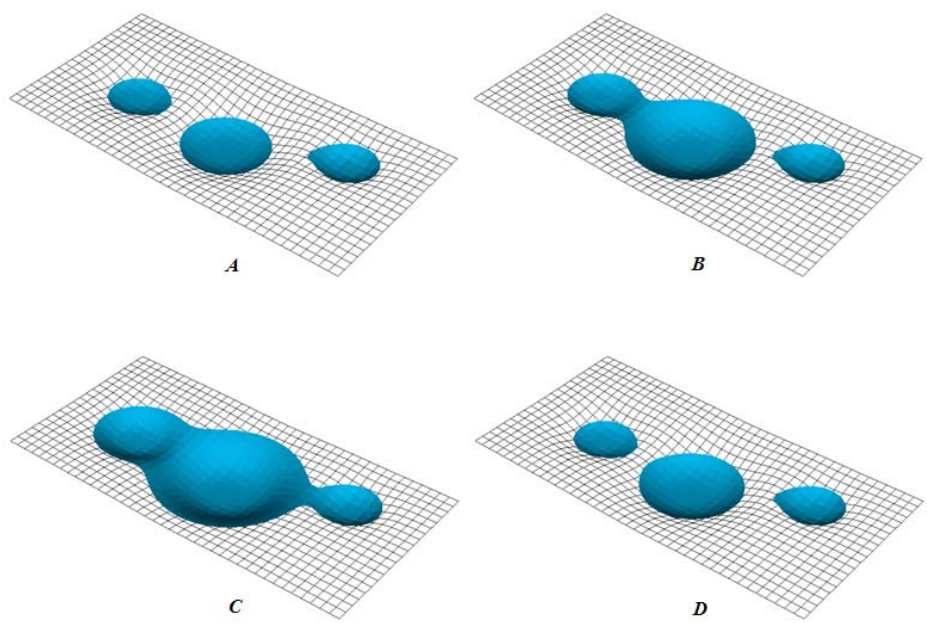

Figure 3.2.3.2 Areas of the model surface covered by lake water (blue) in the lake example. Groundwater flow recharges at higher elevations and discharges at lower elevations, supplying water to form lakes in the topographic depressions. *A*, By 30 weeks, lakes 3 (right) and 4 (left) are full and are spilling over onto lake 5 (middle). *B*, By 60 weeks, lakes 4 and 5 are coalesced into their parent, lake 2. *C*, By 100 weeks, all lakes are coalesced into one large lake (lake 1), and lake-water withdrawal begins. *D*, By 500 weeks, lake stages have declined such that there are once again three distinct lakes, and inflows nearly balance outflows in each lake, so the flow system is near steady state. (50X vertical exaggeration)

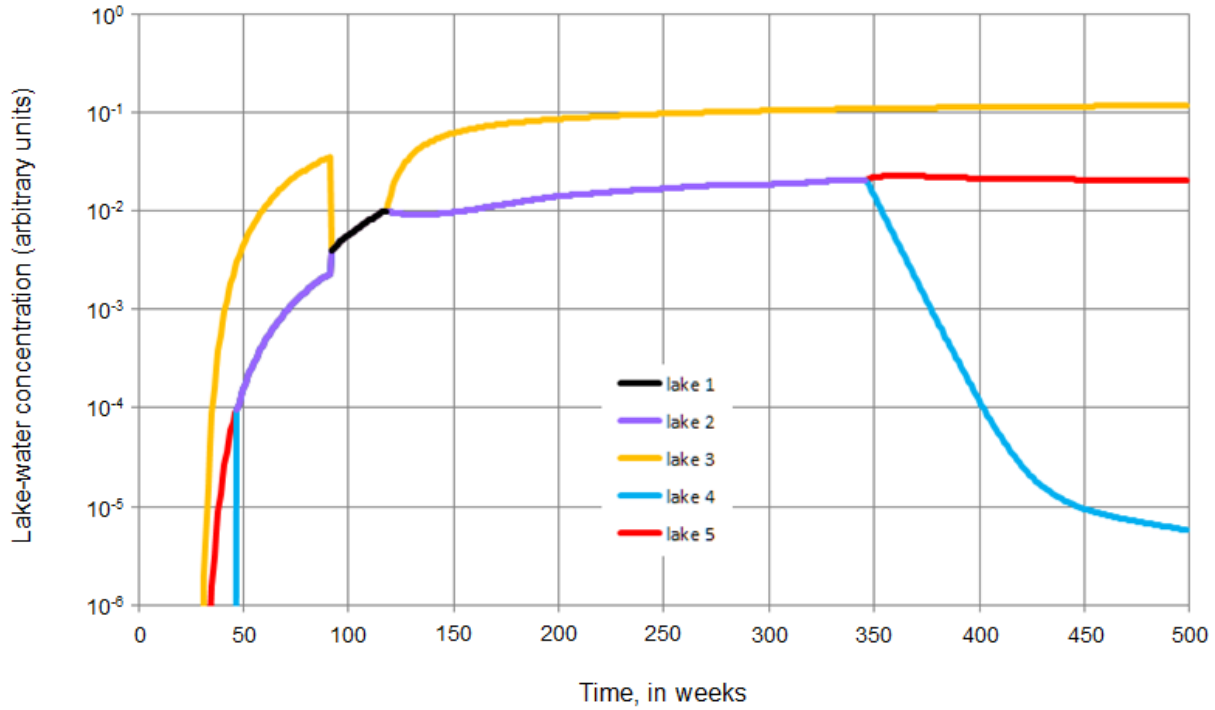

Figure 3.2.3.3 Lake-water concentration as a function of time in the lake example. Concentration is expressed in arbitrary units in which the maximum source concentration is 1. When two lakes coalesce (lakes 4 and 5 at 47 weeks, and lakes 2 and 3 at 92 weeks), the water in the parent lake is a mixture of the concentrations in the two child lakes. When a lake splits into its children (lake 1 at 119 weeks, and lake 2 at 347 weeks), the concentration in each child lake is initially the concentration from the parent lake. Over time, the concentrations in the two child lakes diverge.

4. Geophysical Investigations

Geophysical field investigations were conducted at two sites in interior Alaska in late summer 2011, 2012, and 2014. Geophysical methods demonstrated included ground penetrating radar, frequency-domain electromagnetics, direct-current resistivity, and time-domain electromagnetics. Operation and information acquired from these methods are illustrated schematically in Figure 4.0.1.

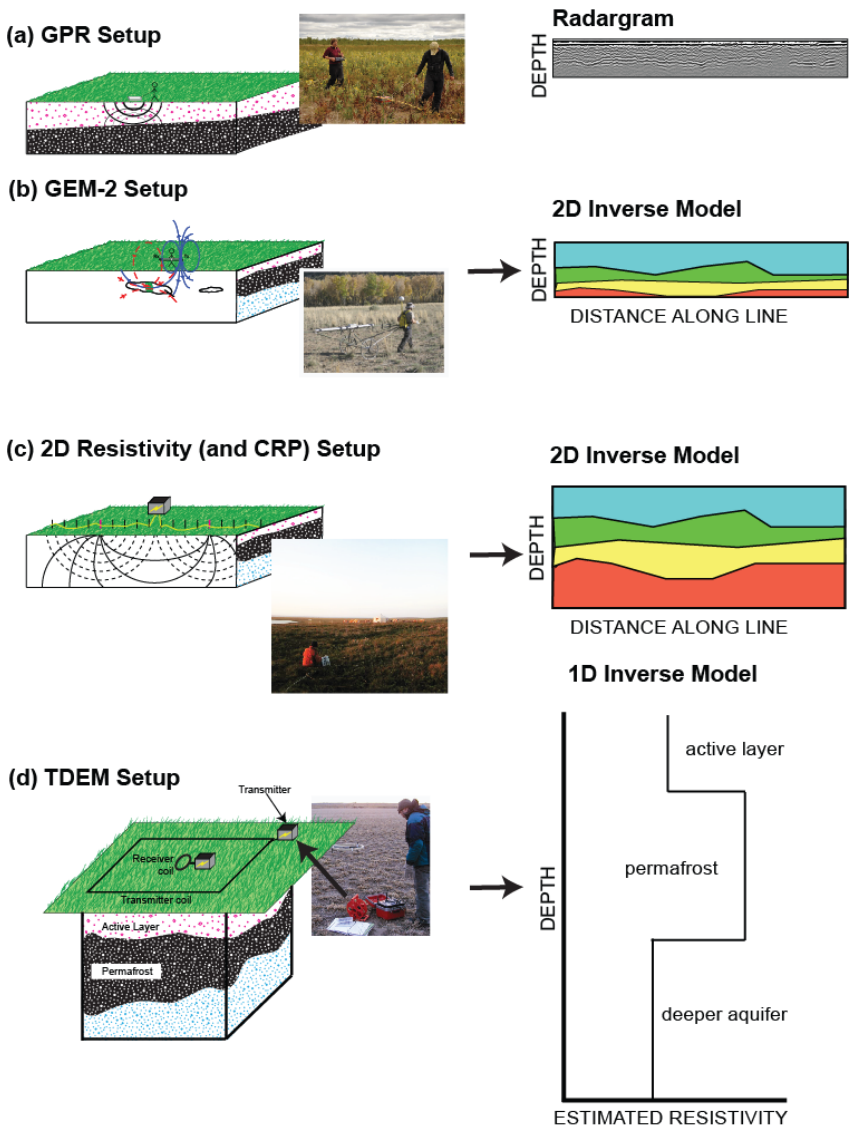

Figure 4.0.1 Schematic diagram illustrating setups and data products for geophysical methods used in this work: (a) ground penetrating radar (GPR); (b) multi-frequency electromagnetic induction using a GEM-2 instrument; (c) two-dimensional electrical resistivity (2D Resistivity) and continuous resistivity profiling (CRP); and (d) time-domain electromagnetics (TDEM).

The geophysical methods used in our work were selected based on their complementary and overlapping spatial resolutions and coverage (Figure 4.0.2). In addition to our ground-based geophysical methods, another USGS group recently collected airborne electromagnetic (AEM) surveys under related research in Alaska (Minsley et al., 2012). We collaborated with the other USGS group to integrate the AEM information with the ground-based geophysical information collected in this study. As illustrated in Figure 4.0.2, the various methods provide information over different ranges of depth, or with varying spatial resolution, or with different spatial coverage. For example, airborne electromagnetics provides the best spatial coverage of methods considered but at low resolution compared to several other methods, such as ground-penetrating radar. In addition, we also collected passive seismic, temperature, and frost-probe data. Passive seismic was conducted as a test of a new method, not previously (to our knowledge) used in permafrost settings. Temperature and frost-probe data were collected for ground truth.

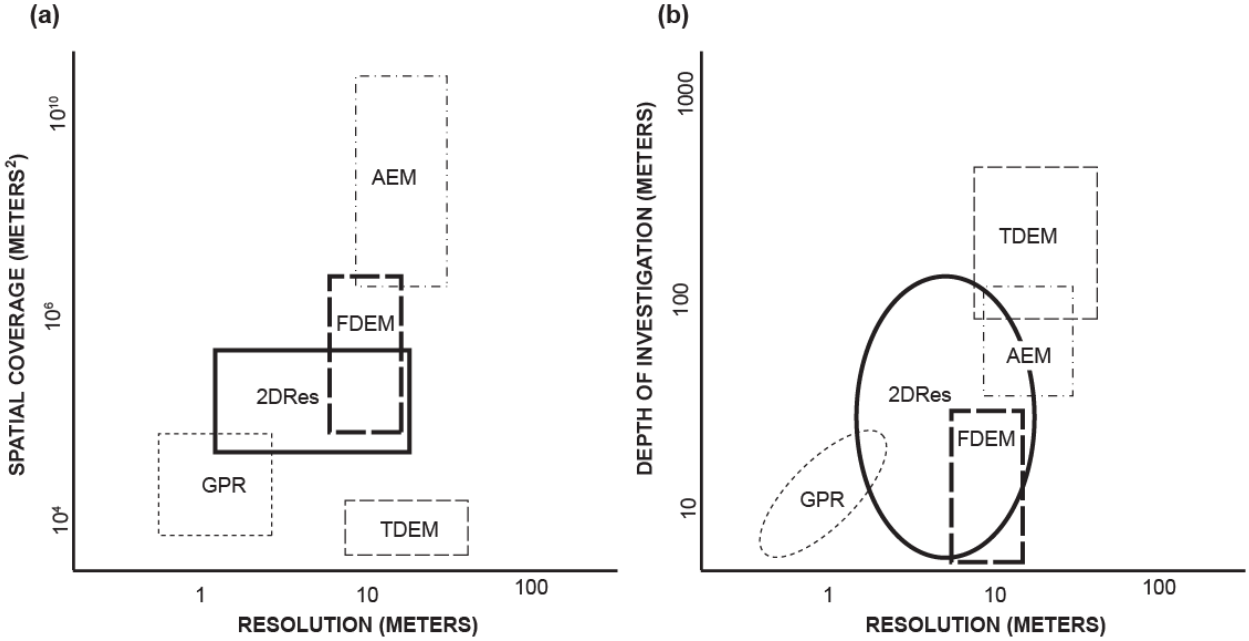

Figure 4.0.2 Schematic diagram illustrating the tradeoff in coverage and resolution for geophysical methods used in this work.

4.1 Study Area

The Yukon Flats is located within the discontinuous permafrost zone in eastern interior Alaska (Jorgenson et al., 2008). Geophysical surveys were conducted at two sites in the Yukon Flats: Beaver Meadow Lake near Fort Yukon north of the Yukon River, and the Twelvemile Lake study area, which is situated ~18 km (~12 miles) southwest of Fort Yukon, and ~12 km south of the Yukon River main channel (Figure 4.1.1). The Twelvemile Lake location has been a USGS research site, hence our research there was synergistic with past and concurrent research. The site is remote and accessed primarily by float plane. The Beaver Meadow site is close to Fort Yukon,

Alaska and accessed by roads, and thus provided a more cost-effective test site for method demonstration of geophysical approaches. Additional field demonstrations were conducted around Fairbanks during a training course put on by project PI's as a tech-transfer and outreach effort in August 2014.

From a lack of inlet or outlet, Twelvemile Lake was stagnant for decades (until flooding in 2013), yet numerous relict sediment-filled channels surround the lake. The two most obvious and recently active channels are located in the northwest and southeast corners of the lake. The Northwest channel meanders and breaks off into multiple sub-channels. The southeast channel is more defined and evidence suggests that it is an old inlet to Twelvemile Lake with flow originating from Buddy Lake, 2-3 km distant. This drainage feature originates from grasslands surrounding Buddy Lake and immediately narrows into a series of disconnected water-filled thermokarst features and hummocks. Jepsen et al. (2012b) show an abrupt 2 m water table elevation drop between Buddy Lake and Twelvemile Lake within this beaded stream. The thermokarst beaded stream continues for approximately 500 m before it widens as it approaches Twelvemile Lake. The overall elevation range between Buddy and Twelvemile Lake is < 20 meters. Vegetation is characterized by black spruce transitioning into aspen, low growth shrubs, and grasses with increasing proximity to current or recent water bodies.

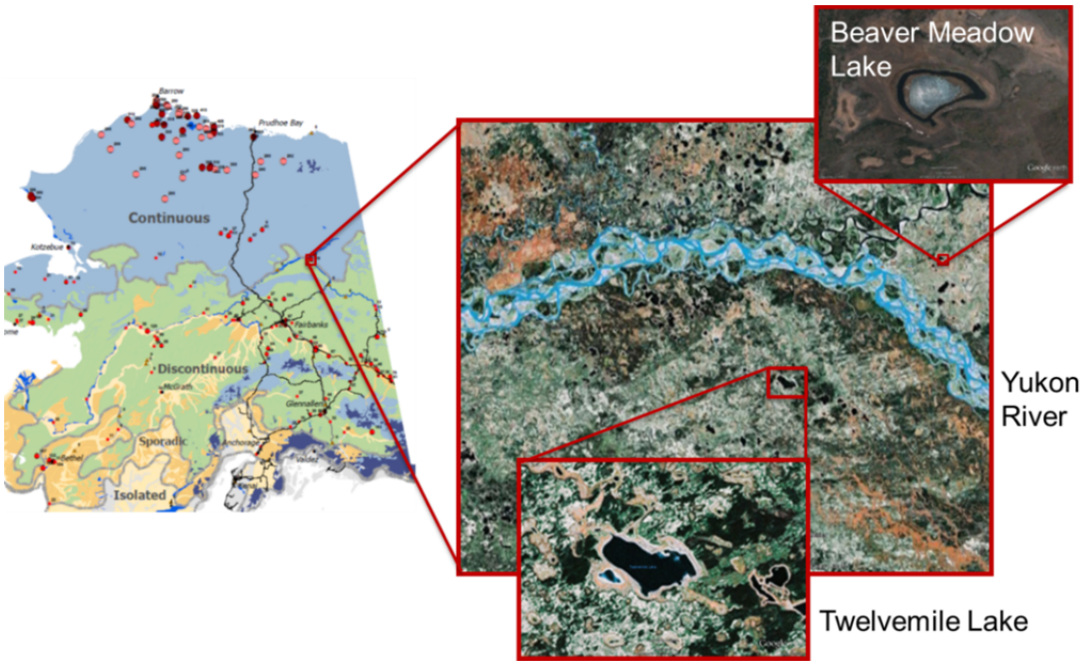

Figure 4.1.1 Location map of Beaver Meadow and Twelvemile study areas.

4.2 Materials and Methods

Field geophysical campaigns were conducted with SERDP support in August of 2011, 2012, and 2014 and April of 2012. Additionally, our group collected field data in August 2010 with USGS funding. Complementary geophysical methods were employed, providing information about

subsurface conditions at different depths or with different spatial coverage. Co-located surveys were conducted to compare results from different methods and to evaluate depth of investigation and spatial resolution. Several transects from 2011 were reoccupied in 2012 for repeat surveys to evaluate changes over time.

4.2.1 Resistivity

Direct-current electrical resistivity measurements were collected using a 10-channel IRIS Syscal Pro instrument and inverted using several different software packages. The method can image to a depth of approximately one fifth the maximum spread between electrodes (e.g., 100 m for a 0.5-km line). Resistivity increases in saturated porous media with freezing, hence the ability of the method to detect permafrost. In total, 5 resistivity lines were collected at Twelvemile (~2 km) and four at Beaver Meadow (~1.5 km). Several lines were collected at multiple electrode spacings to provide multi-resolution information. Whereas longer spacing provides superior depth of investigation and coverage, shorter spacings provide superior resolution. Representative results are shown in Figure 4.2.1.1.

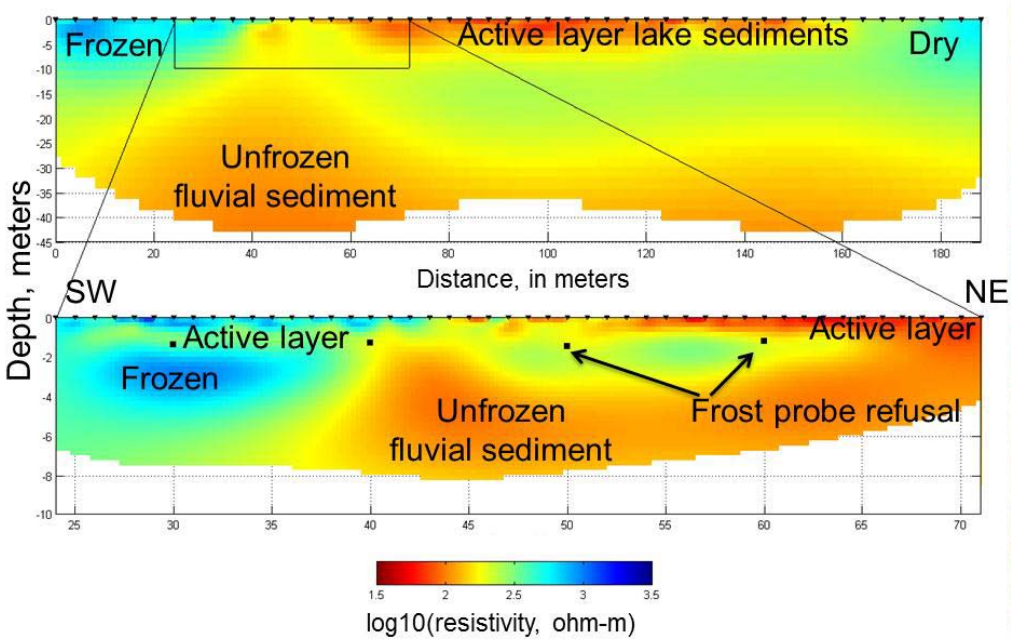

Figure 4.2.1.1 Resistivity line 2 from Twelvemile Lake collected August 2011, with images for 4-m and 1-m electrode spacing, providing multi-resolution information about subsurface conditions.

To understand the ability of resistivity to resolve shallow permafrost, we conducted numerical experiments on hypothetical permafrost configurations and various survey geometries. SUTRA models were run to produce physically based distributions of soil moisture and temperature, which were converted to cross sections of resistivity using the petrophysical relation Archie's Law. Synthetic resistivity data were computed using a finite-difference model, random noise

(2%) was added for realism, and data were inverted using the same codes and procedures applied to field data. This analysis provides valuable insight into survey design. For example (Figure 4.2.1.2), a 2-meter electrode spacing is capable of revealing shallow resistivity variations undetected by inversions of data collected using a 4-meter electrode spacing.

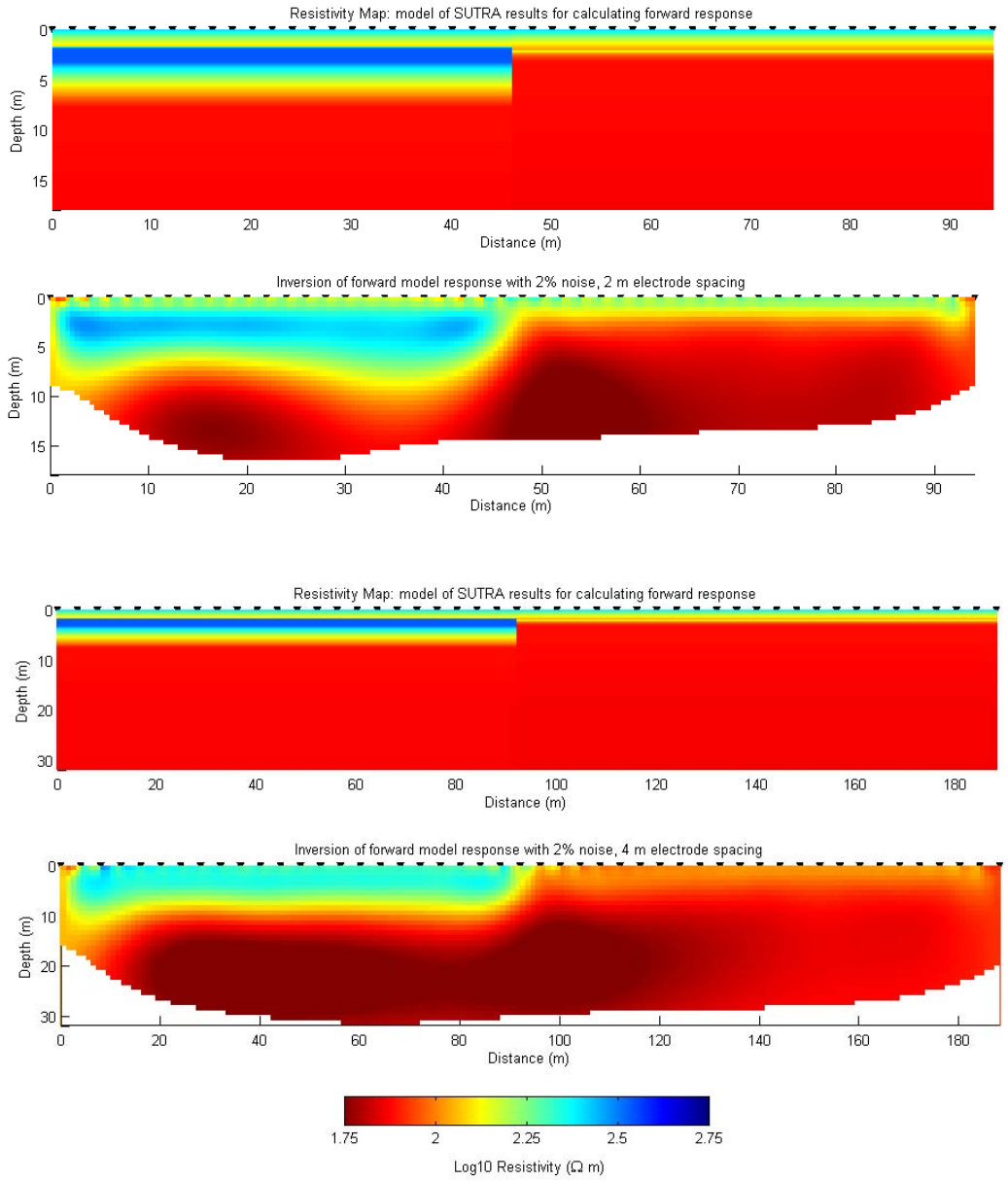

Figure 4.2.1.2 Synthetic examples illustrating the resolving power of 2D resistivity using different survey geometries. The top plot shows the true, hypothetical resistivity cross section based on SUTRA model output for soil moisture and temperature. The second plot shows the resulting resistivity inversion, assuming 2% noise and 2-meter electrode spacing. The third plot shows the same true, resistivity cross section at a larger scale. The fourth plot shows the resistivity inversion resulting from data collected with a 4-meter electrode spacing.

4.2.2 Electromagnetics

Frequency domain electromagnetic (FDEM) induction data were acquired using a Geophex GEM-2 instrument along ~30 linear km at Twelvemile Lake and ~15 linear km at Beaver Meadow. The GEM-2 is sensitive to earth electrical conductivity to several meters to several tens of meters depth depending on site conditions and data quality. Data are acquired rapidly relative to TDEM or resistivity but require calibration. Cross-sectional images of conductivity can be obtained through inversion. Representative results from Twelvemile Lake are provided in Figure 4.2.2.1, 4.2.2.2, and 4.2.2.3.

A new software package for frequency-domain electromagnetic inversion (FEMIC) was developed to meet the data interpretation needs of our project. Commercially available software is not amenable to inversion of large, areally distributed electromagnetic data, as produced in our work. The code includes a graphical user interface to inversion and calibration routines. FEMIC supports 2D and 3D inversion with a variety of regularization criteria. The code can take advantage of multi-core computers and can run on desktop computers or supercomputers. The code is currently undergoing internal testing at USGS prior to submission for publication in a peer-review journal. The code and executable will enter the public domain, enabling follow-on research and expansion.

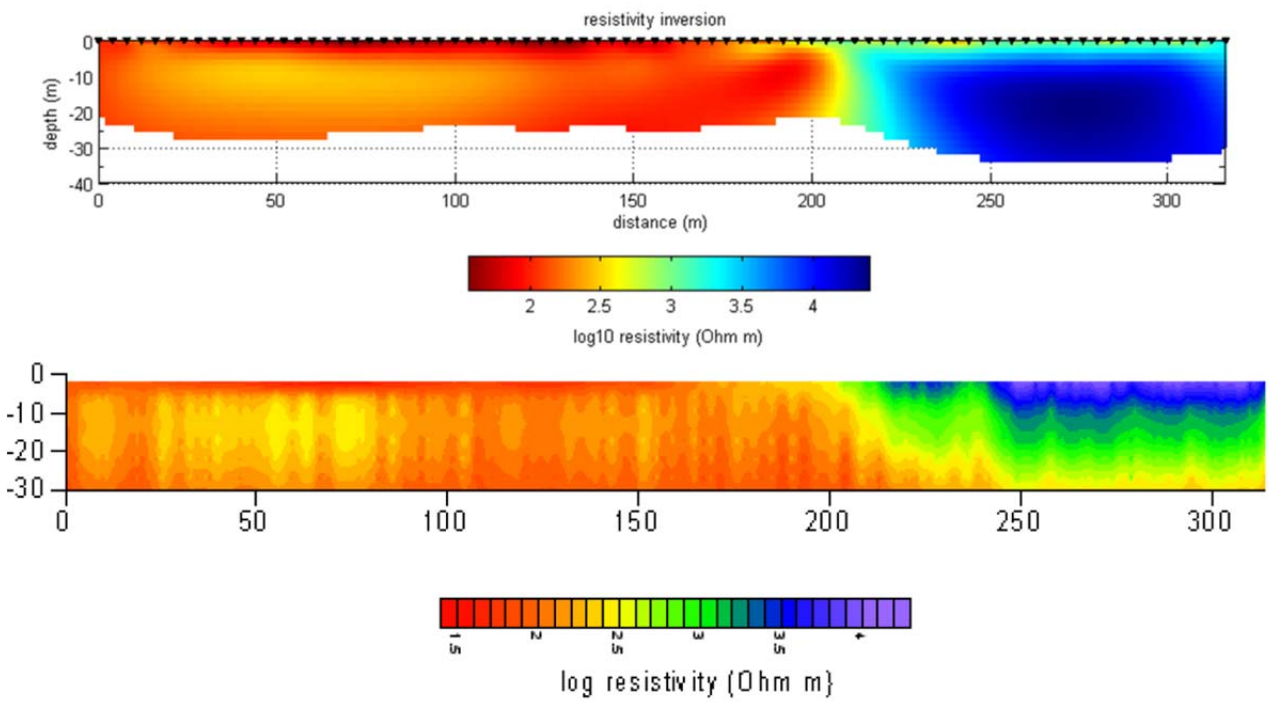

Figure 4.2.2.1 Comparison of direct-current resistivity results (top) and multi-frequency electromagnetic data (bottom) for Line 1, Twelvemile Lake.

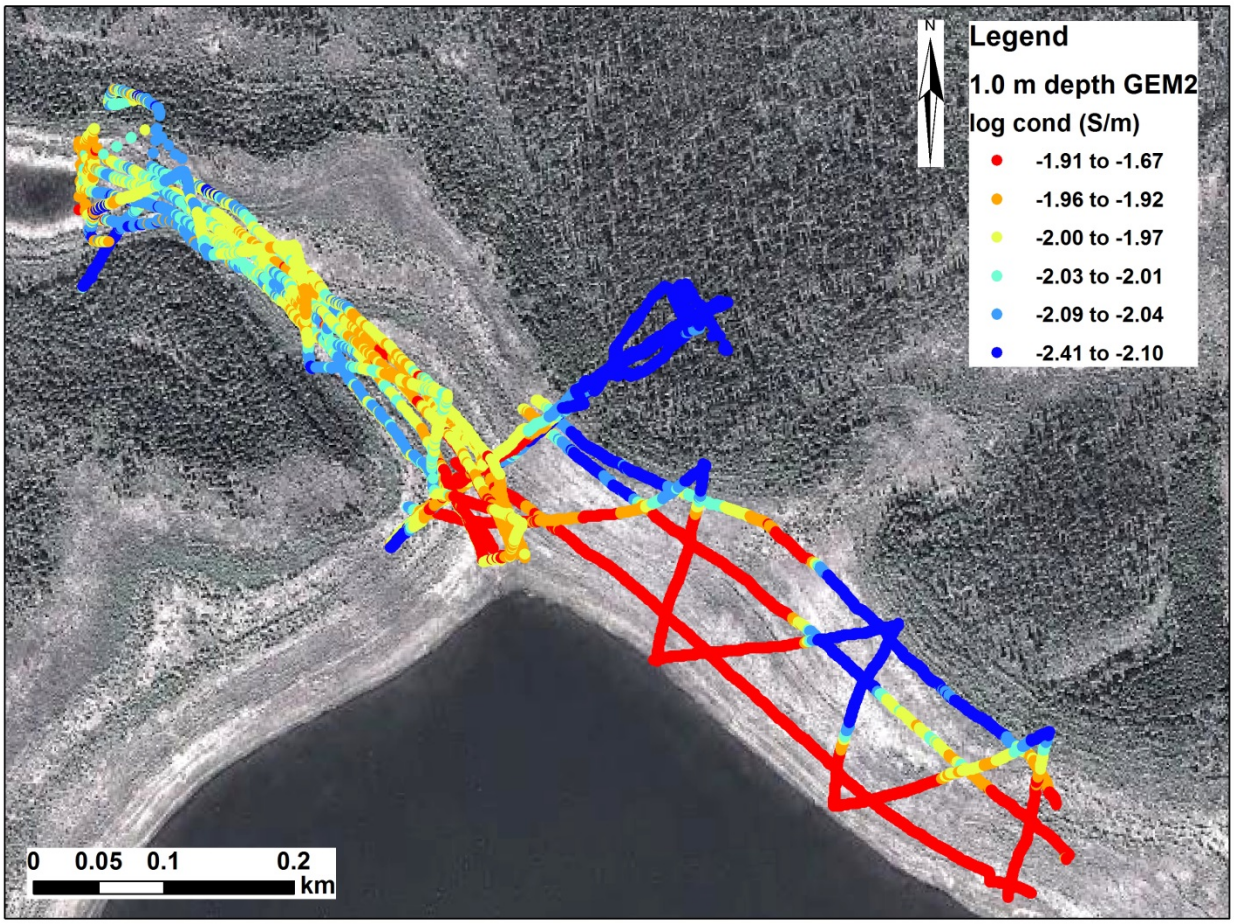

Figure 4.2.2.2 FEMIC inversion results of data from GEM2 transects for 1-m depth. FEMIC results for this dataset include 2D vertical cross sections along transects, but results are displayed here for only the 1-m depth.

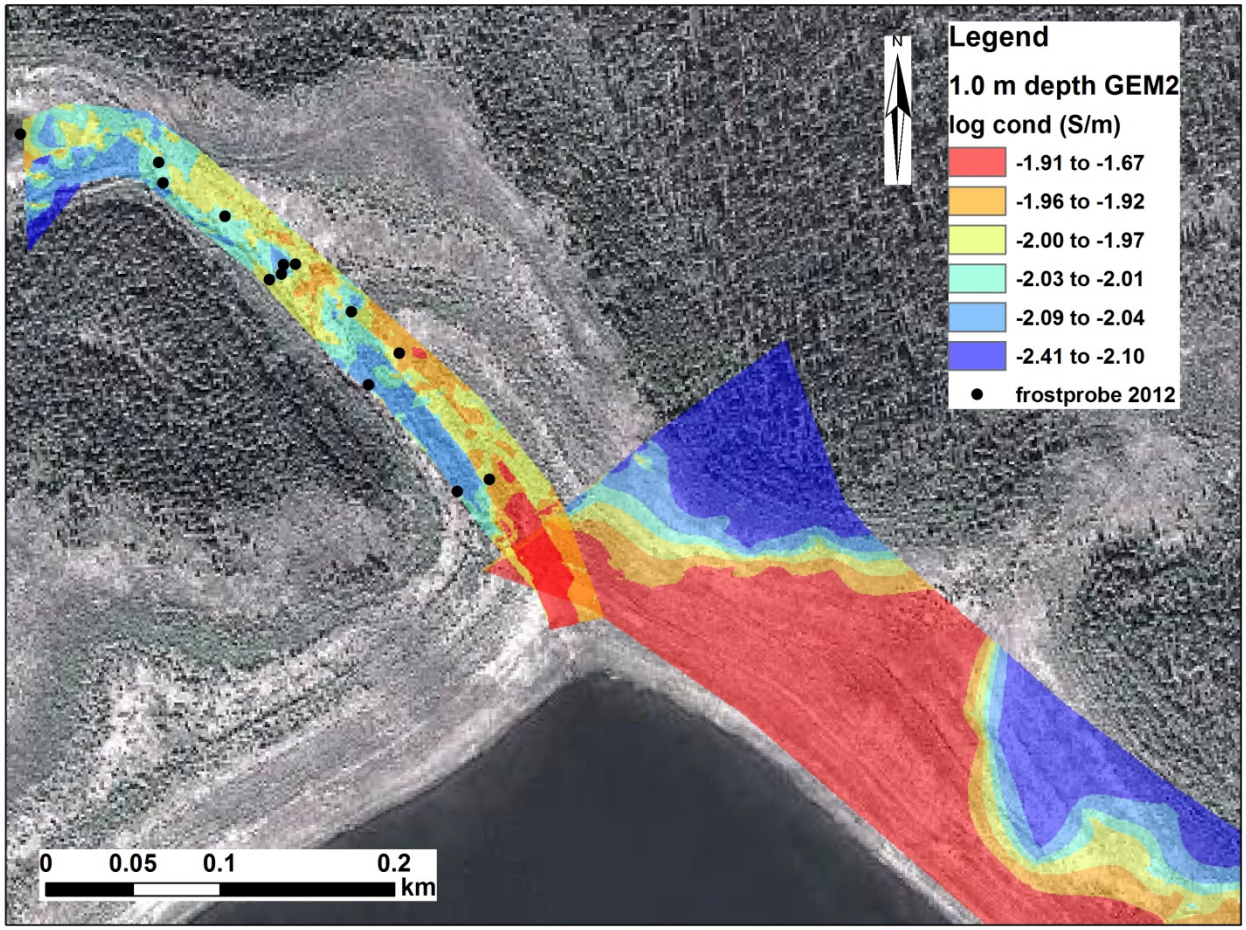

Figure 4.2.2.3 Interpolated GEM2 inversion results from FEMIC at the 1-m depth. Results show strong correlation with vegetation, which also is an indicator of permafrost presence. Low conductivity (blue) in regions covered by spruce indicate permafrost. Patches of low resistivity elsewhere indicate 'islands' of shallow permafrost formed under more recent deciduous vegetation growth.

Due to extreme precipitation patterns over the summer of 2014, the open meadow and willlow shrub area in the North-Western corner of Twelvemile Lake was flooded with 1-2 m of surface water. This unexpected condition presented the opportunity to evalutate the effects of periodic flooding on new permafrost formation. EM data were collected using a raft throughout the area where new permafrost had been observed in 2011, 2012, and 2013. Preliminary data interpretation indicates that new permafrost still exists in the flooded area (Figure 4.2.2.4); in the future, SUTRA models will be adjusted to included flooding events to predict the longer-term effects on new permafrost development.

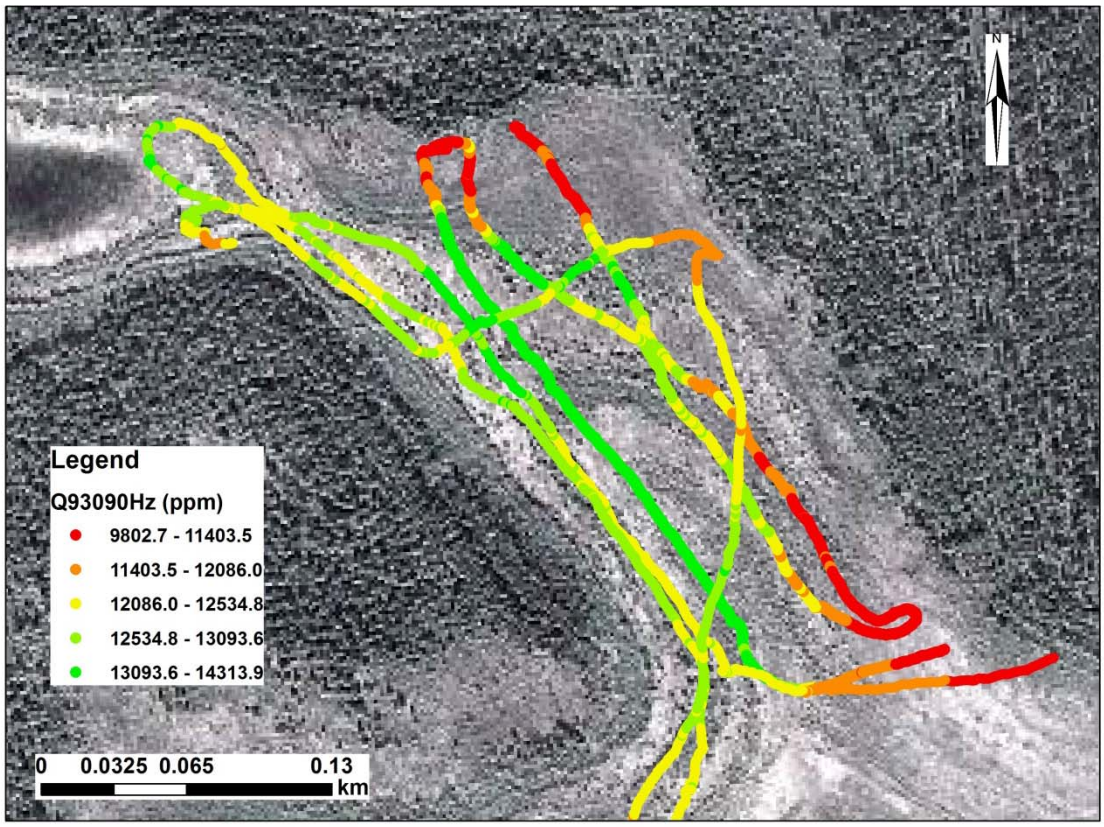

Figure 4.2.2.4 Raw GEM2 data indicates electrical conductivity of the subsurface in the 2014 flooded meadow area. Preliminary review of the EM data and physical ground-based measurements indicate that at this early stage of flooding, the new permafrost still exists in the shallow subsurface.

4.2.3 Time-domain electromagnetics

Time-domain electromagnetic (TDEM) data were acquired using a Geonics PROTEM 57 instrument, capable of soundings to several hundred meters depth. Data were acquired at 9 sites distributed around Beaver Meadow, Twelvemile Lake, and between Fort Yukon and Twelvemile Lake. Representative TDEM sounding results for a site between Fort Yukon and Twelvemile Lake are shown in Figure 4.2.3.1, which indicate permafrost between depths of several meters to about 45 meters at this location.

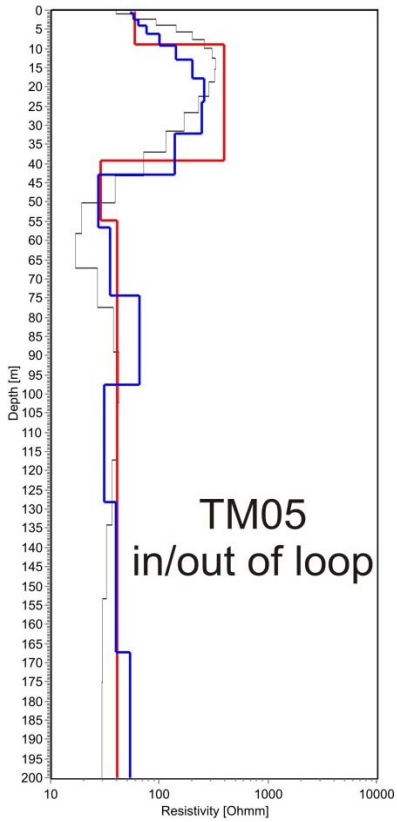

Figure 4.2.3.1 Time-domain electromagnetic sounding for site TM05 between Fort Yukon and Twelvemile Lake for minimum layer inversion (red line), smooth-model inversion (blue line), compared to results from airborne electromagnetic sounding (gray line).

4.2.4 Ground Penetrating Radar

In August 2011 we used a Geophysical Survey Systems Inc. (GSSI) SIR-3000 control unit coupled with a GSSI model 5103 400 MHz bistatic antenna to survey the near surface geology as well as the depth and spatial extent of the seasonal thaw zone through various vegetation regimes at Twelvemile Lake near Fort Yukon, Alaska. The antenna was hand towed at 0.5 m s^{-1}, oriented orthogonal to data collection, and traces lasted between 80-140 ns with 1024-2048 16-bit samples per trace. Profiles were recorded with range gain, bandpass filtering, and stacking to reduce noise and improve signal to noise ratios, particularly for flat lying reflectors. Survey lines were repeated and expanded upon in April 2012 at Twelvemile Lake by towing a GSSI model 3107 100 MHz monostatic transceiver coupled with the SIR-3000 behind a snowmobile at 2-5 km hr^{-1}. The lower frequency radar data was used to reach greater depths for an improved assessment of permafrost extent and local near surface geology. The low frequency system was impossible to use in August due to the thick shrub ground vegetation which hampered travel with the larger low frequency system relative to the smaller 400 MHz antenna. The snow and frozen

conditions likely improved signal penetration relative to depths expected to be reached in the summer due to decreased attenuation rates from less free water. The last GPR survey in August 2012 at Twelvemile Lake was conducted using the 400 MHz antenna and similar parameters to resurvey profiles collected in August 2011. Profiles were also significantly expanded to cover a remnant and mostly dry (at the time) drainage system between Twelvemile Lake and nearby Buddy Lake.

The 400 MHz profiles discussed here were ground-truthed through frost probing, shallow (2-3 m) sediment cores and dirt pits with placed metal reflectors at known depths to determine relative permittivity and associated radio-wave velocities. Shallow (0.5-1.0 m) temperatures and frost probe depths were also recorded at random locations relative to these profiles. Ground truth of the low frequency data was not possible at these remote field sites however galvanic resistivity and GEM2 electromagnetic profiles were collected along several of the GPR profiles for comparison to both the 100 and 400 MHz GPR results. Approximately ~15 km of GPR profiles were collected over the three field seasons. Interpreted GPR results are shown for the Twelvemile Lake area in Figure 4.2.4.1.

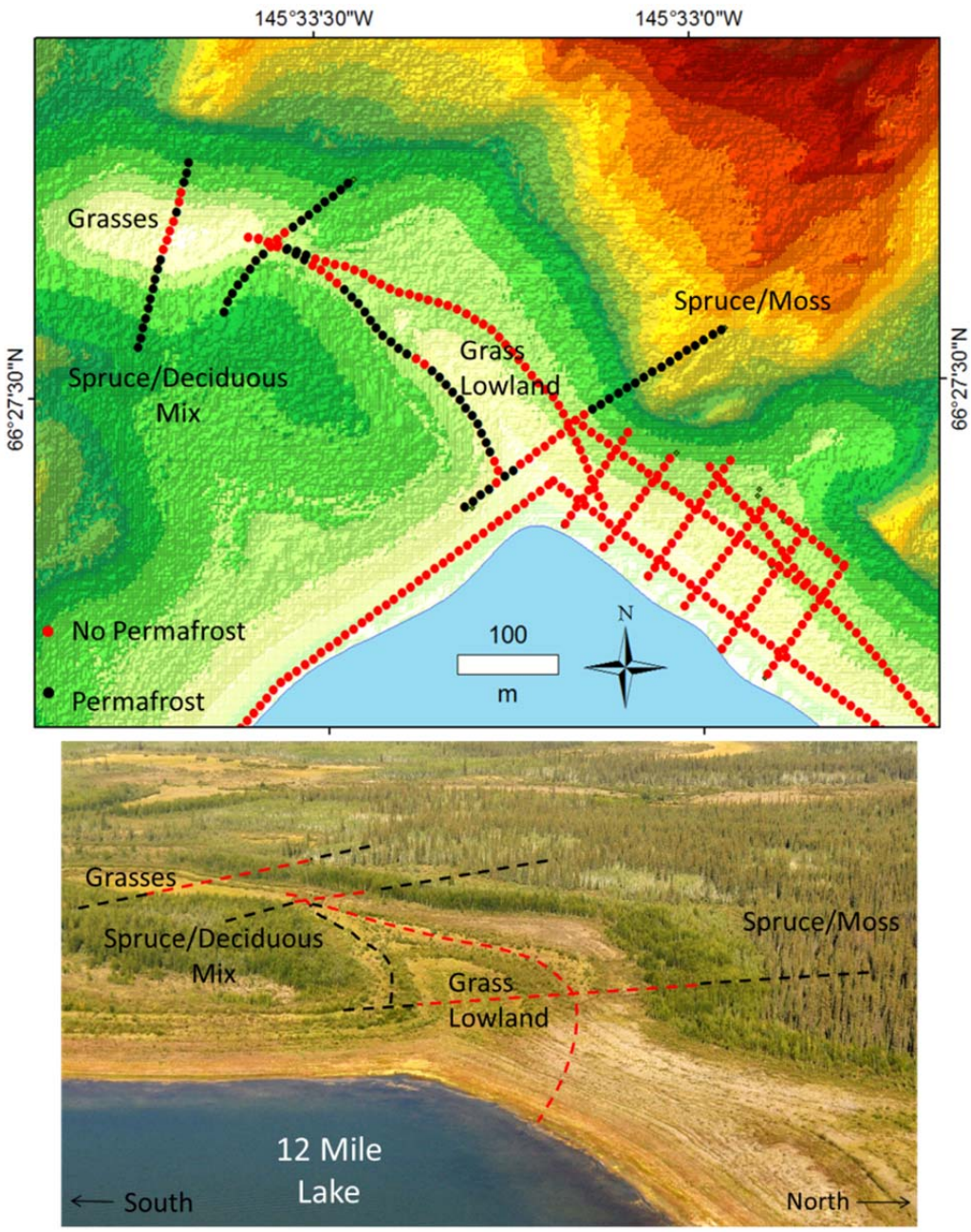

Figure 4.2.4.1 Interpreted permafrost distribution based on ground-penetrating radar collected in 2011-2012, in the vicinity of Twelvemile Lake.

4.2.5 Passive Seismic

The horizontal-to-vertical seismic-noise ratio (HVSR) method is a novel, non-invasive technique that can be used to rapidly estimate the depth to bedrock. The field equipment is compact, light-weight and easy to transport. The HVSR method uses a single, broad-band three-component seismometer to record ambient seismic noise. The ratio of the averaged horizontal-to-vertical frequency spectrum is used to determine the fundamental site resonance frequency, which can be

interpreted using regression equations to estimate sediment thickness and depth to bedrock (Ibs-von Seht and Wohlenberg, 1999; Parolai et al., 2002). To the best of our knowledge, HVSR has not been used previously to investigate depth to permafrost. We employed the technique at sparse locations around Beaver Meadow and Twelvemile Lake, including a line along which resistivity measurements were made at Beaver Meadow (Figure 4.2.5.1). Application of HVSR at the field locations was supplemental to our original geophysical data collection plan. Results indicate that HVSR may prove a cost-effective method for determination of permafrost depth.

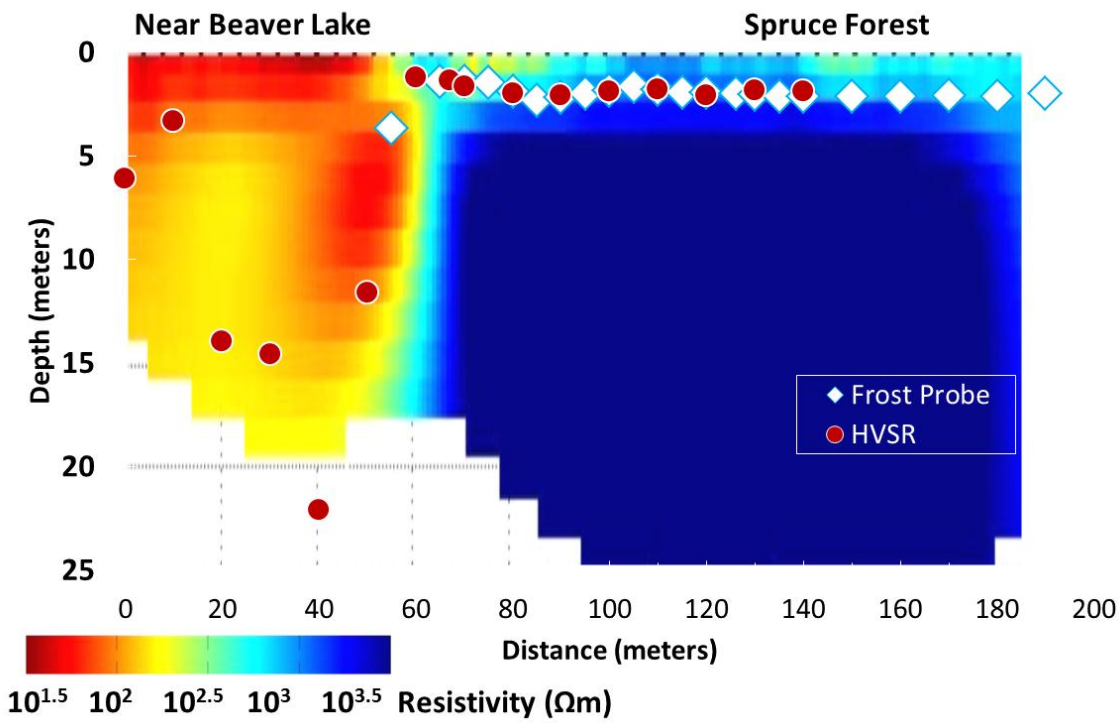

Figure 4.2.5.1 Representative passive-seismic results overlayed on resistivity cross-sectional image, showing strong relation between seismic interface and depth to permafrost derived from frost probe.

4.3 Results and Discussion

Geophysical results from our multi-method investigation have provided information about permafrost distribution around Twelvemile Lake across a range of scales (Figure 4.3.1), demonstrating the effectiveness of our multi-scale geophysical toolbox (Figure 4.0.2). Sub-meter and meter-scale information from ground-penetrating radar, frequency domain electromagnetics, electrical resistivity and passive seismic indicate has served to reveal complex lake/permafrost interactions, where new permafrost was forming in the margin of a receding lake. Using geophysical information to help constrain SUTRA modeling, we have explained how new

permafrost can form in seeming contradiction of climate warming trends (see Section 5.6). Information at the scale of meters to tens of meters from resistivity, time-domain electromagnetics, and airborne electromagnetics has provided information about permafrost depth and large-scale areal distribution of permafrost; these data provide a snapshot against which future studies can compare to infer changes in permafrost distribution over time, for assessment of climate-change impacts.

In addition to providing basic insight into permafrost distribution and processes, our SERDP efforts include methods development and examples of methods demonstrations. To the best of our knowledge, our work includes the first application of HVSR for permafrost study, showing the potential of this cost-effective method for use in remote areas. Development and publication of the FEMIC code will allow for follow-on studies and enable more widespread application of FDEM and also AEM. Our well attended training course, conducted at University of Alaska, Fairbanks, in August 2014, supported the transfer and transition of our approach to cooperators from academia, federal government, and state agencies. Participants included engineers and other staff from University of Alaska, Alaska Department of Transportation, Alaska Geological Survey, Department of Defense, Alyeska, and an Alaska legislative staffer.

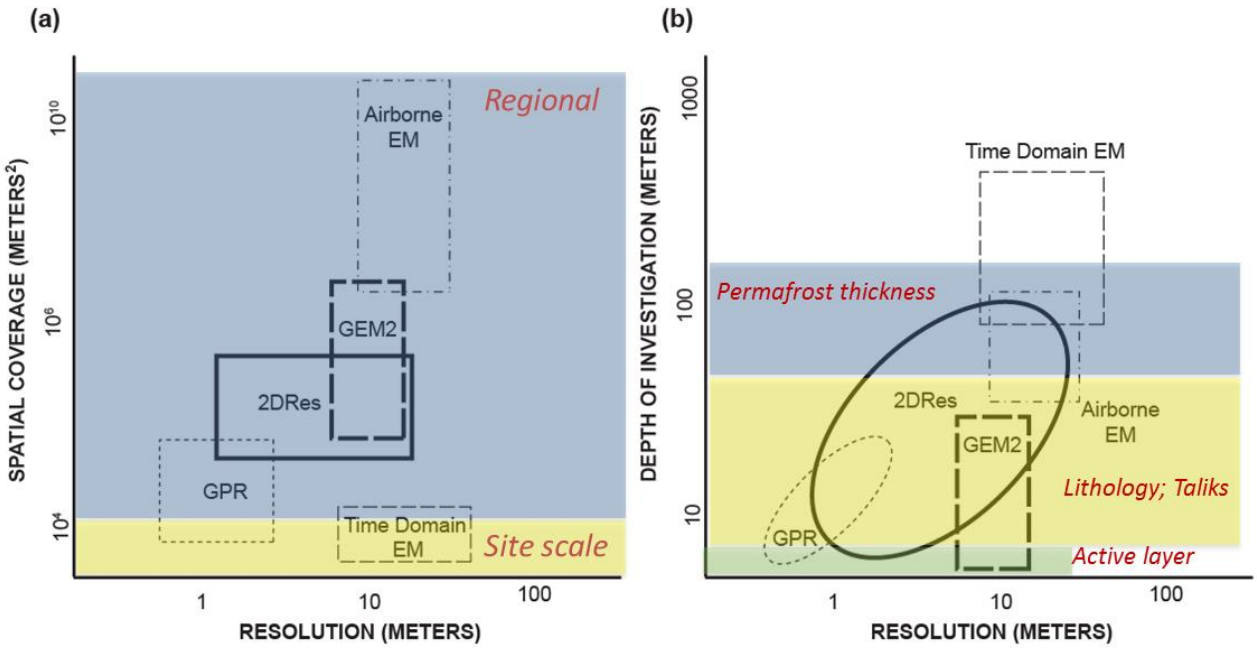

Figure 4.3.1 Summary of geophysical methods useful for characterizing cold region features of interest at variable scales and resolution.

5. Hydrologic Analyses and Model Applications

The hydrologic analyses and model applications completed as part of this project are interrelated, but can be partitioned into seven sub studies described herein. The first study (Section 5.1), a groundwater modeling study of the overall study region, utilized an existing standard groundwater computer code that simulated permafrost as a very low conductivity unit and required manual manipulation of changes in permafrost distribution to assess the influence of permafrost on groundwater flow. The next study presented (Section 5.2) demonstrated the use of the modified SUTRA code to simulate dynamic permafrost/groundwater flow relations for a generalized nested groundwater flow system. The next four sub studies (Sections 5.3-5.6) developed multiple approaches for evaluating cryohydrologic processes at the primary study lake, Twelvemile Lake, in the Yukon Flats. In each case, information from geophysical investigations was used to inform the model/analytical analysis. Finally, section 5.7 describes synthesis efforts at the Yukon Flats regional scale, using geophysical characterization, remote sensing, flow analysis, and insight gained through the course of this project to better understand the controls on lake mass balance and surface water distribution in discontinuous permafrost.

Additional details supplementary to this report can be found in: Walvoord et al. (2012) (section 5.1); McKenzie and Voss (2013) (section 5.2); Jepsen et al. (2013a) (section 5.3); Wellman et al. (2013) (section 5.4); Minsley et al., (2014) (section 5.5); Briggs et al. (2014) (section 5.6), and Jepsen et al., (2013b) (section 5.7).

5.1 Regional Groundwater Flow in the Yukon Flats Basin

Groundwater and the exchange between groundwater and surface water bodies are key components that influence vegetation community, species habitat, biogeochemical cycling, and biodiversity. Understanding the role of permafrost in controlling groundwater flowpaths and fluxes is central in studies aimed at assessing potential climate change impacts on ecosystems. Basin-scale studies in interior Alaska show evidence of hydrologic changes hypothesized to result from permafrost degradation (e.g., Striegl et al., 2005; Walvoord and Striegl, 2007). We conducted a groundwater modeling study of the Yukon Flats Basin to assess the hydrologic control exerted by permafrost and taliks (unfrozen zones within permafrost), elucidate modes of regional groundwater flow for various spatial permafrost patterns, and evaluate potential hydrologic consequences of permafrost degradation at the regional scale.

5.1.1 Materials and Methods

A regional three-dimensional groundwater flow model of the Yukon Flats Basin (Figure 5.1.1.1) was generated using the USGS-MODFLOW code (Harbaugh, 2000) to (1) illustrate the control that permafrost exerts on regional groundwater flow systems, and, (2) reveal potential trends and behavior in groundwater flow that might result from climate warming. Although MODFLOW is an isothermal model, it was selected for the initial phase of hydrologic analysis in this permafrost basin, because of its efficiency in simulating regional scale hydrology. Results from the

MODFLOW simulations with variable, but static, permafrost distributions provide a regional framework for subsequent finer scale dynamic permafrost hydrology simulations using the enhanced SUTRA model.

The Yukon Flats Basin is a large sub-basin within the Yukon River Basin in Alaska. The basin includes an alluvial lowland (90 - 353 m in elevation and occupying 24,080 km^2) transected by the Yukon River, a dissected to rolling marginal upland (30 – 150 m higher than the lowlands and occupying 15,460 km^2), and bordering highlands (occupying 78,800 km^2). The most recent map of generalized permafrost distribution and characteristics in Alaska by Jorgenson et al. (2008), indicates that Yukon Flats Basin spans the transition between continuous permafrost (defined as >90 % coverage) to the north of the Yukon River and discontinuous permafrost (50-90% coverage) to the south.

The watershed boundary for Yukon Flat Basin, encompassing an area of 118,340 km^2, defines the model domain. Lateral grid spacing for all simulations presented here is 1500 m, and there are 26 vertical layers, ranging from 1 – 25 m thick. Modeled basin thickness is 400 m. The hydrogeology of the basin, based on descriptions in Williams (1962) and the State Surficial Geology Map of Alaska (NPS, 1999), and data from a deep borehole at Fort Yukon (Clark et al., 2009) are here interpreted as belonging to 6 lithologic units with different hydraulic properties: upper alluvium (sand and gravel mix), lower alluvium (sand to fine silt mix), loess, bedrock, mountain alluvium and colluvium, and permafrost. Permafrost was represented in the regional model as hydrogeologic units with very low hydraulic conductivity (e.g., Burt and Williams, 1976; Horiguchi and Miller, 1983; McCauley et al., 2002) that extended to a maximum depth of 90 m as influenced by the geothermal gradient and determined by borehole information (Clark et al., 2009). For the permafrost distribution considered plausible under present climate conditions, the model was calibrated using baseflow estimates for major rivers with the Yukon Flats Basin (streamflow stations denoted in Figure 5.1.1.1). Calibration was accomplished automatically, using the inverse model (parameter estimation) functionality of MODFLOW-2000. Using the present-day roughly-calibrated model as a reference or 'base case', permafrost distribution was varied in subsequent simulations, and the impacts of permafrost distribution on groundwater flow were evaluated to assess sensitivity, magnitude, and implications of differences. A full sequence of cases from full permafrost (no taliks, or unfrozen zones, within the permafrost layer) to permafrost-free conditions allowed testing the influence of permafrost on groundwater fluxes and flowpaths for a full range of possible conditions. Primarily steady-state groundwater flow was considered, but transient analyses were also carried out to check the magnitude of variation resulting from the simplifying steady-state assumption. Groundwater flowpaths were determined with post-processing using MODPATH (Pollock, 1994). Water budgets were calculated in a post-processing step by ZONEBUDGET (Harbaugh, 1990). Using ZONEBUDGET, total horizontal and vertical inflow/outflow was determined for each of the following hydrologic regions within the Yukon Flats Basin:

(1) supra-permafrost aquifer (0 m to 1-4 m below surface in regions overlying permafrost),

(2) taliks-shallow aquifer (0 m to 4 m below surface in permafrost-free areas, not directly overlain by river),
(3) river zone (0 m to 4 m below surface of river),
(4) taliks-deep aquifer (4 m to 90 m below surface in permafrost-free areas),
(5) permafrost (1-4 m to 90 m below surface; i.e., regions containing permafrost),
(6) sub-talik aquifer (90 m below surface to aquifer bottom below taliks), and
(7) sub-permafrost aquifer (90 m below surface to aquifer bottom below permafrost).

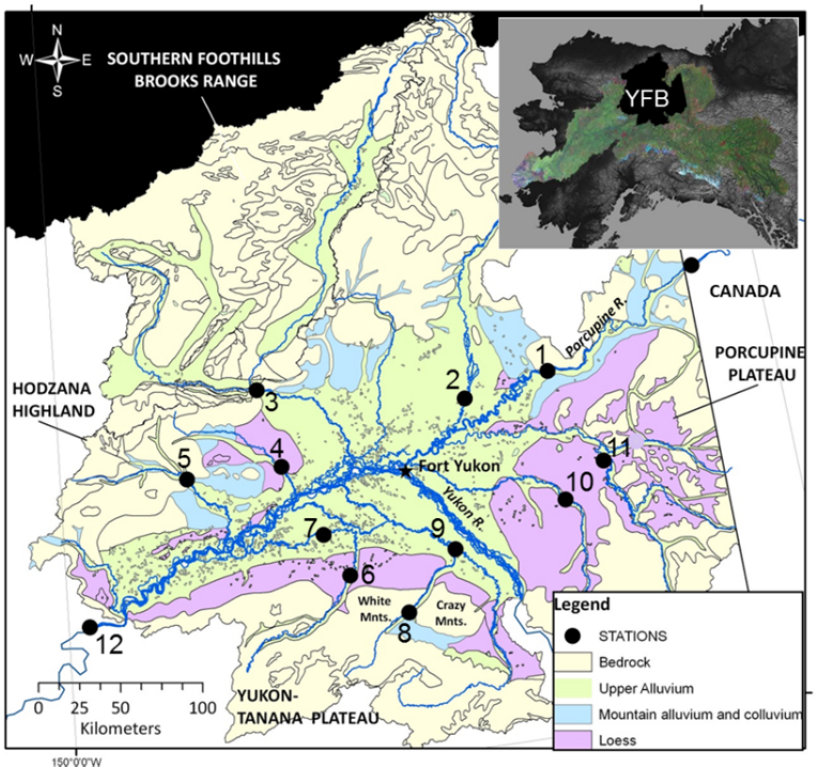

Figure 5.1.1.1 Location map of the Yukon Flats Basin (after Williams, 1962). Surficial geology represents substrate above permafrost (after Karlstrom et al., 1964). Streamflow stations with baseflow information available are denoted. Numbers apply to stations described in Table 1 of Walvoord et al. (2012). Inset shows Yukon Flats Basin location.

5.1.2 Results and Discussion

Permafrost was shown to function as an effective confining layer in the model, resulting in relatively high hydraulic head below the permafrost in low-lying regions of Yukon Flats Basin (Figure 5.1.2.1 a, b). Large modeled regions of upward gradient across the permafrost layer coincided with locations of concentrated lake distributions in the low-lying Yukon Flats, suggesting a possible link between the existence and persistence of lowland lakes and upwelling of deep groundwater. The confining effect of permafrost also served to partition flowpaths into shallow/young and deep/old components. Model-calculated residence times for porewater in the

supra-permafrost aquifer (shallow) were on the order of 10^1 years, compared with residence times of $10^3 – 10^4$ years for porewater in aquifers below permafrost.

Overall water budget results from the base case indicate a groundwater-flow system that supports recharge equivalent to 55 mm/yr, or 11% of the basin-wide PRISM-estimated precipitation (PRISM Climate Group, Oregon State University, http://prism.oregonstate.edu, created 2/2000). The budget results (reported and schematically illustrated in Figure 5.1.2.2) demonstrate the important role of open taliks (unfrozen zones) in the circulation of groundwater in permafrost-dominated systems, emphasizing the importance of understanding and characterizing talik extent and morphology. Surficial fluxes represent flow across the water table for each shallow zone; downward fluxes represent recharge (precipitation – ET) and upward fluxes represent groundwater discharge. For the base case, 76% of the total groundwater recharge through the ground surface occurs above open taliks, which comprise only 11% of the total area. Flow through the supra-permafrost aquifer totals 43.7 x 10^5 m^3/d representing 25% of groundwater flow through the system. Although the supra-permafrost zone covers 89% of the basin in area, it comprises less than 1% of the basin by volume. Thus, the result that a relatively large proportion (25%) of groundwater flows through the supra-permafrost zone signifies relatively rapid flushing.

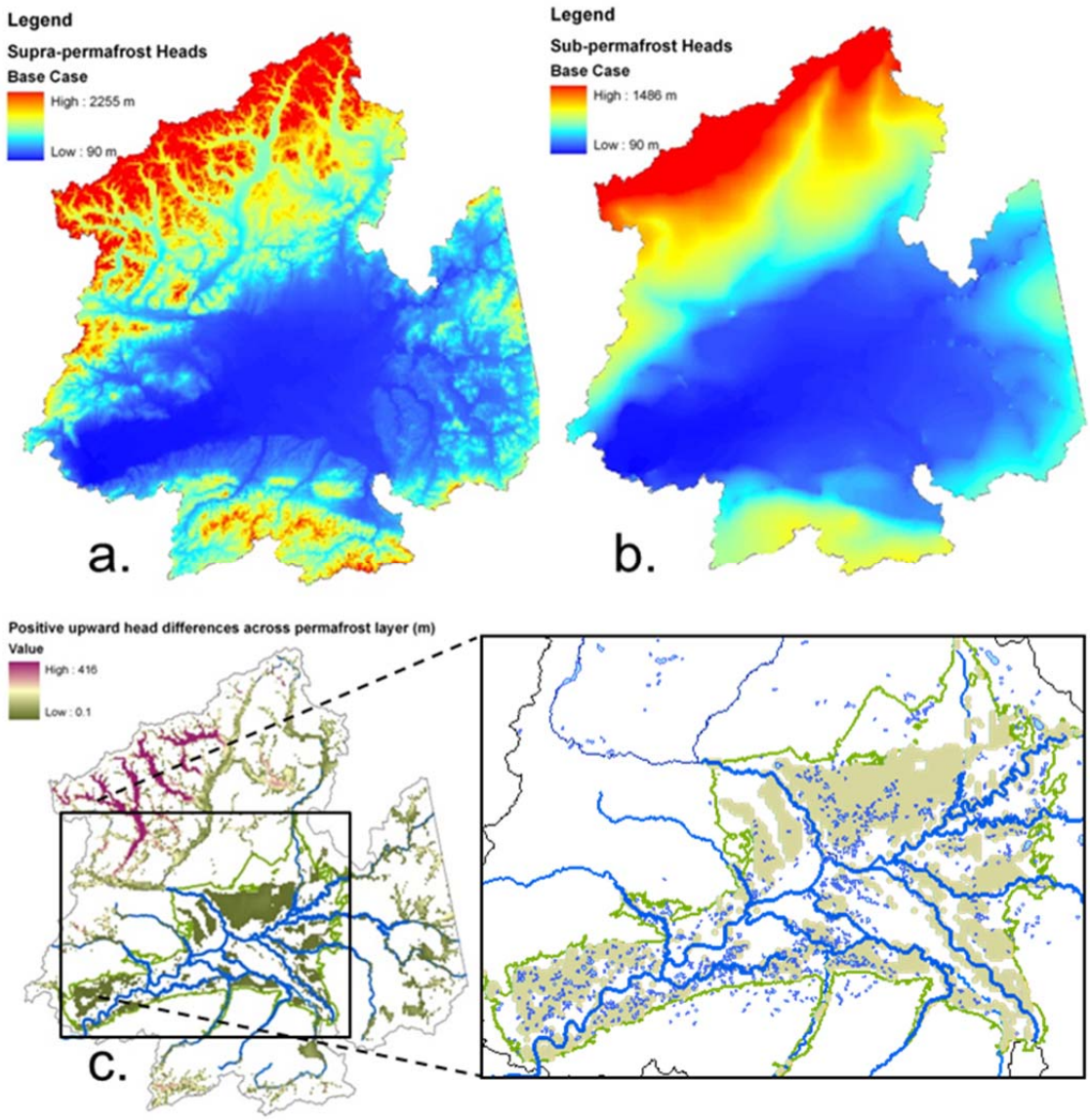

Figure 5.1.2.1 Steady-state head distribution for the supra-permafrost zone (for base case PDISC1) (a), and the sub-permafrost zone (b).
Areas of upward gradients across the permafrost layer are indicated by the color scheme in the legend (c). The blowup for the lowlands (within green outline) shows the distribution of lakes > 100 m in diameter.

Base case baseflow is 54.0 x 10^5 m^3/d representing 30% of the total groundwater flow in the system. This baseflow is comprised of 19% supra-permafrost groundwater flow, 23% intra-talik flow, and 58% sub-permafrost flow. These results are composite for the entire Yukon Flats Basin; individual sub-basins will have differing proportions of supra- to sub-permafrost contributions that are dependent on basin characteristics.

To evaluate the importance of lowland lake taliks on regional groundwater flow, results from the base case (PDISC1) were compared to the simulation in which lowland lakes > 100 m diameter possess open taliks (PDISC1L). Percent increases in flow resulting from lake taliks (PDISC1L compared to PDISC1) are given in parentheses in Figure 5.1.2.2. In summary, lowland lake taliks comprising only ~1% of the model domain, exert a proportionally large effect on groundwater circulation patterns, increasing some fluxes by nearly 20%. The greatest effects of lake taliks on lateral groundwater flow are localized and are thus, locally substantial.

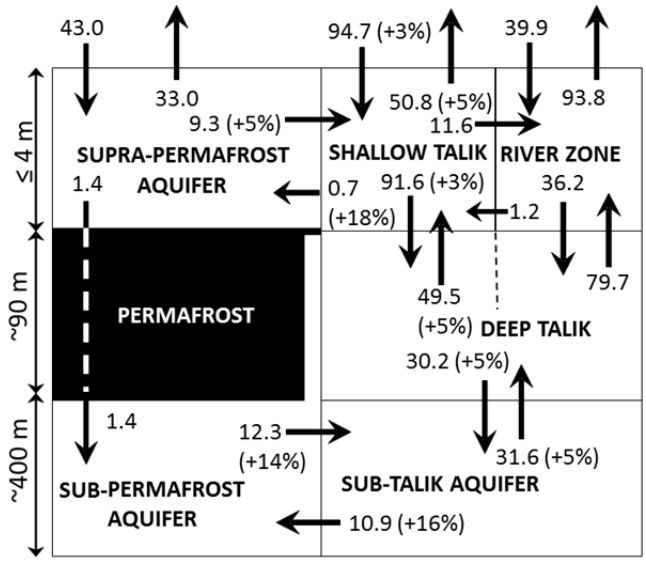

Figure 5.1.2.2 Steady-state zone water budget results (not drawn to scale) for the base case, PDISC1.
Groundwater fluxes reported in units of 10^5 m^3/d. Values in parentheses represent the percent increase in flux for PDISC1L (with lake taliks) relative to PDISC1 flux.

Selected results are presented from permafrost configurations that may be considered to reflect key stages of a permafrost degradation sequence, including: (1) complete permafrost (PALL), (2) continuous permafrost coverage – (PCONT) (95% permafrost), (3) discontinuous I – cold (PDISC1) (base case, 89% permafrost), (4) discontinuous II – warm (PDISC2) (67% permafrost), and (5) permafrost-free conditions (PNONE) (Table 5.1.2.1 and Table 5.1.2.2). Numerous other intermediate permafrost configurations were simulated, described, and reported in Walvoord et al., (2012). The greatest hydrologic changes to the system occur within the continuous to discontinuous sections of the permafrost coverage spectrum, and results presented here focus on this range. Figure 5.1.2.3 illustrates the strong control of permafrost distribution on groundwater discharge patterns. For the continuous permafrost case (PCONT), groundwater discharge is focused in the permafrost-free Yukon River valley and to upland river valleys with the greatest vertical relief (Figure 5.1.2.3a). The widening of taliks under the Yukon River and opening of taliks beneath all major tributaries for PDISC1 has the effect of focusing discharge through river taliks in the lowlands (Figure 5.1.2.3 b). The increase in vertical connectivity in the system, concurrent with progressive loss of permafrost (PDISC1 to PDISC2 to PNONE, shown in the figure) results in expanded regions of groundwater discharge in the lowlands (Figure 5.1.2.3 b-d).

Model	Short Name	Permafrost Coverage (%)	Description
Complete Permafrost	PALL	100	No open taliks
Continuous Permafrost	PCONT	95	Narrow open taliks only beneath 2 largest rivers– Yukon and Porcupine Rivers
Base Case Discontinuous I	PDISC1	89	Open taliks beneath all major rivers
Discontinuous I with Lake Taliks	PDISC1L	88	Same as above + open taliks beneath lowland lakes
Discontinuous II	PDISC2	67	Open wide (+5 km each side from base case) river taliks + lake taliks
Permafrost Free	PNONE	0	Entirely unfrozen material

Table 5.1.2.1 List of select model simulations and corresponding permafrost distribution

Model	Average Recharge[a] (mm/yr)	Total Baseflow (m^3/d)	Groundwater Discharged as Baseflow (%)	Supra-Permafrost[b] Contribution to Baseflow (%)	Median Baseflow Travel Times (yr)	Median Baseflow Path Length (km)
PALL	13	7.4×10^5	18	93	3712	5.72
PCONT	28	2.3×10^6	20	47	114	3.56
PDISC1	55	5.4×10^6	30	19	335	3.73
PDISC2	146	1.1×10^7	23	8.5	486	3.67
PNONE	458	2.6×10^7	17	3.7	461	3.26

[a] Value is calculated by the model, reflects an average across the entire model domain, and represents maximum recharge capacity for the prescribed hydrogeologic conditions.[b] For cases in which permafrost is absent, this component represents shallow (≤4 m) aquifer contribution.

Table 5.1.2.2 Model results for a permafrost thaw sequence in the Yukon Flats Basin.

Model results showed total groundwater flow increasing with decreasing permafrost coverage. Average basin-wide recharge values (and thus, total groundwater flow for steady state) increased nearly an order of magnitude from the base case (PDISC1) to permafrost-free conditions (PNONE) (Table 5.1.2.1). Baseflow magnitudes also increased substantially with decreasing permafrost coverage, exceeding an order of magnitude increase from complete permafrost (PALL) to permafrost-free conditions (PNONE) (Figure 5.1.2.4; Table 5.1.2.2). Pertinent substantial baseflow change applicable to the near-term (10^1 - 10^2 yr), as a result of current warming trends, may be represented by the change between one of the stages depicted in Figure 5.1.2.4 and the following stage. Model results that showed an overall trend in increased baseflow with diminishing permafrost coverage are consistent with the hypothesis that permafrost degradation has led to the observed increases in groundwater input to rivers in northern basins, as noted by Smith et al. (2007), Walvoord and Striegl (2007), and St. Jacques and Sauchyn (2009) among others. In addition to considering changes in baseflow magnitude, it is important to address the sources and flowpaths of baseflow and how these may change with permafrost degradation. This is particularly important in evaluating potential changes in aquatic chemical exports as a consequence of permafrost thaw (Frey and McClelland, 2009). Groundwater modeling results for the Yukon Flats Basin indicate a sharp decline in the proportional contribution of lateral flow from the supra-permafrost layer to baseflow near the continuous to discontinuous permafrost transition (Figure 5.1.2.5; also reported in Table 5.1.2.1). Changes in the magnitudes and ratios of organic to inorganic aquatic chemical exports would be expected to accompany the changes in the proportional contributions of supra-permafrost flow to baseflow illustrated in Figure 5.1.2.5 (O'Donnell et al., 2012).

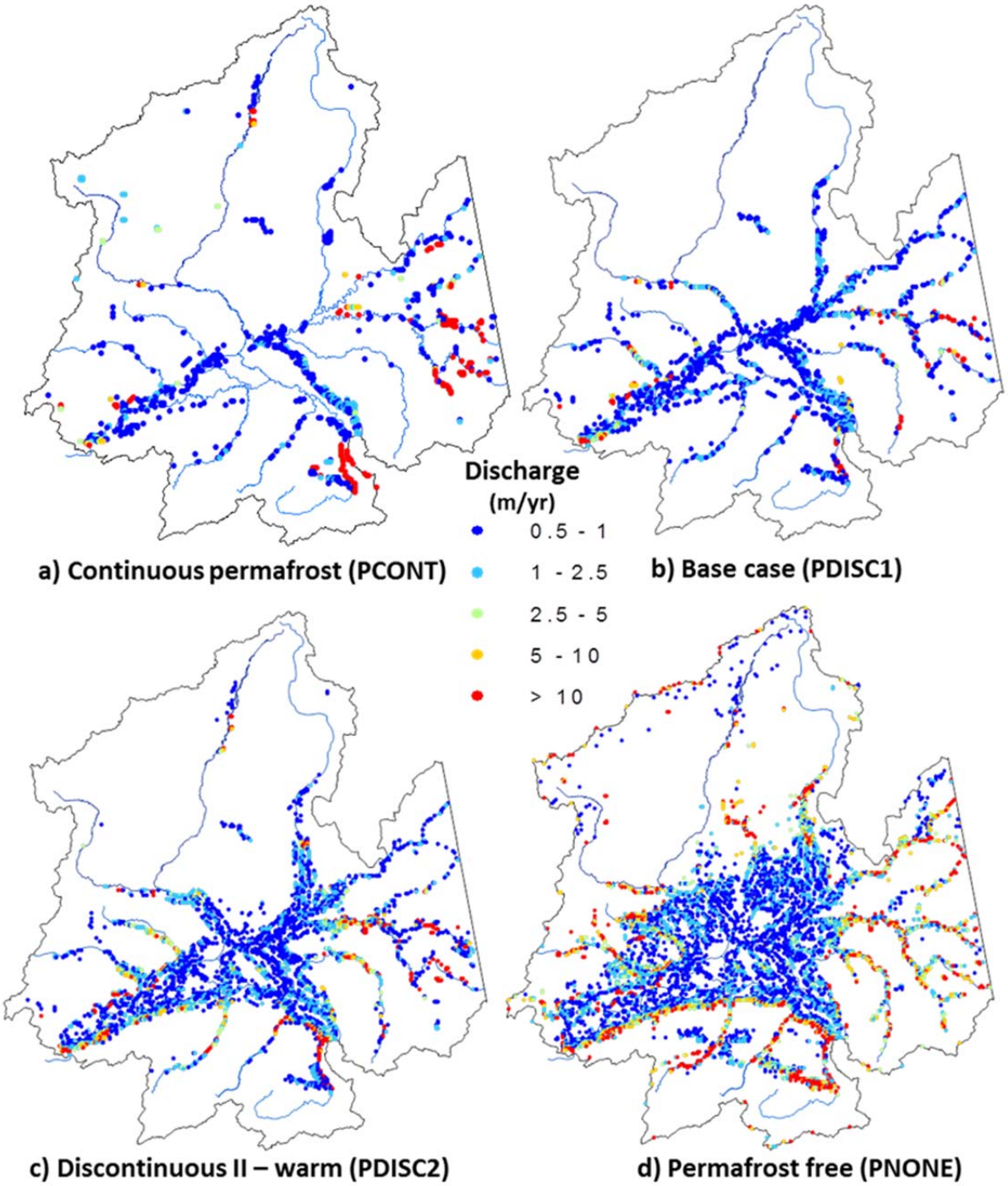

Figure 5.1.2.3 Model results for groundwater discharge patterns with varying permafrost distributions.

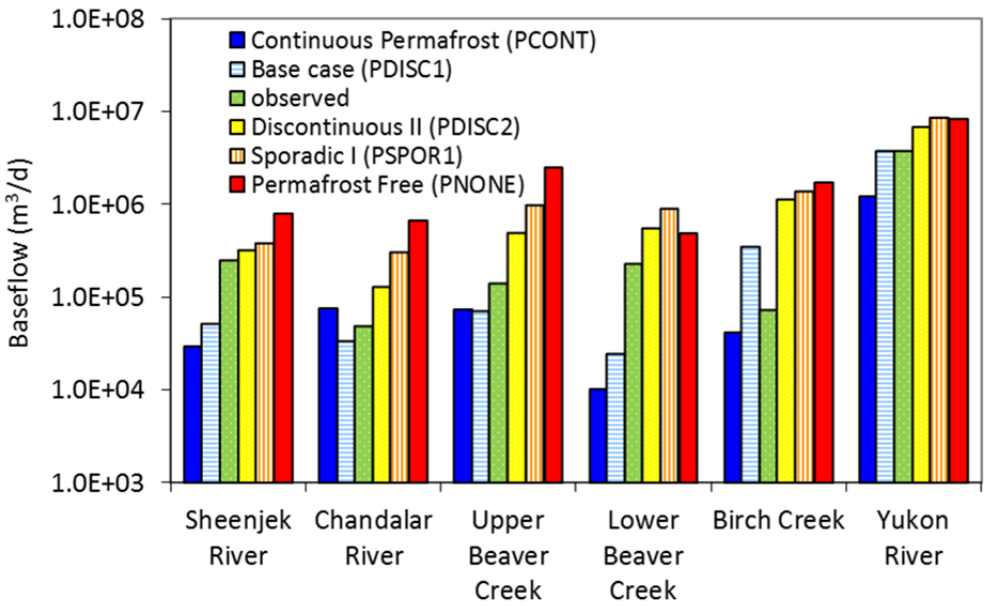

Figure 5.1.2.4 Model-calculated baseflow for selected river reaches with a variety of permafrost distributions.
The streamflow stations are noted by number in Figure 5.1.1.1 map as follows: Sheenjek (2), Chandalar (3), Upper Beaver (6), Lower Beaver (7), Birch (8), and Yukon (12).

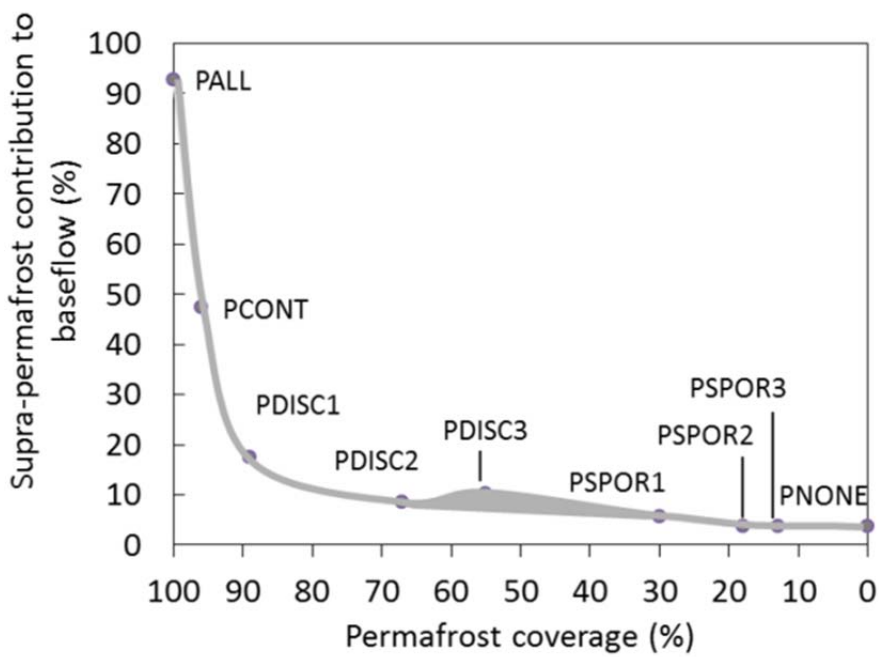

Figure 5.1.2.5 Model-calculated percentage of supra-permafrost (or shallow aquifer in thawed cases) contribution to baseflow.
Range associated with thaw patterns beginning in late discontinuous stages indicated by thicker line.

Model-Predicted Baseflow to Upstream River Segment (m^3/day)

Station[a]	PALL	PCONT	PDISC1	PDISC2	PNONE	OBSERVED
1	1.12×10^5	1.15×10^5	1.31×10^5	1.35×10^5	3.19×10^6	3.03×10^5
2	3.32×10^4	2.97×10^4	5.02×10^4	3.20×10^5	7.94×10^5	2.50×10^5
3	1.61×10^4	7.50×10^4	9.36×10^4	1.28×10^5	6.73×10^5	4.92×10^4
4	5.45×10^3	5.40×10^3	2.27×10^4	1.92×10^5	5.14×10^5	9.79×10^3
5	4.77×10^4	4.89×10^4	1.45×10^4	6.12×10^4	1.44×10^6	1.42×10^5
6	7.27×10^4	7.45×10^4	7.01×10^4	4.96×10^5	2.52×10^6	2.26×10^5
7	1.02×10^4	1.03×10^4	3.26×10^4	5.51×10^5	4.86×10^5	8.56×10^5
8	4.12×10^4	4.20×10^4	3.48×10^5	1.14×10^6	1.71×10^6	7.34×10^4
9	2.55×10^4	2.61×10^4	1.95×10^4	3.96×10^4	8.79×10^5	1.96×10^4
10	2.50×10^4	2.55×10^4	1.27×10^5	9.03×10^5	1.19×10^6	1.22×10^4
11	1.25×10^5	1.28×10^5	1.33×10^5	1.39×10^5	3.77×10^6	1.10×10^5
12	2.26×10^5	1.22×10^6	3.88×10^6	6.92×10^6	8.37×10^6	3.84×10^6

[a] station numbers correspond to streamflow stations located in Figure 5.1.2.1.

Table 5.1.2.2 Model-predicted baseflow for select permafrost distributions.

In summary, model simulations that represented an assumed permafrost thaw sequence revealed the following trends with decreasing permafrost: 1) increased groundwater discharge to rivers, consistent with historical trends in baseflow observations in the Yukon River Basin, 2) potential for increased overall groundwater flux, 3) increased extent of groundwater discharge in lowlands, and, 4) decreased proportion of supra-permafrost (shallow) groundwater contribution to total baseflow. These trends directly affect the chemical composition and residence time of riverine exports, the state of groundwater-influenced lakes and wetlands, seasonal river-ice thickness, and stream temperatures. Presently, the Yukon Flats Basin is coarsely mapped as spanning the continuous-discontinuous permafrost transition that model analysis shows to be a critical hydrogeologic threshold; thus, the Yukon Flats Basin may be on the verge of major hydrologic change should the current permafrost extent decrease. This possibility underscores the need for improved characterization of permafrost and other hydrogeologic information in the study area via geophysical techniques and ground-based observations.

5.2 Generalized Permafrost Thaw/ Groundwater Flow Interaction

The modified SUTRA code described in Section 3.0 was applied to a nested groundwater flow system subjected to mean annual sub-freezing temperatures as a means of evaluating the importance of groundwater flow in accelerating climate-driven permafrost thaw. This modeling study was not intended to be comprehensive regarding behavior of ground ice in groundwater flow settings; rather, was intended to identify some of the most important processes and phenomena that warrant further study.

5.2.1 Materials and Methods

In order to investigate the interplay of heat conduction and heat advection via groundwater flow with both seasonal ground ice and permafrost in arctic hydrologic systems, an idealized typical cold-regions terrain was modeled with the modified SUTRA code. The region represents an area with undulating topography. For a similar terrain and within a set of nested groundwater flow systems, the study evaluated the impacts of a key (though not exhaustive) set of surface and hydrogeologic controls on the timing and pattern of permafrost thaw during climate warming. The controls considered (though only select results are discussed in this report) were:

- frequency and amplitude of topographic (i.e. water table) undulation,
- permeability value ('zero' permeability giving conduction-only heat transport, and also a range of low to high realistic values),
- vertical anisotropy in permeability (ratio of horizontal to vertical permeability, ranging from no anisotropy to high values representing the upscaled effect of low-permeability layers),
- heterogeneity in spatial distribution of permeability (patchiness consisting of high- and low-permeability structures),
- lakes/streams in valleys with perennially-unfrozen bottom water (none, one, or more water bodies),
- initial permafrost state (permafrost initially much colder than thaw temperature range, and, permafrost initially ready to thaw with only minor temperature increase),
- extent of groundwater flow through permafrost body (no throughflow, and, some throughflow),
- climate warming rate (low and high estimates), and,
- amplitude of seasonal temperature variation (none and a range from low to high) superimposed on a linear temperature trend representing a warming climate.

The two-dimensional, 'Tothian hills' cross-sectional model domain was created in the spirit of the classic nested groundwater flow analysis of Tóth (1963). The water table coincides with the top of the model. The uppermost one meter of the domain was used to explicitly model heat transfer through an equivalent thermal boundary layer that represents the roughness of ground surface, vegetation and snow pack, as described below. The mean ground surface elevation of

the domain rises linearly from left to right, with a single uniform slope. Sinusoidal hills of uniform frequency and amplitude were superimposed on the sloping surface. Figure 5.2.1 illustrates the finite-element mesh and the overall extent of the domain (5 km length, approximately 2 km depth) for one example of topographic undulation superimposed on the linearly-increasing mean ground-surface elevation. The same value of the mean slope (20 m/km) was used for all analyses. Depending on the topographic shape and permeability values, a nested combination of local flow systems (e.g., one below each hill) and a larger-scale domain-wide flow system (driven by the regional slope) may exist in the domain. Spatial discretization consists of 1 m by 50 m finite elements in the top (finest) band of elements, 10 m by 50 m in the middle band, and approximately 50 m by 50 m in the deepest band. For some simulations with high permeability or heterogeneous permeability a finer discretization was employed (as little as 0.5 m vertical spacing in the upper band of elements).

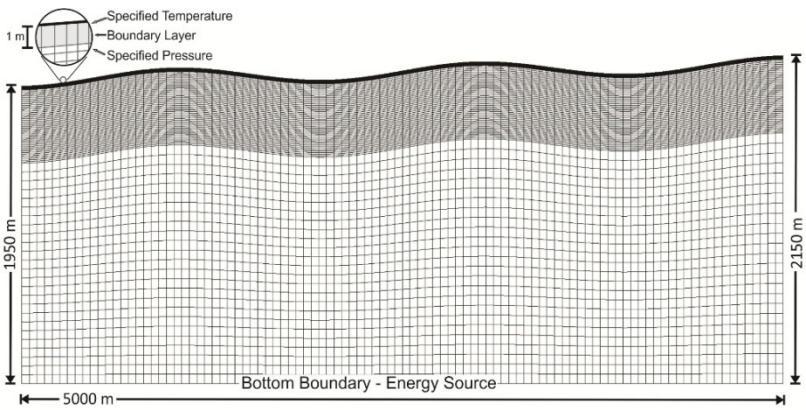

Figure 5.2.1 'Tothian Hills' model domain (no vertical exaggeration) for reference topographic shape with finite-element mesh (coarsest of several used for simulations) and boundary conditions.

Boundary conditions for the energy balance were defined as follows. A no-flux (insulated) condition was specified along the vertical sides of the domain. Along the bottom, a heat source of 0.085 J/(s m^2) was specified, equivalent to the heat flux that occurs for a typical vertical lapse rate of 26.5 °C/km when a typical thermal conductivity of geologic fabrics of 3.21 J/(s m °C) is employed in the model. A specified temperature boundary condition with a time-varying temperature value representing air temperature was specified all along the top of the domain on the upper surface of the thermal boundary layer.

A general function was specified for air temperature, allowing simulation of a constant or linear increase in mean yearly air temperature with time, or additionally with a superimposed sinusoidal seasonal variation. This air-temperature function, with increasing mean air temperature, was applied to all simulations in this study. At a given time, t (in years), the air temperature, T_{Air} (in degrees C), is calculated as:

$$T_{Air} = T_{Initial} + T_{Slope}\, t + T_{Amplitude}\, sin(2\pi t),$$

where the angle of the sin is in radians, $T_{Initial}$ (°C) is the starting temperature, T_{Slope} (°C) is the change in mean annual air temperature per year, and $T_{Amplitude}$ (°C) is the amplitude of yearly air temperature variation (i.e. half of the difference between maximum and minimum temperature in each one-year cycle).

For all analyses (except one considering initially warmer permafrost), the initial atmospheric temperature was -6 °C and the increase of mean annual air temperature was either +1 °C per 100 years (pertains to results presented here) or +6 °C per 100 years (additional examples provided in McKenzie and Voss, 2013). These rates of increase bracket the very low end and very high end of the IPCC (2007) and SNAP (Scenarios Network for Alaska and Arctic Planning, 2012) warming prediction range. The amplitudes of the yearly temperature variations considered were ±5°C, ±10°C, ±15°C and ±20°C. An initial condition with initial permafrost distribution was obtained for a system dominated by heat conduction with a constant sub-zero air temperature.

5.2.2 Results and Discussion

The divergent evolutions of permafrost thawing during climate warming in conduction-only and advection-influenced hydrogeologic systems are described in reference to results displayed in Figure 5.2.2.1. In this simulation, the air temperature warms from -6 to 0 °C during the first 600 years. Initially, there is a uniform layer of continuous permafrost from the ground surface downwards, ranging in thickness from 220 m below valleys to 300 m below hilltops, with a mildly undulating bottom (initial ice saturation at -600 years in Figure 5.2.2.1 a).

For the case of advection-influenced thaw (simulation with groundwater flow), permafrost completely disappears by 770 years (Figure 5.2.2.1). This is about one-third less than the time required for complete permafrost loss in the equivalent conduction-only system (1100 years). It is notable that the configuration of residual permafrost is quite different between the two cases. For conduction-only thaw (no groundwater flow), the residual permafrost bodies are located below hilltops; in contrast, for advection-influenced thaw, the residual permafrost bodies are located below valley bottoms. For conduction-only thaw, the thinnest parts of the permafrost layer thaw through first. For advection-influenced thaw, most thaw occurs where warm recharge water is directed against the permafrost, directly below hilltops; less thaw occurs laterally because groundwater temperature decreases as it flows towards valley discharge points due to the loss of latent heat during thawing that occurred below the hilltops. Results of this simulation analysis demonstrate that where groundwater flows readily in unfrozen ground surrounding permafrost bodies, groundwater flow is an important control on the temporal and spatial evolution of permafrost during periods of thaw. Systems with groundwater flow will experience accelerated rates of permafrost degradation overall, and regional patterns of residual permafrost can be very different in conduction-only and advection-influenced groundwater systems. Conversely, where groundwater flow in unfrozen ground is minimal, such as where the subsurface has very low permeability inhibiting flow, where the subsurface is highly stratified with low vertical permeability, or where ground ice is spatially continuous over large areas

(blocking recharge), heat conduction is the primary thaw process affecting permafrost evolution during climate warming.

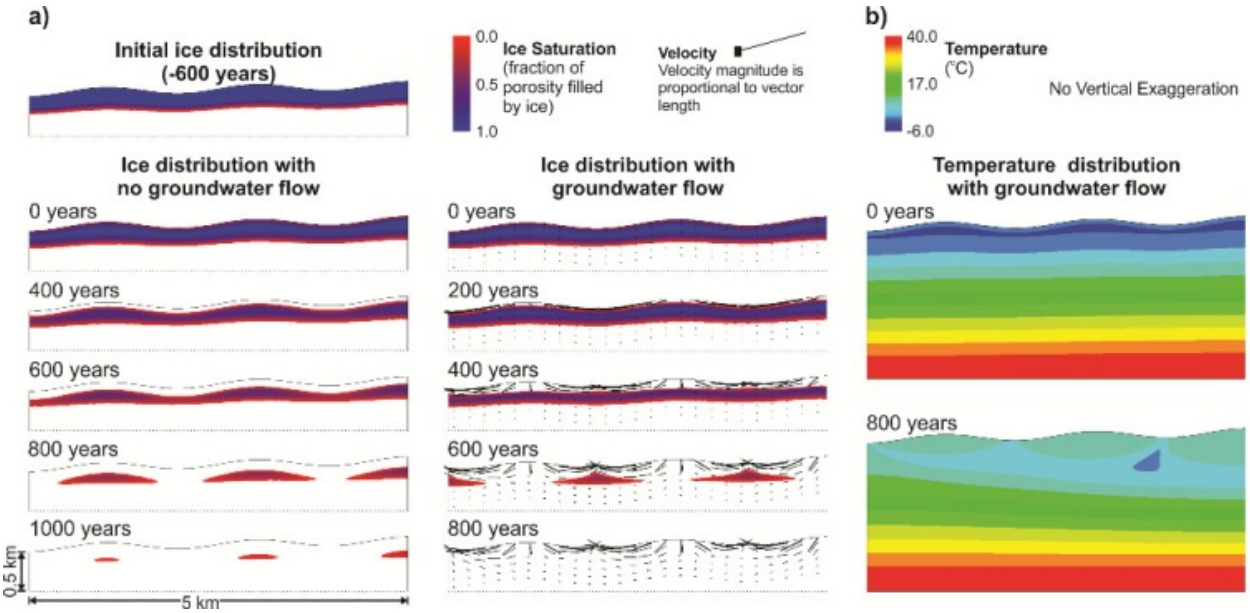

Figure 5.2.2.1 Comparison of conduction-dominated (left) and advection-influenced (middle) permafrost thaw during climate warming.
Results illustrate: (a) permafrost distribution and groundwater flow field in the uppermost 0.5 km of the 2 km deep model domain and (b) temperature distribution in entire model domain. Horizontal permeability, 10^{-12} m^2; vertical anisotropy, 10.

For given landforms with particular hydraulic driving forces for groundwater flow, the magnitudes of fluid flux and potential advective heat transport are dependent on the permeability of the geologic fabric. It follows then, that permeability and permeability distribution exert important controls on thawing of ground ice. Additional simulations were designed and performed to quantify the reduction in permafrost thaw elicited from increases in permeability. Impacts on permafrost thaw of two types of permeability heterogeneity in the geologic fabric, simple layers and patchiness, are illustrated in Figure 5.2.2.2 and 5.2.2.3.

Comparison of the thaw evolution and timing from the three simple layer heterogeneity situations with initially continuous permafrost reveals that, if the high-permeability zone is located anywhere below the permafrost, it has little or no effect on the thaw process; the bottom and below-permafrost results (Figure 5.2.2.2 a, b) are practically equivalent. High flow in the zone (see Figure 5.2.2.2 b at 700 years) begins only once permafrost becomes discontinuous, and by that time, most thaw has already occurred, so the higher groundwater flux has little impact. In contrast, a high-permeability zone located at the top of permafrost (Figure 5.2.2.2 c) enhances supra-permafrost groundwater flow, accelerating thawing from the top and causing much earlier breakthrough and complete permafrost disappearance.

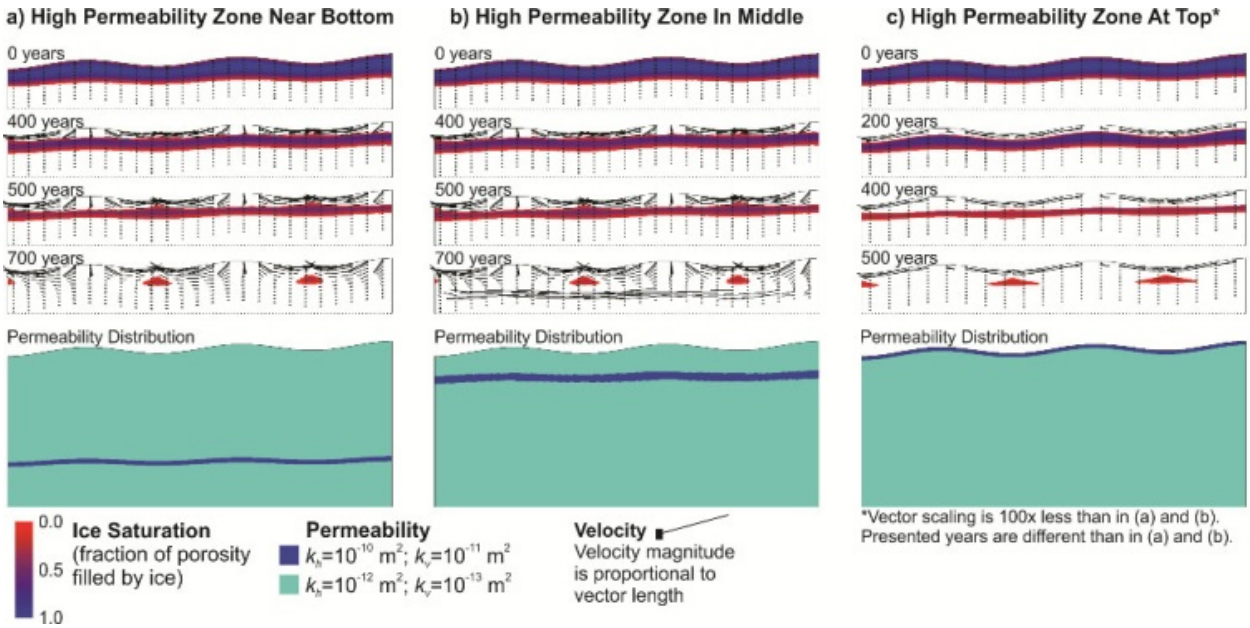

Figure 5.2.2.2 Effect of heterogeneity in permeability on evolution of permafrost thaw patterns: high-permeability layers.

An example of patchy permeability heterogeneity was also simulated as shown in Figure 5.2.2.3. The times to first breakthrough and complete disappearance of permafrost in the patchy heterogeneous case are 200 years and 750 years, respectively, and in the homogeneous case are 600 and 770 years, respectively. A through-going talik forms in the heterogeneous case in one-third of the time required in the equivalent homogeneous case, but complete loss of permafrost takes about the same amount of time. Inspection of the patterns of residual permafrost (Figure 5.2.2.3) indicates that thaw occurs preferentially in the high-permeability patches, with much earlier creation of taliks within and near these zones due to higher localized groundwater flow. In contrast, the low-permeability patches preserve permafrost for an extended time due to very low flow and essentially conduction-only conditions within the patch. Permafrost is also preserved in some regions below the low-permeability zone within more-permeable fabric, perhaps as a result of the patch shielding its underside from groundwater flow.

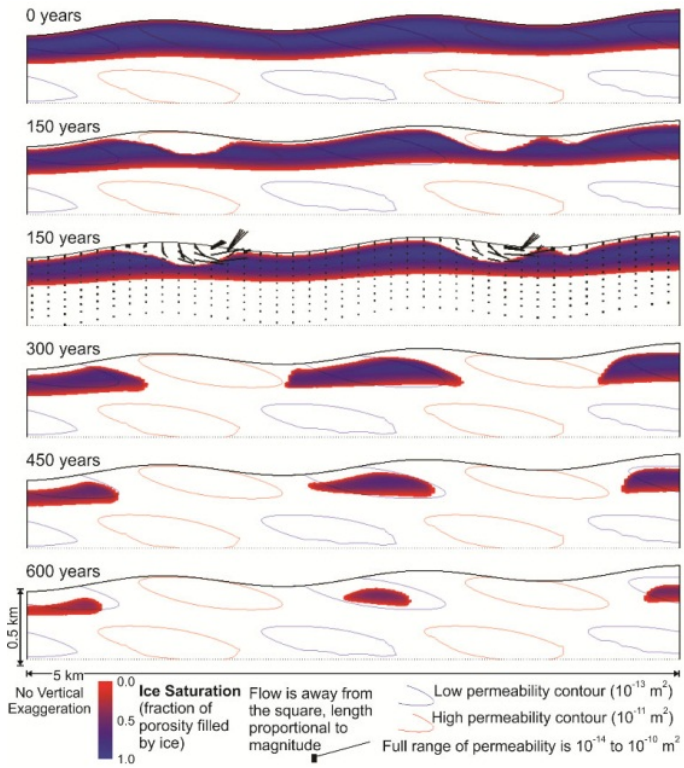

Figure 5.2.2.3 Effect of heterogeneity in permeability on evolution of permafrost thaw pattern: example with high- and low-permeability patches.

Surface water bodies such as lakes and streams have a thermal impact on the subsurface region below and immediately surrounding the water body. Most surface water bodies, particularly for those that do not freeze to the bottom in winter, support an ice-free zone (talik) below the surface water body. Here, the interaction of surface water bodies and nested groundwater flow systems were examined by introducing lakes with variable configurations into the cross-sectional simulations. Simulated thaw evolutions with surface-water bodies in different valleys are compared in Figure 5.2.2.4, and these may all be compared with the equivalent hydrogeologic situation without surface water (second panel of Figure 5.2.2.1). One result of a lake is the absence of an initial permafrost layer below its valley. Thus, for a sub-lake valley, there will be no long-lasting residual permafrost, as occurs below a lake-free valley when all other permafrost has thawed. Times for total thaw should thereby be reduced. This is borne out by the results, in which total thaw occurs by 600 years or 700 years, depending on the number of lakes, in comparison with total thaw time of 770 years for the no-lake situation. Further, it might be expected that when there are two or more lakes with through-going taliks, some regional groundwater flow occurs even at the beginning of the time period, shortening thaw times due to advection. In this light, it may be noted that the cases with a single lake experience thaw (complete in about 700 years) in a manner similar to the no-lake case, because no regional flow occurs until breakthrough in an additional location. Note in Figure 5.2.2.4 (clearest at early times) that flow enters higher lakes, passes laterally downhill below permafrost bodies, and

discharges to lower lakes. This accelerates thaw somewhat, with complete thaw occurring by 600 years. However, despite the contribution of large-scale deep groundwater flow, the primary thaw mechanism in cases with surface water remains heat advection in the downward flow below hilltops.

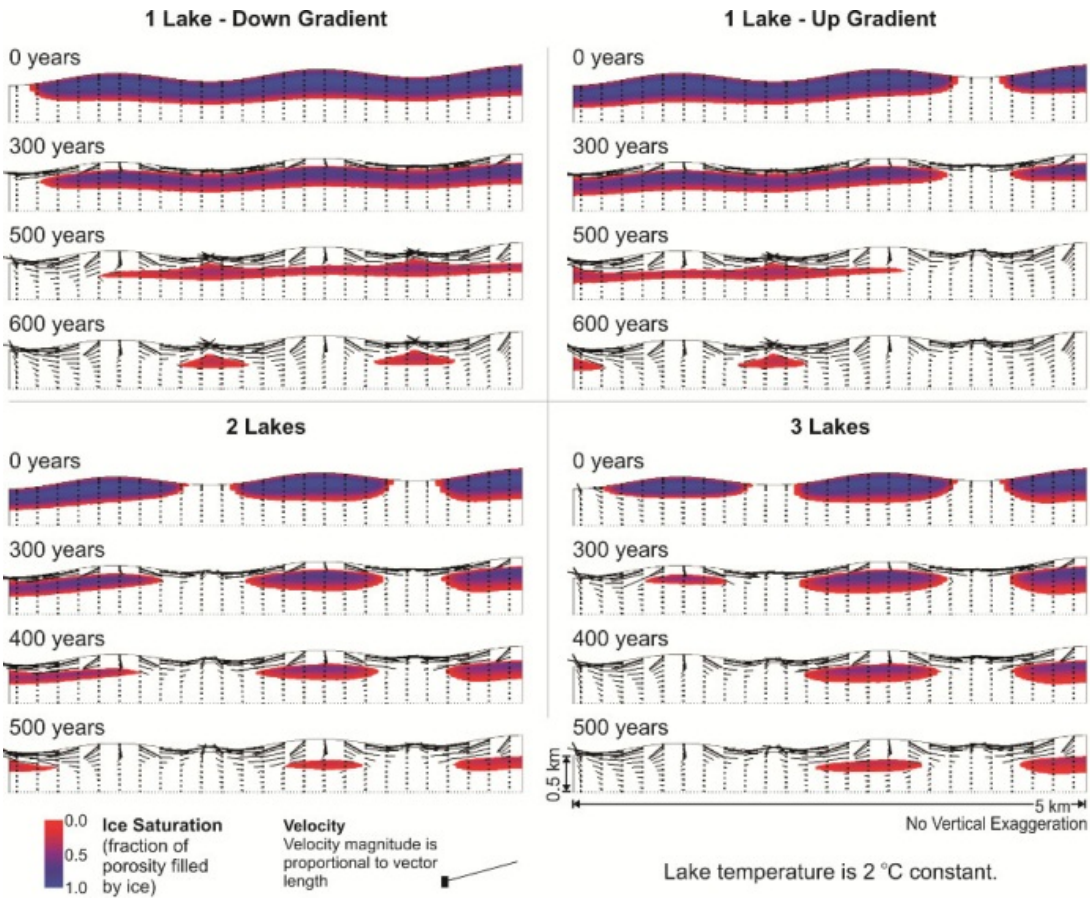

Figure 5.2.2.4 Effect of lakes on evolution of permafrost thaw patterns.

Results of this modeling study (described more fully in McKenzie and Voss, 2013) demonstrate how specified climate warming rates affect permafrost thaw. Simulated times for total thaw under the 1 °C and 6 °C per 100 years warming rates are respectively: 1100 years and 700 years for conduction-only, and 770 years and 500 years for the advection-influenced case.

5.3. Lake Mass Balance Analysis

Many lakes in northern high-latitudes have undergone substantial changes in surface area over the last four decades. In the discontinuous permafrost of Yukon Flats, interior Alaska, these changes have been non-uniform across adjacent watersheds (Rover et al., 2012), suggesting local controls on lake water budgets. In the lake mass balance analysis conducted here, multiple

mechanisms were explored to explain the decreasing mass of the primary study lake, Twelvemile Lake, in the Yukon Flats (Figure 5.3.0.1). Twelvemile Lake was chosen because of (1) its substantial reduction (~60%) in surface area since the early 1980's at a rate of approximately 12 cm yr^{-1} ($p < 0.001$), and (2) the nonuniformity displayed between Twelvemile Lake and a neighboring lake (Buddy Lake), 2 km to the southeast, which has shown no apparent change in surface area since the early 1950's (Figure 5.3.0.2). Changes in snowmelt mass and infiltration, permafrost distribution, and climate warming were considered in this quantitative analysis. The analysis was carried out by testing the sensitivity of lake volume to assumed changes in different plausible water flowpaths. The effect of climate, between 1950 and 2010, on the mechanisms considered are both direct (evaporation, snow/rain partitioning) and indirect (configuration of permafrost).

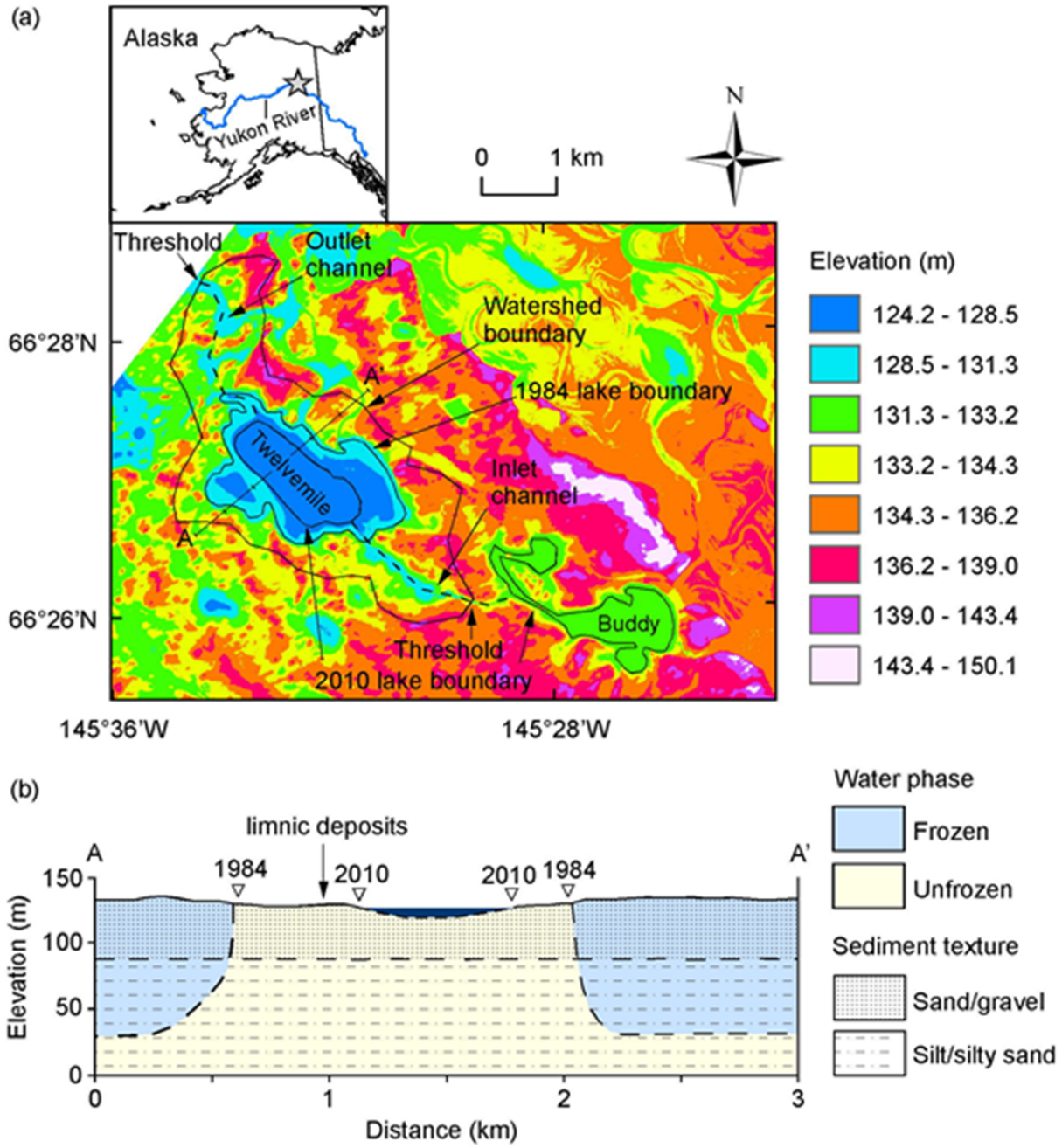

Figure 5.3.0.1 Study site location.

Topographic map of the Twelvemile Lake watershed, based on a 2.5 m-resolution LIDAR DEM (Gesch 2007) (a). Lake boundary of Buddy Lake during 1984 is similar to that in 2010 and thus not shown. Schematic cross-section view of soil textures and permafrost distribution, triangles denote lake margin locations (b), line AA' shown in panel (a).

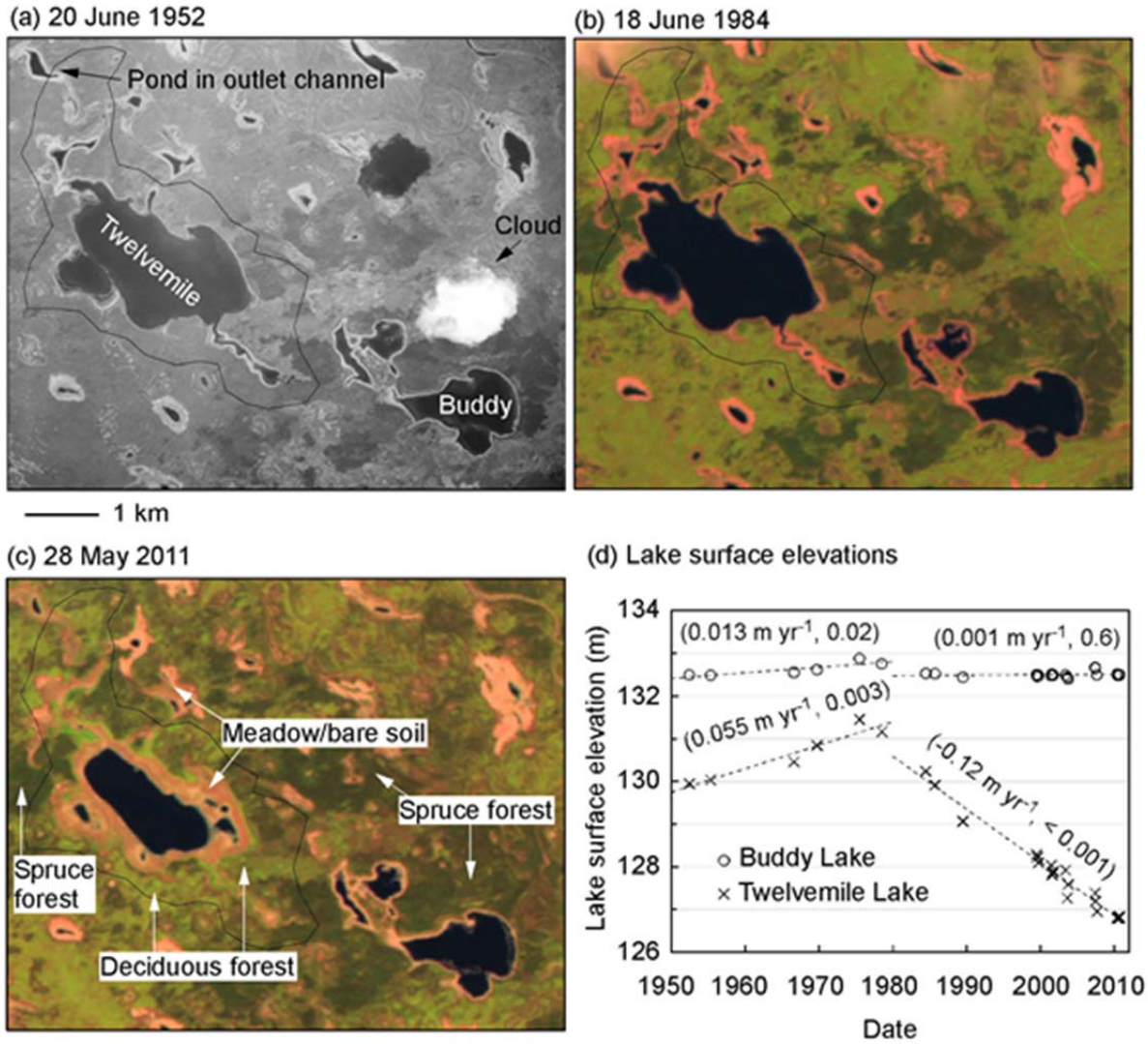

Figure 5.3.0.2 Images of Twelvemile and Buddy Lakes between 1952 and 2011 (a-c) and time series of lake surface elevation (d).

5.3.1 Materials and Methods

Water fluxes to and from Twelvemile Lake were estimated via a scoping analysis for variable partitioning of precipitation between snow and rain, different flowpaths of snowmelt, and historic changes in growing season air temperature (May-September). The past and present spatial distribution of permafrost, which acts as an aquiclude at the spatial scale necessary for this study, is not completely known; therefore, a variety of permafrost configurations and associated flow pathways are considered in order to address different plausible boundaries of the hydrologic system. Some water fluxes to/from the lake occur directly from the atmosphere (direct flux), while other fluxes occur indirectly as groundwater or overland flow (indirect flux). Direct fluxes are defined to be snow, rainfall, and lake evaporation. Indirect fluxes (Q_i) are

enumerated as follows (Figure 5.3.1.1): (i) flows from the contributing-area slopes of the watershed ($Q_{contrib}$, L^3 T^{-1}), (ii) subsurface flow across the watershed boundary over a "low spot" ("threshold") formed by a topographically depressed permafrost table (Q_{thresh}, L^3 T^{-1}), and (iii) flows to or from the lake through an open talik (Q_{talik}, L^3 T^{-1}). Indirect fluxes are determined based on the hydraulic forces and hydraulic properties along multiple assumed flowpaths. The spatial distribution of land features and water surface elevations are determined using aerial photos and satellite images and a LIDAR 2.5 m-resolution DEM (Gesch, 2007). Constraints on the current spatial distribution of permafrost and water table elevation are determined from augering and frost probing during 2010 and 2011. Mapped resistivity from an airborne electromagnetic (AEM) survey conducted during 2010 helped to visualize the overall pattern of ground ice in the watershed.

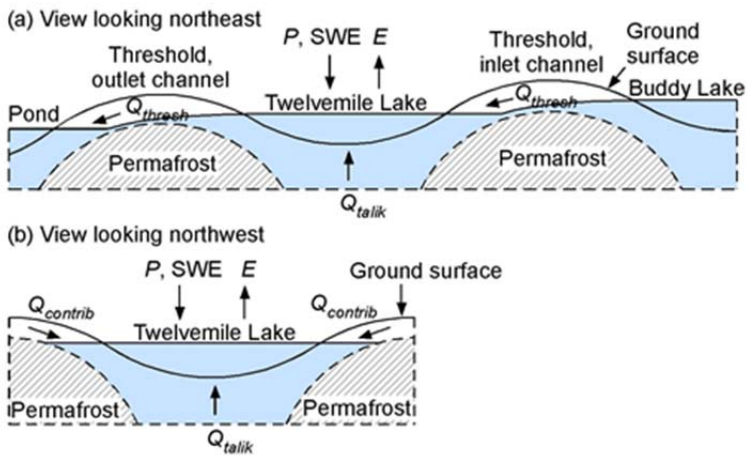

Figure 5.3.1.1 Conceptual model of water fluxes considered in this study.
View looking northeast, perpendicular to the inlet and outlet channels (a), and view looking northwest (b).

Time periods of 1950-1980 and 1980-2010 were considered, the former period assumed to represent conditions prior to onset of lake lowering beginning in the early 1980's. Years 1984 and 2010 were used to represent lake geometries during the earlier and latter periods, respectively. Here, an indirect flux was defined to be significant if it alone provides at least half of the indirect flux required to produce the observed average rate of lake level change between 1950 and 2010. The lake water budget was considered to have significant sensitivity to change in a particular water flux if that change would produce at least half of the observed change in lake lowering beginning in the early 1980's.

5.3.2 Results and Discussion

Permafrost was not found via frost probing and soil pit analysis at 19/21 sites within the 1984 lake boundary, and was found at 0.4-2.5 m depth at 25/36 sites outside of the 1984 lake boundary (Figure 5.3.2.1 a). Most of the ice-free sites outside of the 1984 lake boundary are in the inlet and outlet channels, where ground penetration near the watershed boundary was limited due to the presence of shallow gravel and water (Jepsen et al., 2012). These observations indicate that the early 1980's lake margin approximately separates watershed areas with and without permafrost,

excluding the channels. This pattern is consistent with that from the AEM resistivity interpretation (Figure 5.3.2.1 b), where resistivities greater than about 530 ohm·m (i.e., orange color in Figure 5.3.2.1 b) generally reflect the presence of permafrost. Based on these observations, the outer and inner contributing areas used for the $Q_{contrib}$ calculation was defined to be the areas outside and inside, respectively, the 1984 lake boundary.

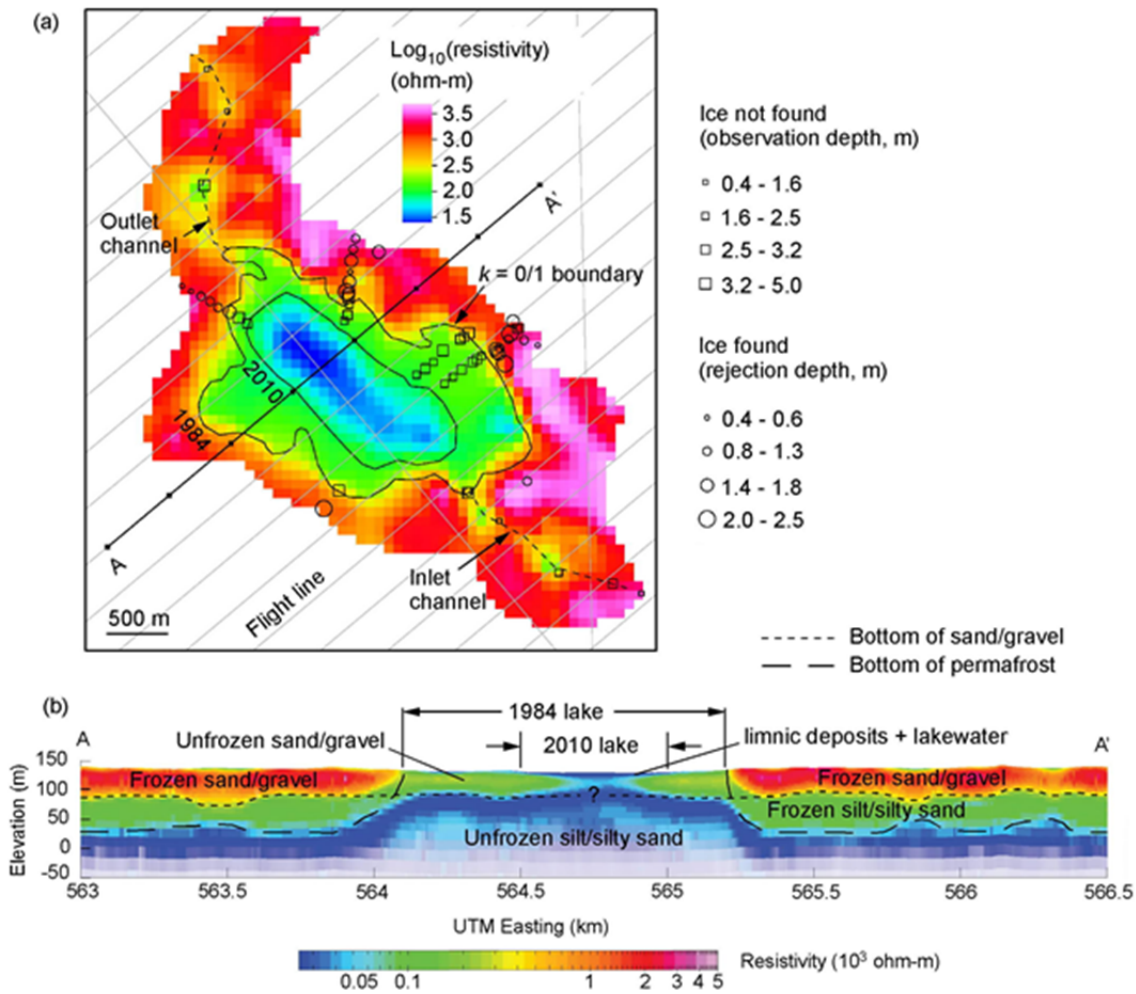

Figure 5.3.2.1 Maps showing resistivity of subsurface (upper 10 m) from the AEM survey and depth to ice from ground-based observations (a), and AEM-based resistivities and lithology-ice interpretations along cross section AA' through Twelvemile Lake (b). Frozen material in (b) indicates permafrost. Vertical exaggeration 2.6× in panel (b). The boundary separating the outer (*k* = 0) and inner (*k* = 1) contributing areas is shown in (a).

The increase in lake evaporation since the early 1980's due to increased May-September air temperatures was calculated to be 2 cm yr^{-1}, which is an order of magnitude lower than the observed 17.5 cm yr^{-1} change in mass balance, indicating that increased air temperature warming alone is not likely to be a primary mechanism. Decreased duration of the ice-covered season may

be as much as 1-2 weeks since the late 1970's due to springtime warming (Brown et al., 2010; Foster et al., 2008). This would increase the duration of the open-water season, and hence lake evaporation (Woo, 1980), by perhaps 10%, which is still not adequate to be a primary mechanism.

Analytical results using the equations and parameters provided in detail in Jepsen et al. (2013a) demonstrate that the following mechanisms are possible explanations for the lowering of Twelvemile Lake beginning in the early 1980's: (1) changes in lateral, shallow (< ~40 m) groundwater flow across the watershed boundary, through gravel, (2) changes in groundwater flow resulting from the development of an open talik, provided that sub-permafrost flow is through sand, layers of which are sparse relative to lacustrine silt, (3) a decrease in the mass of maximum-accumulation snowpacks in conjunction with increased infiltration of snowmelt into, and subsequent evaporation from, fine-grained sediment around the lake.

Increased lateral, shallow groundwater flow from a lake's watershed (mechanism 1) would occur if a lake overtopped the permafrost-table threshold at the watershed boundary, resulting in a type of shallow-subsurface flooding (Michel and van Everdingen, 1994). This process would represent a subsurface analogue of lake drainage via overland flow through surface channels, as observed in other studies (Woo and Mielko, 2007; Brewer et al., 1993; Mackay, 1992), and may lead to sustained lake lowering if the rate of thermal erosion at the permafrost threshold could equal or exceed the rate of lake lowering (Marsh and Neumann, 2001). Thawing of the transient layer (permafrost that freezes and thaws on decadal time scales) (Shur et al., 2005) in gravelly material could facilitate onset of this process. This mechanism was found to be potentially important despite the low topographic gradients of Yukon Flats because of the high hydraulic conductivity of gravel.

The requirement of high permeability in the subpermafrost aquifer for open-talik development (mechanism 2) to be an important mechanism of lake lowering results from the low hydraulic gradients in Yukon Flats, which are 2-3 orders of magnitude lower than gradients observed near Council, Alaska, where open taliks are an important mechanism for thermokarst pond drainage (Yoshikawa and Hinzman, 2003). In the Yukon Flats, subpermafrost sand layers are minor in abundance relative to lacustrine silt (Williams, 1962; Clark et al., 2009), suggesting that lake drainage through open taliks on a large scale in Yukon Flats may be limited by the permeability of the subpermafrost aquifer.

In regard to increased snowmelt infiltration (mechanism 3), previous studies have revealed a wide range of infiltration capacities of frozen soil (for reviews, see Ford and Bedford, 1987; Dingman, 1975). In environments where frozen soil has been found to prevent snowmelt infiltration and enhance overland flow (Woo and Steer, 1983; Granger et al., 1984; Kane and Stein, 1983; Kane, 1980), which may be associated with relatively cold, moist soils, lake mass would have a high sensitivity to snow water equivalent (SWE). In contrasting environments where much or all snowmelt can infiltrate into frozen soil (Suzuki et al., 2006; Carey and Woo,

1999), lake mass would have low sensitivity to SWE because of how little snowmelt reaches the lake. This would be especially true in areas of gentle topography and fine-grained soils, such as Yukon Flats. Progressive lake lowering produces a gradient in the exposed land surface in vegetation and permafrost distribution. How this process affects soil moisture and snowmelt infiltration, and possible feedbacks on lake recharge, merits further study.

All of the plausible mechanisms for lake level lowering identified in this study require the presence of certain geologic and/or permafrost conditions, known to display high spatial variability across the Yukon Flats. This finding is consistent with the high degree of non-uniformity observed in lake level changes in Yukon Flats (Rover et al., 2012; Riordan et al., 2006). Examples of these spatially varying characteristics include discontinuity of permafrost, depth to the permafrost table, and SWE at maximum accumulation (Sturm et al., 2010, 2011).

5.4 Lake Talik Evolution

In cold regions, hydrologic systems possess seasonal and perennial ice-free zones (taliks) within areas of permafrost that control and are enhanced by groundwater flow as demonstrated by model simulations described in sections 5.1 and 5.2. To further develop that concept within the framework of our study area on the lake watershed scale, a series of simulations were designed to understand talik development that follows lake formation in watersheds modeled after conditions in the Yukon Flats. The goal was to provide insight on the coupled interaction between groundwater flow and ice distribution. The modified SUTRA code with freeze-thaw physics was used to examine timescales and controlling factors of talik formation. This work was the first numerical study published (Wellman et al., 2013) that addressed both sub-lake talik evolution and supra-permafrost (active layer) near-lake talik evolution under the influence of seasonal temperature fluctuations over the millennium (1000 years) timescale for a range of environmental conditions. Controlling variables explored in this analysis include lake depth (and related lake size), hydrologic gradient with respect to the lake, and shifts in climate-driven surface temperature. Information derived from this study provides insight into the impact of these controls on expected times of lake-talik development, on shallow and deep water fluxes to and from lakes, and on lake-basin permafrost distribution, thus supplying a supporting foundation for important scientific linkages such as biogeochemical and ecological studies of arctic lake changes (Zimov et al., 2006; McGuire et al., 2009).

5.4.1 Materials and Methods

The basic scenario considered in this modified-SUTRA modeling study was the talik evolution associated with a newly-formed lake above thick (90-m) permafrost. The model enabled thawing by a combination of thermal conduction and advective heat transport. Building from the general climatic and structural features of Twelvemile Lake (Figure 5.4.1), a suite of 36 simulation scenarios was generated to address variations in climate, lake size, and groundwater flow

direction on talik evolution. The suite of scenarios allowed examination of hydrologic and cryologic processes under a range of conditions that typify lakes in Yukon Flats and in other circumpolar regions of relatively thick discontinuous permafrost and low topographic relief.

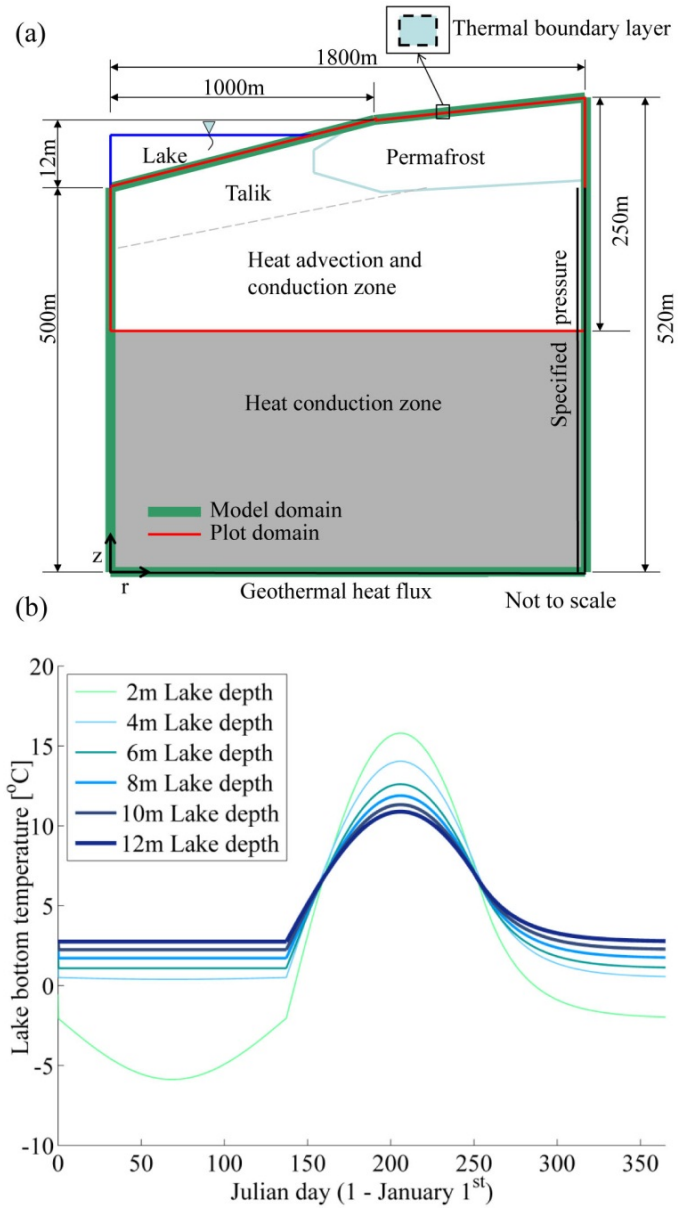

Figure 5.4.1 Cross-section of two-dimensional cylindrical model with boundary conditions of temperature, fluid pressure, and heat flux (a).
Top surface consists of a thermal boundary layer between air temperature (or lake temperature) and aquifer surface temperature, with a specified air (or lake) temperature on the top surface and a specified pressure on the lower surface representing the land surface pressure (p=0) or lake bottom pressure (p=hydrostatic pressure at local lake depth). Annual synthetic lake bottom temperature as a function of various lake depths patterned after Burn (2002, 2005) (b).

Generalized geologic layer representation for the 2-D cylindrical model followed the basic lithology of the Fort Yukon area as reported in Clark et al. (2009) and Williams (1962) and as interpreted from the AEM survey of the region (Minsley et al., 2012). A thin (2 m) surficial sedimentary deposit characterized as silt and sand exists above a thick (28 m) gravel and sand layer, which is underlain by an extensive undifferentiated deposit believed to be predominately silt in composition.

Constant and time-varying conditions that specify temperature, fluid pressure, and subsurface geothermal energy flux were applied to the model boundaries (Figure 5.4.1). The ground surface at 0 m depth consisted of an idealized lake bottom with prescribed fluid pressures and oscillating seasonal temperatures reflective of an overlying lake body

Prescribed head (pressure) conditions in the sub-permafrost aquifer were used to control the direction of water movement between the sub-permafrost groundwater and simulated lake bottom surface. The examined scenarios include: (1) hydrostatic conditions without an exchange of water between the lake and underlying sub-permafrost aquifer, (2) gaining lake conditions with the potential for sub-permafrost groundwater to discharge to the lake, and (3) losing lake conditions with the potential for water to discharge from the lake.

Three climates were examined, reflective of the present, colder than present, and warmer than present. The yearly temperature cycles for the "colder" and "warmer" climate scenarios were modified from that of the current climate by reducing and raising, respectively, temperatures by 2°C for the terrestrial areas and by 1°C along the lake bottom. The adjustments of temperature assumed an incremental change to the mean conditions while the amplitude of seasonal fluctuations was preserved. The rationale for exploring different climates was based on documented changes in historic air temperature (Serreze et al., 2000) and projected GCM (global climate model) changes in future air temperatures in Alaska (Chapman and Walsh, 2007; Walsh et al., 2008). The selected 2°C temperature adjustment was based on the 50-year projected GCM annual average temperature increase for the Yukon Flats assuming mid-range emissions (Scenarios Network for Alaska and Arctic Planning (SNAP), 2012). For consistency, an equivalent reduction in temperature for a climate colder than present was also explored indicative of conditions half a century or longer in the past.

5.4.2 Results and Discussion

A detailed comparison of transient results for the 12-m deep losing, gaining, and static lake conditions, all under the current climate, provides an opportunity for describing the inter-relations and temporal patterns of ice structure and groundwater flow. Figure 5.4.2.1 a,b, and c illustrates the temporal progression in flow and ice volume through time since lake formation for the losing, gaining, and static lake conditions, respectively. The amplitude of yearly fluctuations in ice volume and groundwater flow are expressed in Figure 5.4.2.1 as the vertical thickness of the color bands, because the individual yearly fluctuations appear as a continuous band on the

long time scale plotted. Ice volume present under the lake decreases with time. Sub-lake talik breakthrough is coincident with a break in the slope indicating the change in ice volume with time for regions with > 0.1 ice saturation and is denoted by the vertical dashed line in Figure 5.4.2.1. After breakthrough, the sub-lake talik expands laterally outward from the lake, further reducing the ice volume under the lake through time. Sub-lake talik breakthrough occurs in 215 years for the losing lake, 240 years for the gaining lake, and 598 years for the static lake, yielding an effective rate of sub-lake vertical thaw of approximately 0.42 m yr^{-1}, 0.38 m yr^{-1}, and 0.15 m yr^{-1} respectively. The rate of total ice volume decrease (approximated by the decline in ice volume with an ice saturation > 0.10), and the sub-lake groundwater flow both increase once an open talik is developed for the losing and gaining systems, providing a feedback mechanism that enhances the thaw rate via heat advection. Prior to this point, reduction in ice volume is largely controlled by heat conduction, because groundwater flow is restricted by pore ice that impedes groundwater flow. Yearly fluctuations in ice volume diminish with time for the losing and gaining lakes thereafter as the ice structure along the lake margin tends toward equilibrium.

Four cases of talik evolution are illustrated for a 12-m lake: hydrostatic and gaining lakes under the current climate (Figure 5.4.2.2 a, b), and gaining and losing lakes under a warmer climate (Figure 5.4.2.2 c, d). Results are examined at 100, 250, and 1000 year elapsed times representing early to late phases in talik development. At 100 years, thaw in all of the scenarios examined is conduction-controlled, because ice saturation is sufficient to impede groundwater flow irrespective of whether a hydraulic gradient exists between the lake and aquifer or if a warmer climate is imposed. At 250 years elapsed time, the hydrostatic lake has a thaw bulb that extends to a depth of about 40 m at the lake center. For a gaining lake with current and warmer climates, Figure 5.4.2.2 b and c, respectively, permafrost thaw is enhanced relative to the hydrostatic lake situation due to advection of heat in the upward-flowing groundwater. The situation with a losing lake under the warmer climate, exhibits the fastest thawing among the four 12 m lake cases considered (Figure 5.4.2.2 d). The talik structure is advanced within 250 years and possesses a width nearly four times greater than that of the gaining lake under the current climate. After 1000 years, the system exhibits extensive permafrost loss with the thaw front extending 200 m beyond the lake margin. The reduction in permafrost within the lake watershed is due to warmer surface temperatures that couple with flowing groundwater to alter both the temperature distribution and ice saturation.

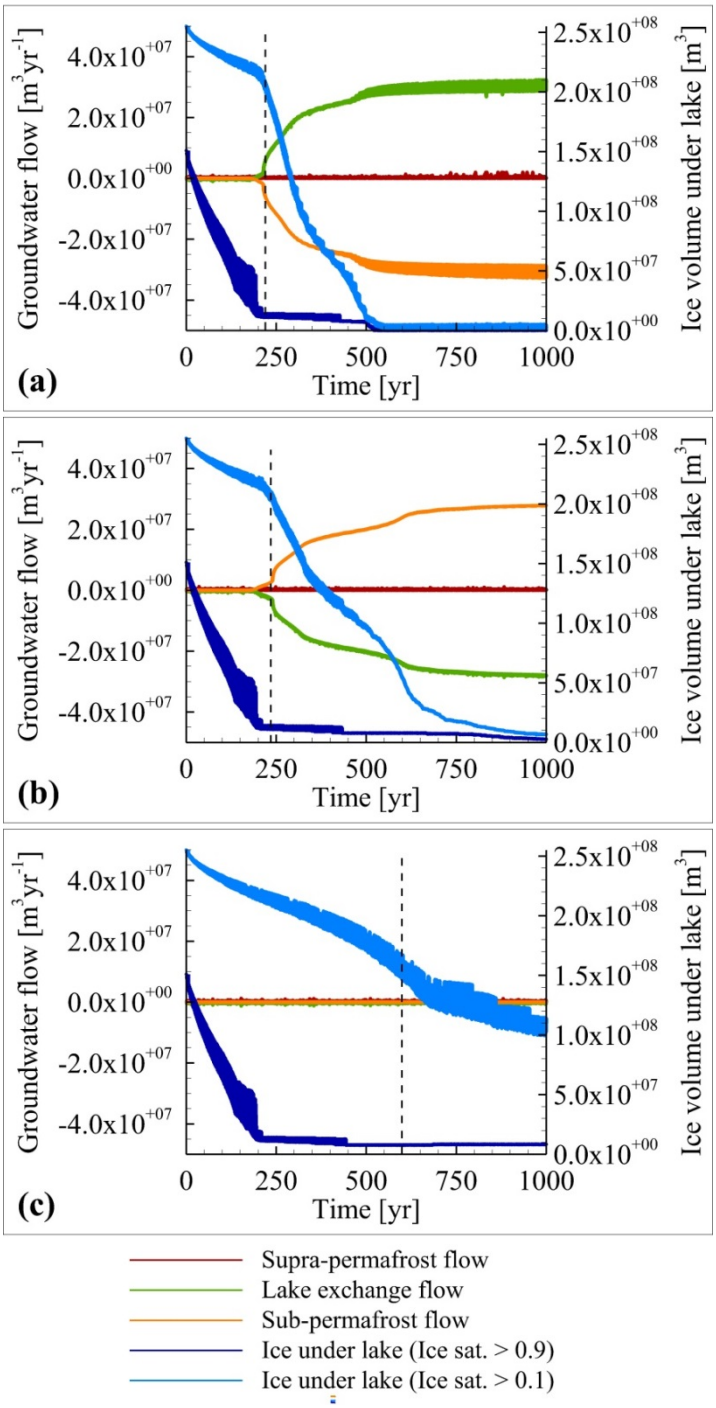

Figure 5.4.2.1 Temporal evolution of groundwater flow and ice volume for the case of a 12m lake that is losing (a), gaining (b), and hydrostatic (c) for the current climate.
The left axis measures groundwater flow (> 0 groundwater enters aquifer, < 0 groundwater leaves aquifer) and the right axis measures the volume of ice for ice saturations > 0.1 and >0.9. The dashed line in a-c indicates the talik breakthrough time for each case. Broad color bands result from yearly oscillations of the plotted factor.

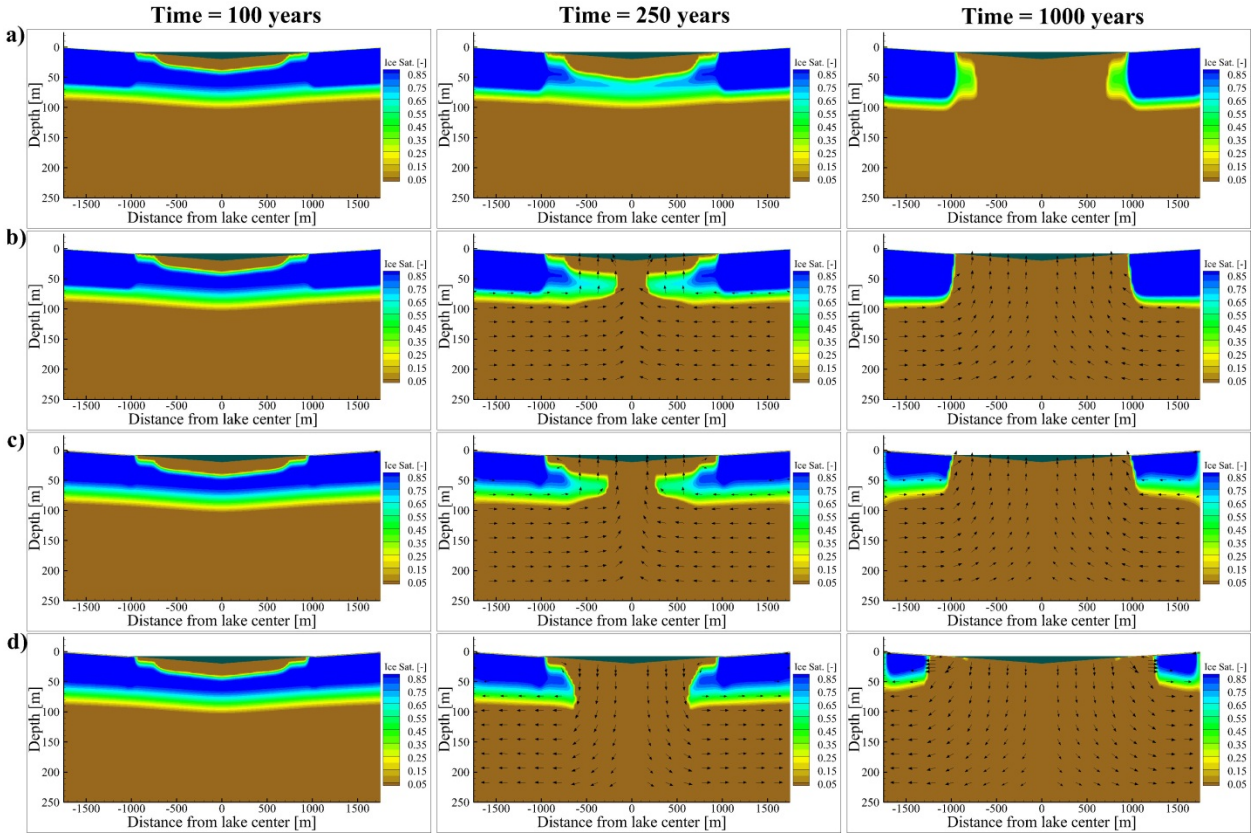

Figure 5.4.2.2 Cross-sections of 2D cylindrical model (mirrored) showing states of lake-talik formation, ice saturation, and groundwater movement where a 12m lake forms over a continuous permafrost layer of about 90m in thickness.
Figure columns distinguish early, middle, and late-time conditions at 100, 250, and 1000 years, respectively, from the time of lake formation. Figure rows differentiate four scenarios: (a) current climate with hydrostatic (no flow) lake, (b) current climate with gaining lake, (c) warmer climate with gaining lake, and (d) warmer climate with losing lake.

Average times of sub-lake talik breakthrough for the different climates, directions of lake flow, and lake depths reveal relational patterns (Figure 5.4.2.3 a). For processes exceeding the time of analysis, the maximum analysis time is used to determine group averages, thereby yielding minimum estimates. For the warmer climate simulations, talik breakthrough times are shorter than for cooler climates. Time required for open talik formation decreases by ~30 % from the colder climate scenarios to the warmer climate scenarios on average. Talik breakthrough time can vary by more than a factor of five between hydrostatic (requiring >1000 years for some cases) and gaining or losing conditions (forming as quickly as ~200 years) due to the additional component of heat advection for the latter cases. The presence or absence of groundwater flow to/from the sub-permafrost aquifer also exerts a large influence on equilibrium times of lake/groundwater exchange (Figure 5.4.2.3 b). In the case of a hydrostatic lake, inflow is derived

only from the supra-permafrost aquifer, and equilibrium, sensitive to processes near the lake margin, is quickly achieved in just 1 to 9 years (< decade). Times of flow equilibrium for losing and gaining lakes are much longer and average 661 and 694 years, respectively.

Calculated times to achieve equilibrium in permafrost volume average 606 and 711 years for permafrost ice saturations of 0.90 and 0.10, respectively, with a range between 206 to > 900 years. In terms of group averages, climate has minimal impact on cryologic equilibrium times for regions of high ice saturation permafrost (ice saturation > 0.9), and a moderate impact for the bulk of the permafrost volume (ice saturation > 0.1) (Figure 5.4.2.3 c, d).

Comparison between groundwater flux within the supra-permafrost aquifer and net flux of water to the lake at equilibrium exhibits stark differences depending on system conditions (Figure 5.4.2.3 e, f). Groundwater exchange with the lake through the open talik is greater than flow within the supra-permafrost aquifer by more than ~1.5 orders of magnitude, on average. For the gaining or losing lakes evaluated, flow through the supra-permafrost aquifer is relatively small (typically < 1 %) compared to flow exchanged between the lake and sub-permafrost aquifer. However, for a hydrostatic lake, supra-permafrost flow is the dominant groundwater contribution to the lake.

Climate warming causes flow within the supra-permafrost aquifer to increase by approximately 2 orders of magnitude from 10^3 to 10^5 m^3 yr^{-1} across the spectrum of climate regimes considered (Figure 5.4.2.3 f). This trend results from thickening of the supra-permafrost aquifer and thus greater groundwater exchange across a more developed lake margin that is permeable for a prolonged part of the year for progressively warmer scenarios.

The results demonstrate the influence of time, climate, lake size, and hydraulic conditions on talik development for cold-region lakes. Regardless of the condition evaluated, early-time thaw after the formation of a lake (periods of 100 years or less) is controlled by heat conduction below the lake bed. At later times, the transfer of heat by groundwater flow, where significant groundwater flow occurs, is an important mechanism that accelerates permafrost thaw and expedites breakthrough of sub-lake taliks. Warmer climates generally increase thaw rates and for the systems examined exhibit: (a) thickening of and increased flow through the supra-permafrost aquifer, (b) reduction of sub-lake open talik formation times and more rapid talik expansion, thereby enhancing earlier hydraulic communication between the lake and sub-permafrost aquifer, and (c) greater overall loss of permafrost.

Hydrologic connections between the lake and sub-permafrost aquifer that depart from hydrostatic conditions are expected to allow intense transfers of water and energy for short time periods in cases such as sub-lake talik formation. Given that lakes in Yukon Flats are observed to change in size, appear, disappear, and even reappear in pre-existing locations, brief periods of thawing, refreezing and occasional intense vertical groundwater exchange may be a recurring process throughout the region.

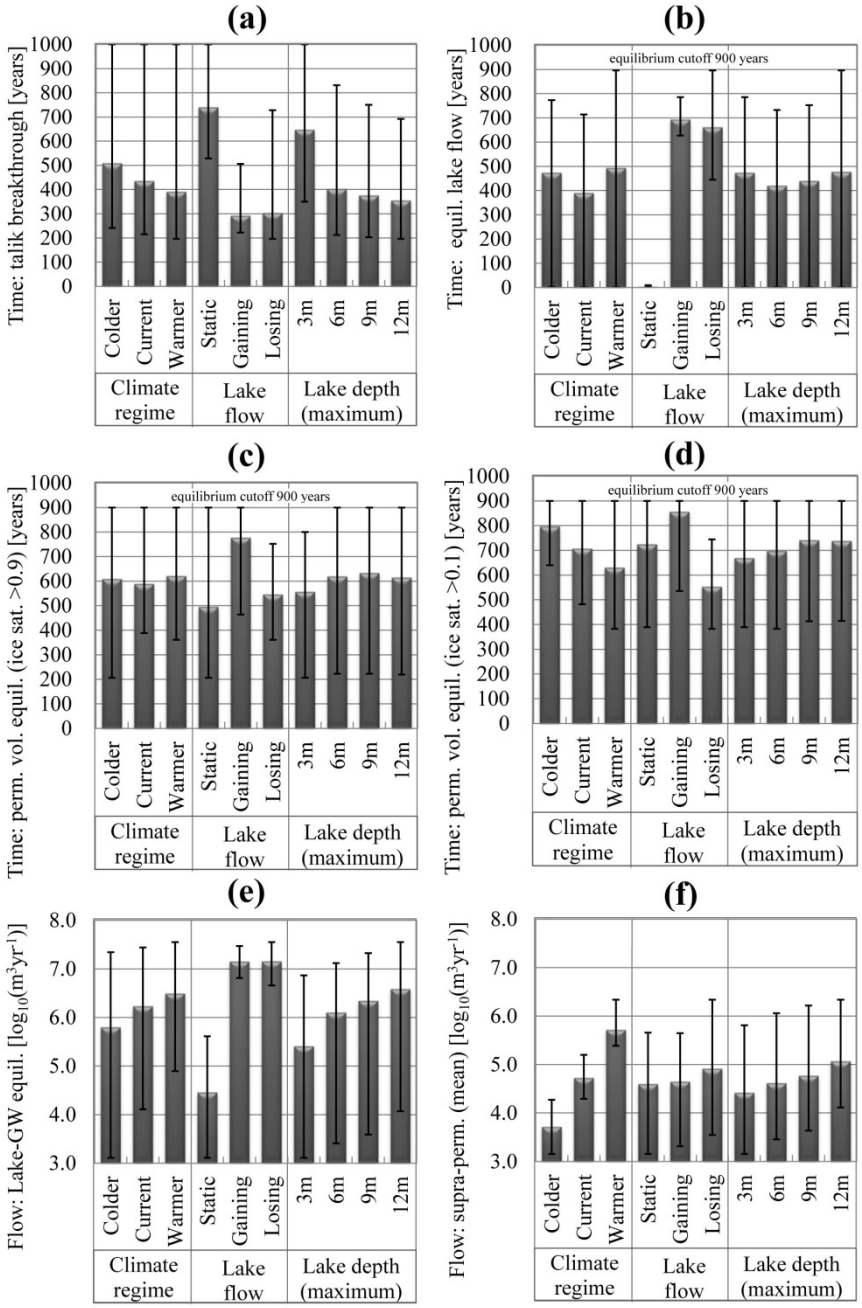

Figure 5.4.2.3 Group averages of simulation results for three categories: climate regime, lake flow, and maximum lake depth.

Tabulated results for the 36 simulations are presented in Table 3 of Wellman et al., 2013. Results are shown for: talik breakthrough time (a), time to reach flow equilibrium at the lake bottom(b), time to reach equilibrium in residual permafrost volume for ice saturation >0.9 and >0.1, respectively(c, d), equilibrium groundwater flow across the lake bottom (e), and mean annual groundwater flow to the lake through supra-permafrost aquifer (f). Grey-shaded bars show averages for each analysis and thin black range bars indicate minimum and maximum values among all analyses.

In summary, although it is generally assumed that climate is the dominant environmental driver in cold regions, lake size and groundwater flow are shown to impose equally important controls on evolution of permafrost thaw, timing of talik formation, and lake/groundwater exchange. The distribution of permafrost within a cold-region lake watershed will influence, and be influenced by, lake-groundwater exchange through supra-permafrost and sub-lake taliks. Studies that evaluate changes in lake size and distribution and that predict climate-change-driven hydrologic evolution in cold regions should consider groundwater-ice dynamics.

5.5 Sensitivity Analysis of Geophysical Data to Permafrost Conditions

The general hydrogeologic framework for the coupled thermal-hydrologic simulations, described above, was based largely on interpretations from electromagnetic geophysical information in the Yukon Flats. However, some of the geophysics-derived interpretations, including lake-talik conditions, have very limited ground truth information for calibration and validation due to the paucity of standard hydrogeologic data collected in this remote region. To address potential sources of uncertainty associated with geophysical interpretations, we investigated the ability of geophysical measurements to recover information about the underlying spatial distribution of permafrost and hydrologic properties. This was accomplished in three steps: (1) development of a physical property relation that connects permafrost and hydrologic properties to geophysical properties; (2) simulation of synthetic geophysical data that would be expected for various permafrost hydrologic conditions; and (3) inversion of the synthetic geophysical data using realistic levels of noise to investigate the ability to resolve specific physical features of interest. The focus was on electromagnetic geophysical methods as these types of data had previously been acquired near Twelvemile Lake in the Yukon Flats, Alaska (Ball et al., 2011; Minsley et al., 2012). Twelvemile Lake is the lake that was the basis for the lake simulations described in the previous section.

5.5.1 Materials and Methods

Model output from the lake talik evolution simulations (section 5.4) utilizing the modified SUTRA code was used as the basis for generating synthetic geophysical data. Relevant SUTRA output including temperature, pressure, and ice saturation at each simulation time step for each model scenario was converted to electrical resistivity, the geophysical property needed to simulate electromagnetic data, as follows.

Bulk electrical conductivity is described by Revil (2012) as

$$\sigma = \frac{S_w^n}{F}\left[\sigma_f + m\left(S_w^{-n}F - 1\right)\sigma_s\right],$$

where σ is the bulk electrical conductivity [S/m]; S_w is the fractional water saturation [-] in the pore space, where $S_w = 1 - S_i$ and S_i is the fractional ice saturation [-] in the pore space; σ_f is the conductivity of the saturating pore fluid [S/m]; m is the Archie cementation exponent [-]; n is the Archie saturation exponent [-]; F is the formation factor [-], where $F = \phi^{-m}$ and ϕ is the matrix porosity [-]; and σ_s is the conductivity [S/m] associated with grain surfaces. The Archie exponents m and n are known to vary as a function of pore geometry; here, we use $m = n = 1.5$. Simulation results are presented as electrical resistivity [ohm-m], which is the inverse of the conductivity, i.e. $\rho = 1/\sigma$.

Information about the different lithologic units incorporated in the model analysis (Figure 5.5.1) was used to define static model properties such as porosity, grain mass density, cation exchange capacity, and Archie's exponents (Table 5.5.1). Dynamic outputs from the SUTRA simulations, including temperature and ice saturation, were combined with the static variables to predict the evolving electrical resistivity structure.

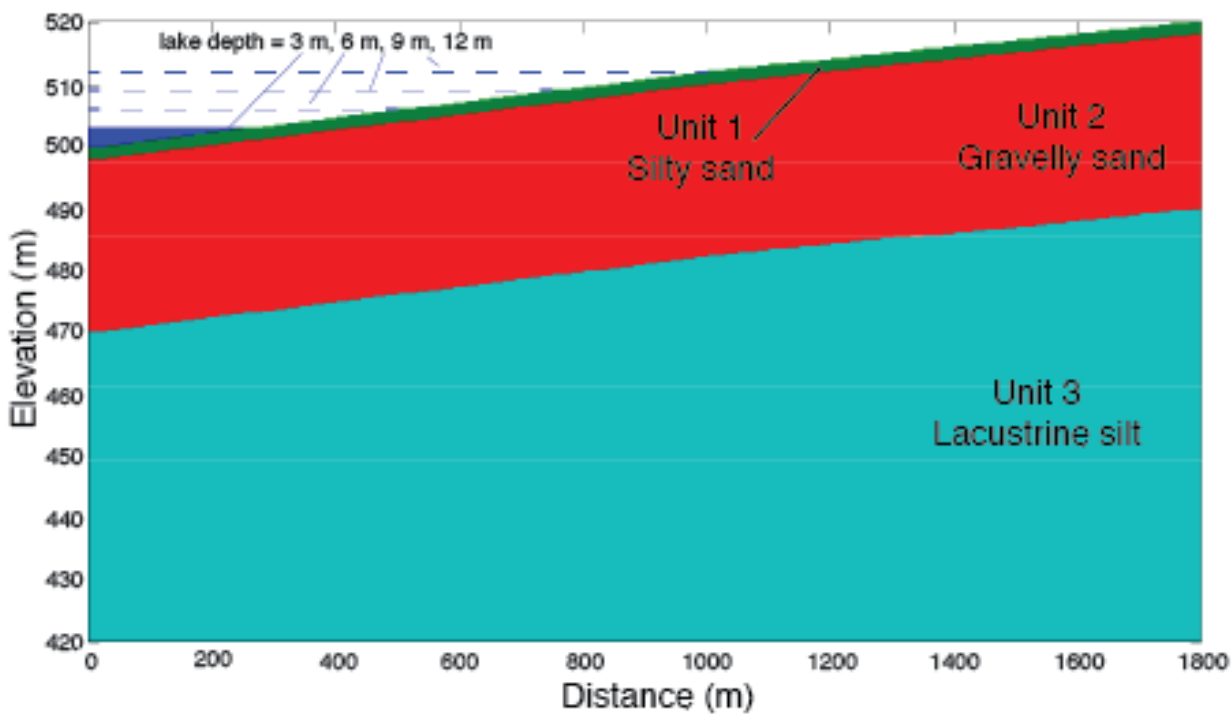

Figure 5.5.1 Axis-symmetric model geometry indicating different lithologic units and simulated lake depths/extents.

Geologic unit properties	
Lithology:	
Unit 1	Sediment (silty sand)
Unit 2	Sediment (gravelly sand)
Unit 3	Lacustrine silt
Unit depth range [m]	0-2, 2-30, 30-250
Porosity [-]	0.25, 0.25, 0.20
Geophysical parameters	
Archie cementation exponent (m) [-]	1.5
Archie saturation exponent (n) [-]	1.5
Water salinity (C) [ppm]	250 (S_i = 0)
Na^+ ionic mobility (β) [m^2/Vs]	5.8 x 10^{-8} (25°C)
Cl^- ionic mobility (β) [m^2/Vs]	7.9 x 10^{-8} (25°C)
Na^+ surface ionic mobility (β_s) [m^2/Vs]	0.51 x 10^{-8} (25°C)
Grain mass density (ρ_g) [kg/m^3]	2650
Cation exchange capacity (χ) [C/kg]	200, 10, 500

Table 5.5.1 Description of geologic units and physical properties used in numerical simulations. Entries separated by commas represent parameters with different values for each of the lithologic units.

Synthetic airborne electromagnetic (AEM) data were simulated for each snapshot of predicted bulk resistivity values using nominal system parameters based on the Fugro RESOLVE frequency-domain AEM system that was used in the Yukon Flats survey (Minsley et al., 2012). Data are simulated at the nominal survey elevation of 30 m above ground surface using the one-dimensional modeling equations described in Minsley (2011). A 200-m vertical profile of resistivity as a function of depth was extracted at each survey location and was used to simulate forward geophysical responses. Forward simulations were repeated for each of the 50 simulation times between 0 and 1,000 years output from SUTRA, resulting in 9,050 data locations per modeling scenario.

Synthetic ground-based electromagnetic data were simulated using nominal system parameters based on the GEM-2 instrument (Huang and Won, 2003). A system elevation of 1 m above ground was assumed, which is typical for this hand-carried instrument.

To address the inherent uncertainty associated with geophysical inversion, a Bayesian Markov chain Monte Carlo (McMC) algorithm developed for frequency-domain EM data (Minsley, 2011) was utilized to explore the ability of simulated AEM data to recover the true distribution of subsurface resistivity values throughout the 1,000-year lake talik simulations. At every data location along the survey profile, an ensemble of 100,000 resistivity models was sampled according to the Metropolis-Hastings algorithm (Hastings, 1970; Metropolis et al., 1953). According to Bayes' theorem, each model was assigned a posterior probability that was a measure of (1) its prior probability which, in this case, was used to penalize models with unrealistically large contrasts in resistivity over thin layers; and (2) its data likelihood, which was a measure of how well the predicted data for a given resistivity model match the observed data within data errors. Numerous measures and statistics were generated from the ensemble of plausible resistivity models, such as: the single most-probable model, the probability distribution of resistivity values at any depth, the probability distribution of where layer interfaces occur as a function of depth, and the probability distribution of the number of layers (model complexity) needed to fit the measured data. Finally, probability distributions of resistivity were combined with assumptions about the distribution of resistivity values for any lithology and/or ice content in order to make a probabilistic assessment of lithology or ice content.

5.5.2 Results and Discussion

For each of the 1,000-year lake talik evolution simulations, the static variables summarized in Table 5.5.1 were combined with the spatially and temporally variable state variables T and Si output by SUTRA to predict the distribution of bulk resistivity at each time step. An example of SUTRA output variables for the 6 m-deep gaining lake scenario at 240 years (the approximate sub-lake talik breakthrough time for that scenario) is shown in Figure 5.5.2.1 A-B, and the predicted resistivity for this simulation step is shown in Figure 5.5.2.1 C. The influence of different lithologic units is clearly manifested in the predicted resistivity values, whereas lithology is not overly evident in the SUTRA state variables. For a single unit, there is a clear difference in resistivity for frozen versus unfrozen conditions. Across different units, there is a contrast in resistivity when both units are frozen or unfrozen. Resistivity can therefore be a valuable indicator of both geologic and ice content variability. However, there is also ambiguity in resistivity values as both unfrozen Unit 2 and frozen Unit 3 appear to have intermediate resistivity values of approximately 100-300 ohm-m (Figure 5.5.2.1 C) and cannot be characterized by their resistivity values alone. This ambiguity in resistivity can only be overcome by additional information such as borehole data or prior knowledge of geologic structure.

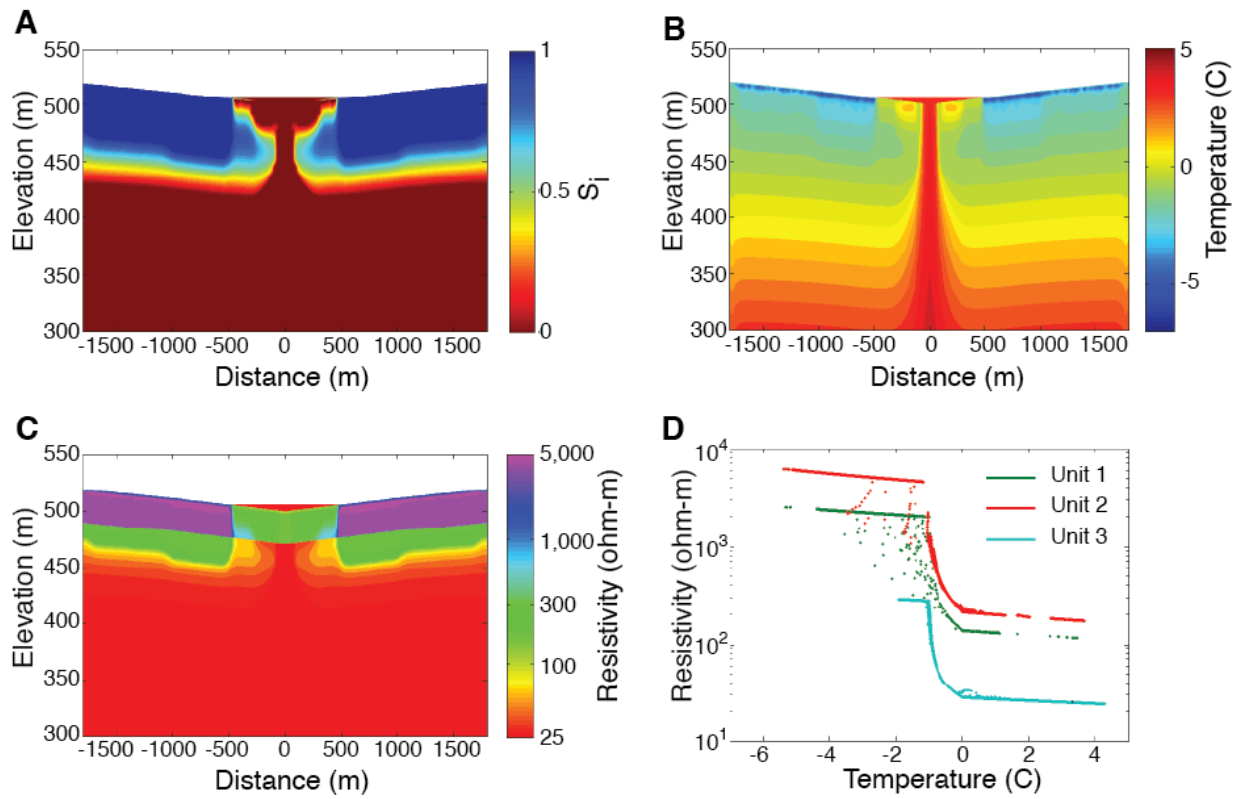

Figure 5.5.2.1 SUTRA model outputs and geophysical transformations from the 6-m gaining lake simulation at 240 years. Ice saturation (A) and temperature (B) are converted to predictions of bulk resistivity (C). Variability in resistivity as a function of temperature is indicated in (D) for lithologic units 1-3.

Lithology and ice saturation are the primary factors that control simulated resistivity values, though ice saturation is a function of temperature. The empirical relation between temperature and bulk resistivity is shown in Figure 5.5.2.1 D by cross-plotting values from Figure 5.5.2.1 B-C. Within each lithology, resistivity is relatively constant above zero degrees, with a rapid increase in resistivity for temperatures below zero degrees. This result is very similar to the temperature-resistivity relationships illustrated by Hoekstra et al. (1975; Fig. 1), lending confidence to the physical property definitions used in this study. Above zero degrees, the slight decrease in resistivity is due to the temperature-dependence of fluid resistivity. The rapid increase in resistivity below zero degrees is primarily caused by reductions in effective porosity due to increasing ice saturation, though changes in surface conductivity and salinity at increasing ice saturation are also contributing factors. Below -1 °C, the change in resistivity values as a function of temperature rapidly decreases. This is an artifact caused by the imposed temperature-ice saturation relationship defined in SUTRA that, for these examples, enforces 99% ice saturation at -1 °C. It is more likely that ice saturation continues to increase asymptotically over a larger range of temperatures below zero degrees, with corresponding increases in electrical resistivity. However, because AEM methods are limited in their ability to discern differences

among very high resistivity values, this artifact does not significantly impact the results presented here.

Geophysical data (not shown) were simulated for each of the electrical resistivity models. The simulated data were then used to recover estimates of the original resistivity values. For example, resistivity parameter estimation results for the 6-m deep hydrostatic lake scenario are shown in Figure 5.5.2.2. At each location along the profile, the average resistivity model as function of depth was calculated from the McMC ensemble of 100,000 plausible models. The overall pattern of different lithologic units and frozen/unfrozen regions was accurately depicted with two exceptions: (1) the specific distribution of partial ice saturation beneath the lake before thaw has equilibrated; and (2) the shallow sand layer (Unit 1) that is generally too thin to be resolved using AEM data. A point-by-point comparison of true versus predicted resistivity values for the hydrostatic 6 m-deep lake scenario at the simulation time 1,000 years is shown in Figure 5.5.2.3. The cross-plot of true versus estimated resistivity values generally fall along the 1:1 line, providing a more quantitative indication of the ability to estimate the subsurface resistivity structure. Estimates of the true resistivity values for each lithology and freeze/thaw state (Figure 5.5.2.3 B) tend to be indistinct; appearing as a vertical range of possible values in Figure 5.5.2.3 A due to the inherent resolution limitations of inverse methods and parameter tradeoffs (Day-Lewis, et al., 2005; Oldenborger and Routh, 2009). Although the greatest point density for both frozen and unfrozen silts (Unit 3) falls along the 1:1 line, resistivity values for these components of the model are also often overestimated; this is likely due to uncertainties in the location of the interface between the silt and gravel units. This is in contrast with the systematic underestimation of frozen gravel resistivity values due to the inability to discriminate very high resistivity values using EM methods (Ward and Hohmann, 1988). Frozen sands (true log resistivity ~2.8 in Figure 5.5.2.3 B) are also systematically overestimated in Figure 5.5.2.3 A; in this case, due to the inability to resolve this relatively thin resistive layer.

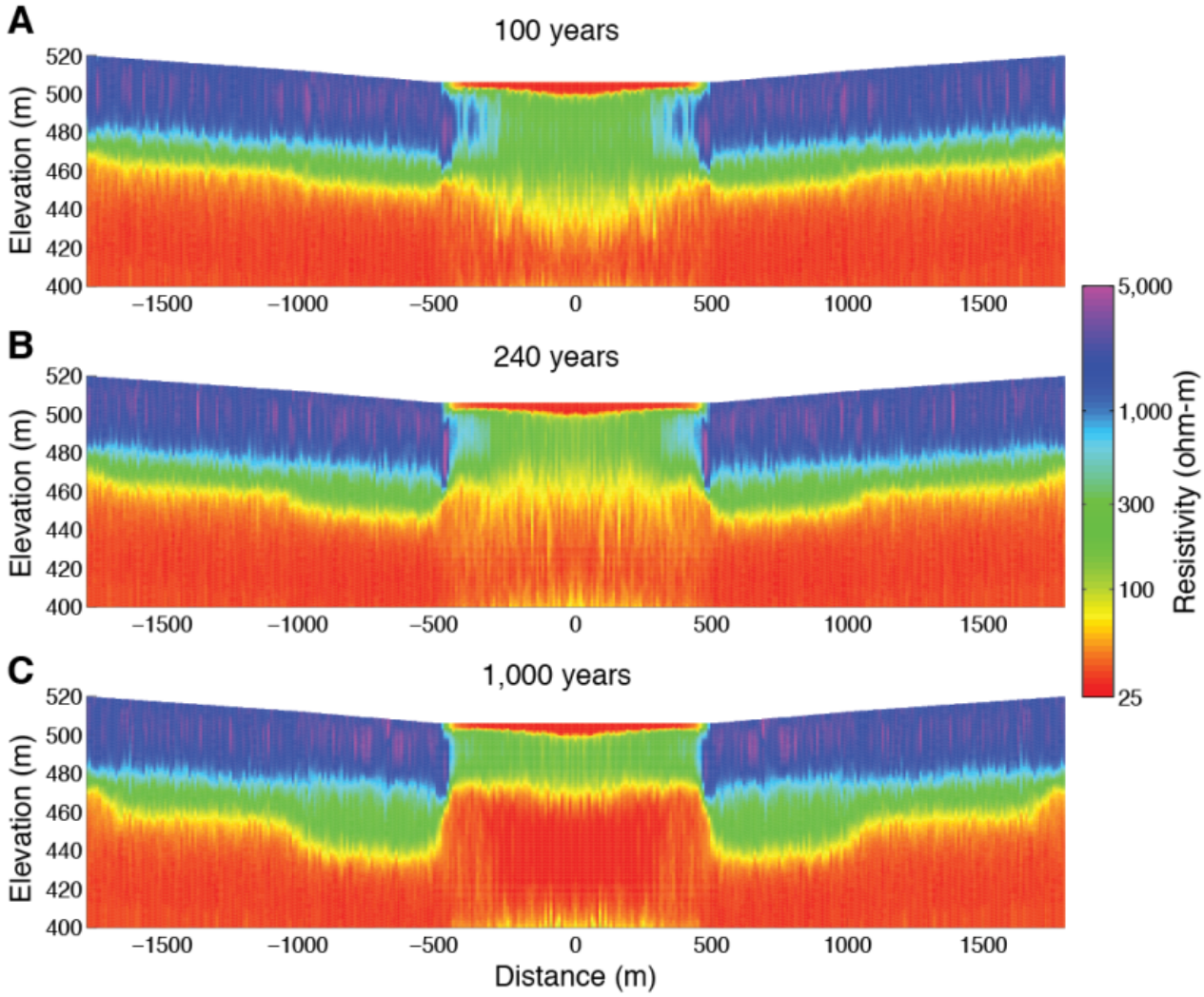

Figure 5.5.2.2 Mean resistivity model extracted from McMC ensembles. **Results are shown for the 6-m-deep hydrostatic lake scenario outputs at (A) 100 years, (B) 240 years, and (C) 1,000 years.**

While useful, single 'best' estimates of resistivity values at any location (Figure 5.5.2.3) are not fully representative of the information contained in the AEM data and associated model uncertainty. From the McMC analysis of 100,000 models at each data location, estimates of the posterior probability density function (pdf) of resistivity were generated for each point in the model. Probability distributions were extracted from a depth of 15 m, within the gravel layer (Unit 2), at one location where unfrozen conditions exist (r = 0 m), and a second location outside the lake extent (r = 750 m) where the ground remains frozen (Figure 5.5.2.4 A). Results from a depth of 50 m, within the silt layer (Unit 3), are shown in Figure 5.5.2.4 B. With the exception of the frozen gravels, whose resistivity tends to be underestimated, the peak of each pdf is a good estimate of the true resistivity value at that location.

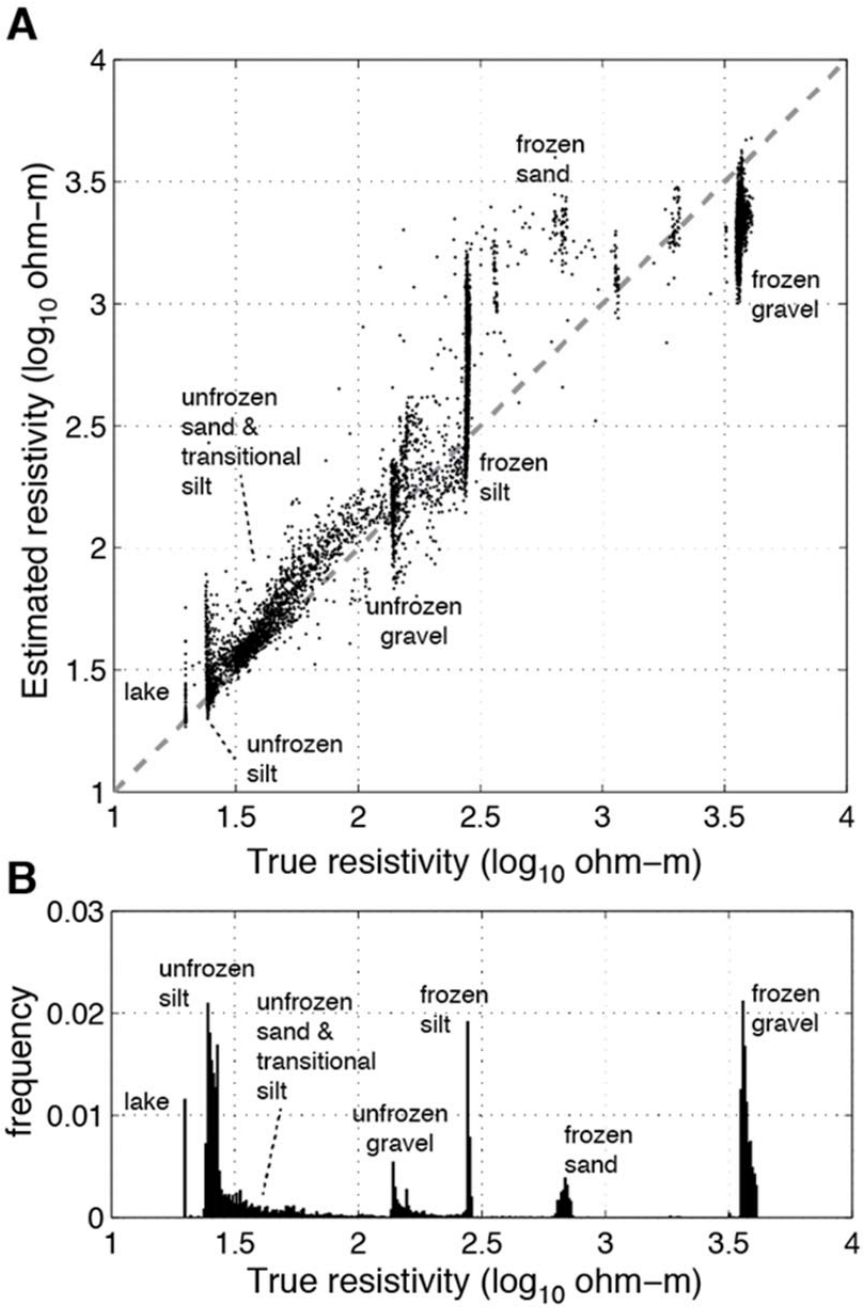

Figure 5.5.2.3 Performance of geophysical parameter estimation in recovering true parameter values. True versus McMC-estimated resistivity values for the hydrostatic 6-m-deep lake scenario at simulation time 1,000 years (A), compared with the frequency distribution of true resistivity values (B). Estimated resistivity values generally fall along the dashed 1:1 line in (A), with exceptions being under-prediction of the resistive frozen gravels, over-prediction of the thin surficial frozen sand, and some over-prediction of the frozen silt where it is in contact with frozen gravel.

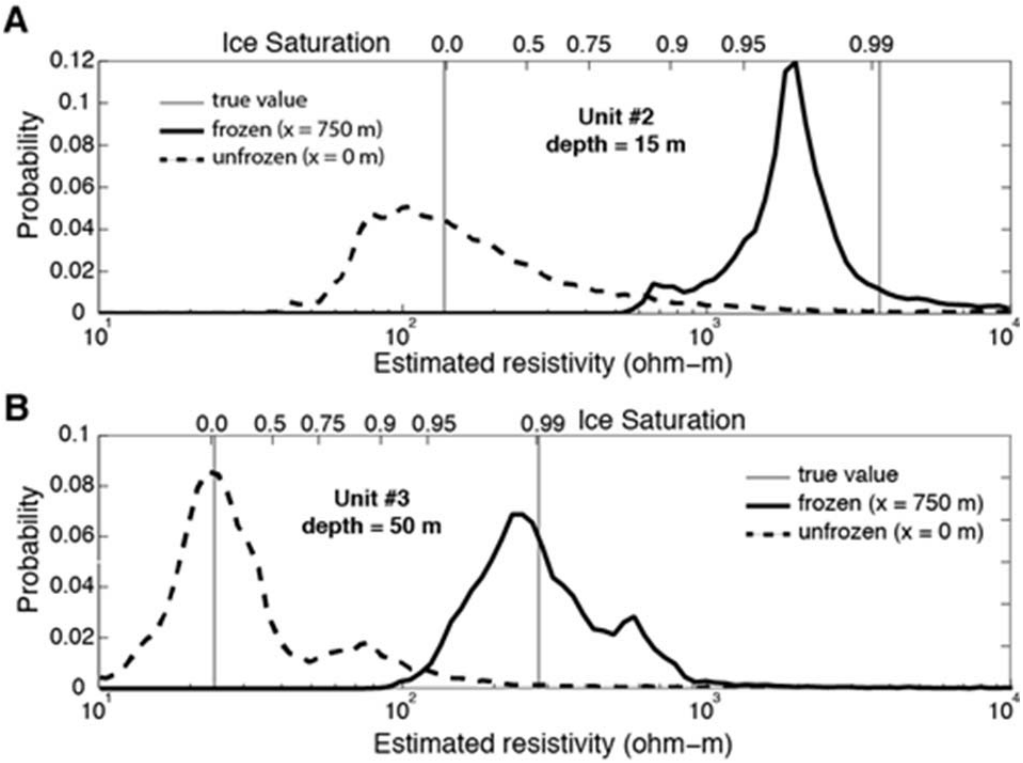

Figure 5.5.2.4 McMC-estimated resistivity posterior distributions within frozen and unfrozen unit #2 gravels (A) and frozen and unfrozen unit #3 silts (B) for the hydrostatic 6-m-deep lake scenario at 1,000 years. Unfrozen resistivity distributions are extracted beneath the center of the lake (r = 0) at depths of 15 m and 50 m for the gravels and silts, respectively. Frozen distributions are extracted at the same depths, but at r = 750 m. The upper x-axes labels indicate approximate ice saturation based on the lithology-dependent ice saturation versus resistivity curves.

Further illustration of the spatial and temporal changes in resistivity pdfs are shown in Figure 5.5.2.5. The resistivity pdf is displayed as a function of distance from the lake center at the same depths (15 m and 50 m) shown in Figure 5.5.2.5, corresponding to gravel (Figure 5.5.2.5 A,C, and E) and silt (Figure 5.5.2.5 B, D, and F) locations. High probabilities, i.e. the peaks in Figure 5.5.2.4, correspond to dark-shaded areas in Figure 5.5.2.5. Images are shown for three different time steps in the SUTRA simulation for the hydrostatic 6 m-deep lake scenario: 100 years (Figure 5.5.2.5 A-B), 240 years (Figure 5.5.2.5 C-D), and 1,000 years (Figure 5.5.2.5 E-F).

Approximate ice-saturation values, translated from the ice versus resistivity relationships for each lithology, are displayed on the right axis of each panel in Figure 5.5.2.5, and true resistivity values are plotted as a dashed line. Observations from Figure 5.5.2.5 include:

(1) Outside the lake boundary, pdfs are significantly more sharply peaked (darker shading) for the gravel unit than the silt unit, suggesting better resolution of shallower resistivity values within the gravel layer. It should be noted however, that this improved resolution does not imply

improved model accuracy; in fact, the highest probability region slightly underestimates the true resistivity value. (2) Probability distributions for the silt layer track the true values, but with greater uncertainty. (3) Inside the lake boundary, gravel resistivity values are not as well resolved compared with locations outside the lake boundary due to the loss of signal associated with the relatively conductive lake water. (4) Increasing trends in resistivity/ice saturation towards the outer extents of the lake are captured in the pdfs, but are subtle. (5) Within the silt layer at early times before the talik is fully through-going (Figure 5.5.2.5 B, D), the AEM data are insensitive to which layer is present, hence the bi-modal resistivity distribution with peaks associated with characteristic silt and gravel values. This ambiguity disappears at later times when the low-resistivity unfrozen silt layer extends to the base of the unfrozen gravels, which is a more resolvable target (Figure 5.5.2.5 F).

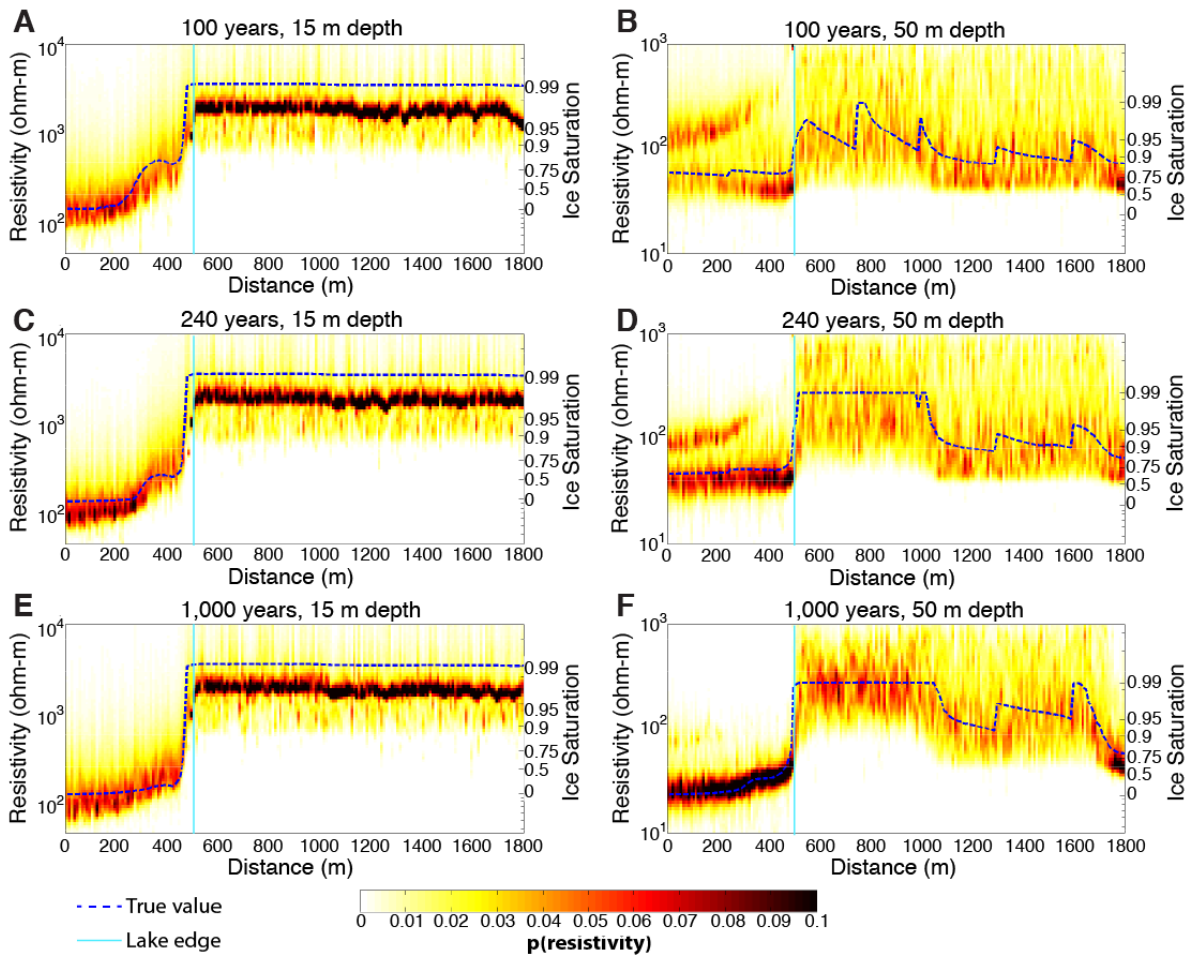

Figure 5.5.2.5 Resistivity probability distributions for the hydrostatic 6-m-deep lake scenario at simulation times 100 years (A-B), 240 years (C-D), and 1,000 years (E-F). Shading in each image represents the probability distribution at depths of 15 m (A, C, E) and 50 m (B, D, F) from the lake center (r = 0 m) to the edge of the model (r = 1800 m). Dashed lines indicate the true resistivity values.

The final component of this analysis focused on the upper sand layer (Unit 1), which is generally too thin (2 m) and resistive (> 600 ohm-m) to be resolved using AEM data; though may be imaged using other ground-based electrical or electromagnetic geophysical methods. Seasonal thaw and surface runoff causes locally reduced resistivity values in the upper 1 m, which is still too shallow to resolve adequately using AEM data. In practice, shallow thaw and sporadic permafrost trends are observed to greater depths in many locations, including inactive or abandoned channels. To simulate these types of features, the shallow resistivity structure of the 6 m-deep hydrostatic lake scenario at 1,000 years was manually modified to include three synthetic 'channels'. These channels are not intended to represent realistic pathways relative to the lake and the hydrologic simulations; they are solely for the purpose of illustrating the ability to resolve shallow resistivity features.

Figure 5.5.2.6 shows the three channels in a zoomed-in view of the uppermost portion of the model outside the lake extent. Each channel is 100 m wide, but with different depths: 1 m (half the Unit 1 thickness), 2 m (full Unit 1 thickness) and 3 m (extending into the top of Unit 2). Analysis of AEM data simulated for this model, presented as the McMC average model, are shown in Figure 5.5.2.6 B. All three channels are clearly identified, but their thicknesses and resistivity values are overestimated and cannot be distinguished from one another. To explore the possibility of better resolving these shallow features, synthetic EM data were simulated using the characteristics of a ground-based multi-frequency EM tool (the GEM-2 instrument) that can be hand carried or towed behind a vehicle, and was commonly used the shallow investigations of the larger project. The McMC average model result for the simulated shallow EM data is shown in Figure 5.5.2.6 C. Channel thicknesses and resistivity values are better resolved compared with the AEM result, though the 1 m-deep channel near r = 800 m appears both too thick and too resistive. In addition, the shallow EM data show some sensitivity to the interface at 2-m depth between frozen silty sands and frozen gravels, though the depth of this interface is over-estimated due to the limited sensitivity to these very resistive features.

In the specific examples of lake talik evolution presented here, which were modeled after the physical setting of the Yukon Flats, Alaska, AEM data were shown to be generally capable of resolving large-scale permafrost and geological features, as well as thermally and hydrologically induced changes in permafrost over time. The Bayesian McMC analysis provided useful details about model resolution and uncertainty that cannot be assessed using traditional inversion methods that produce a single 'best' model. A fortuitous aspect of the Yukon Flats model is the fact that the silt layer (Unit 3) is relatively conductive compared with the overlying gravels (Unit 2), making it a good target for electromagnetic methods. If the order of these layers were reversed, or if the base of permafrost were hosted in a relatively resistive lithology, AEM data would not likely resolve the overall structure with such good fidelity. In addition, knowledge of the stratigraphy helps to remove the ambiguity between unfrozen gravels and frozen silts, which have similar intermediate resistivity values. The methods developed here that use a physical

property model to link hydrologic and geophysical properties provide the necessary framework to test other more challenging hydrogeological scenarios.

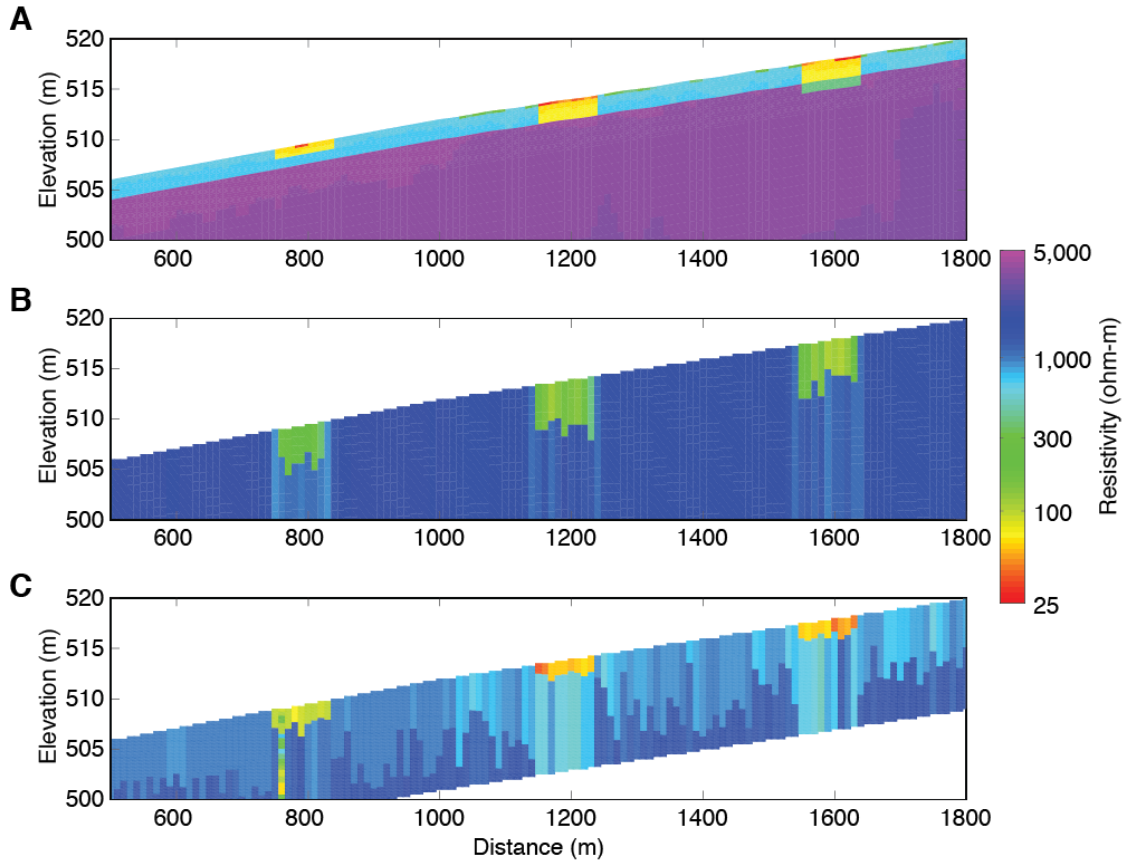

Figure 5.5.2.6 Comparison of airborne and ground-based measurements for recovering shallow thaw features. True shallow resistivity structure extracted from the hydrostatic 6-m-deep lake scenario at a simulation time of 1,000 years, shown outside of the lake extent (distance > 500 m) (A). Three shallow low-resistivity channels with thicknesses 1 m, 2 m, and 3 m were added to the resistivity model to provide added contrast. McMC-derived results using simulated AEM data (B) and ground-based EM data (C) illustrate the capability of these systems to image shallow features.

Analysis of AEM surveys provide a means for remotely detecting subsurface electrical resistivity associated with the co-evolution of permafrost and hydrologic systems over areas relevant to catchment-scale and larger processes. Coupled hydrogeophysical simulations using a physical property relationship that accounts for the effects of lithology, ice saturation, and temperature on electrical resistivity provide a systematic framework for exploring the geophysical response to various scenarios of permafrost evolution under different hydrological forcing. This modeling approach provides a means of robustly testing the interpretation of AEM data given the paucity of deep boreholes and other ground truth data that are needed to characterize subsurface permafrost. A robust uncertainty analysis of the geophysical simulations provides quantitative information about what types of features can be resolved using AEM data given the inherent

resolution limitations of geophysical measurements and ambiguities in the physical property relationships. In the scenarios considered here, we have shown that large-scale geologic and permafrost structure is accurately estimated. Sublacustrine thaw can also be identified, but the specific geometry of partial ice saturation beneath lakes can be poorly resolved by AEM data. Understanding the geophysical response to known simulations is helpful both for guiding the interpretation of existing AEM data, and also to plan future surveys and other ground-based data acquisition efforts.

5.6 Permafrost Response to Lake Recession

Research at Twelvemile Lake in the Yukon Flats of Alaska revealed previously unknown details about permafrost distribution and dynamics associated with lake recession in discontinuous permafrost. Airborne electromagnetic surveys suggest that unfrozen conditions exist below Twelvemile Lake (i.e., an open talik) and relatively thick (~90 m) permafrost exists outside the perimeter of the highstand of the lake in the mid-1980s. Therefore, as the lake receded, exposed open meadow was, at least initially, free of permafrost. Over the past two decades willow shrubs have grown in discrete clumps/bands throughout the previously open meadow area through the process of ecological succession. Ground-based electrical geophysical surveys conducted as part of this project in late summer 2011 and 2012 along a transect of mixed open-meadow and willow shrub showed shallow zones with permafrost located proximal to maturing shrubs, while more open areas did not show evidence of frozen ground. Manual frost and temperature probing confirmed these results. A modeling approach was applied to provide mechanistic understanding into the observations of permafrost aggradation in Twelvemile Lake receding margin.

5.6.1 Materials and Methods

A suite of 100-year vertical one-dimensional (1-D) computer simulations was used to represent various ecosystem effects (reduced recharge and summer cooling from shading) and climate change using the modified SUTRA code to simulate freeze-thaw. Unsaturated zone dynamics had not been considered in previous numerical modeling of permafrost aggradation. The simulations were designed to (1) test the hypothesis that permafrost can form under current conditions in response to lake recession, (2) gain insight into factors controlling permafrost formation, and, (3) evaluate the longer-time response to climate warming. The open meadow with summer recharge (OM-R) scenario serves as a base case representing receded lake conditions prior to shrub succession. Prescribed model ground-surface temperature and recharge boundary conditions for OM-R reflect local observations and history (NRCS SNOw TELemetry Station #961). For comparison, we considered various combinations of shading at two levels (Sh1 and Sh2), summer recharge at the current level and zero level (R and 0R, respectively), and climate warming (CW), for a total of 7 models: OM-R, Sh1-R, Sh2-R, OM-0R, Sh1-0R, Sh2-0R, and Sh2-0R-CW. For the shading scenarios, moderate reductions of 1 °C (Sh1) and 2 °C (Sh2) in

peak summer shallow soil temperatures (defined at 0.06 m model depth) were based on observed willow shrub shading effects in a similar setting (Smith, 1975); these values approximate the average apparent cooling effect of 0.6 °C at 0.5 m depth under discrete willow clumps (n=5) compared to adjacent open meadow areas (n=5) measured at the field site in late summer 2013.

Summer recharge averages 0.1 m in the Twelvemile Lake area (SNOTEL #961), well below the maximum potential for willow evapotranspiration; therefore, effective zero-recharge (0R) is a plausible condition. The strongest ecosystem effect considered was a 2 °C reduction in maximum shallow soil temperatures and no summer recharge (Sh2-0R). The silt-loam soils at Twelvemile Lake were simulated using the recently measured unsaturated soil-water freezing and soil-water retention characteristics of similar materials (Watanabe et al., 2011; Kurylyk and Watanabe, 2013).

The domain spanned an elevation of +1 m to a depth of 20 m, with the datum being the ground surface. The upper 1 m represented a thermal boundary layer with a sinusoidal annual thermal input. The upper model domain spanned 0-5 m in depth and consisted of 0.01-m vertical elements. The water table at -3.0 m was represented as a zero-pressure boundary, simulating the control of a constant lake level on water table, based on observations over the 2011-2012 field seasons. Therefore, the model domain from 0-3 m depth was variably saturated through time. The lower model domain, from 5-20 m depth, comprised a vertical column of elements 0.1-m thick to simulate the deeper saturated zone and the geothermal gradient from below the penetration depth of the annual temperature envelope.

The initial condition for each model was the result of an 80-yr equilibration run of the OM-R model using a sinusoidal annual thermal input with amplitude of 16 °C and a mean of 0.5 °C, similar to observed ground temperatures within the dried lake boundary near the study site. The phase of the annual temperature sinusoid was shifted forward in time by 3 months ($\pi/2$) to best coincide the onset of snowmelt with a few-day lag of boundary temperature rising above 0 °C in April. Once initial conditions were established, predictive models were run for 100-yr simulations, incorporating varied effects of willow shading by reducing annual temperature amplitude and mean by similar magnitudes; in this way the summer thermal maximum is reduced but the cold winter minimum is preserved. Note that potential winter insolation effects of trapped snow were not incorporated.

The climate warming scenario was created by applying a trend to the thermal boundary that resulted in a +2.55 °C change in mean temperature at 0.06 m depth after 100 yr; the 2.55 °C value was chosen by applying a conversion factor of 0.85 for “low shrub-scrub” land-cover (Jorgenson and Kreig, 1988) on soils to the moderate Scenarios Network for Alaska and Arctic Planning (SNAP) (Scenarios Network for Alaska and Arctic Planning, University of Alaska, 2013) predicted air warming over the simulated time period. Little regional trend in recharge is predicted by SNAP, so the recharge boundary was left unchanged. Once the +2.55 °C background temperature trend was established, the climate warming model scenario was re-run

with the added "strong willow effect" of 2 °C summer shading and no summer recharge (model Sh2-0R-CW).

A time varying recharge boundary was set at the ground surface to represent three distinct phases: (1) Winter, no recharge (ordinal days 0-100 and 275-365), (2) Spring snowmelt recharge (days 100-120), (3) Summer recharge (days 120-275). Meltwater temperature was 0.5 ◦C, and volume was determined from average Fort Yukon data (SNOTEL #961) as 0.47 m snow with 0.2 snow/water equivalent. The summer recharge phase delivers 0.1 m of precipitation; this recharge was assigned a value of 12 °C to represent observed area conditions, although models were found to be relatively insensitive to this assumed temperature. To simulate the effects of transpiration/interception by the willow shrub, summer recharge was set to 0 m (0R models), while the melt pulse was preserved as it was assumed the shrubs are not foliated and therefore not using soil water at that time.

Various unsaturated soil properties were investigated, and simulations were found to be strongly sensitive to both the freezing function and residual saturation at strong negative (drying) pressure. Therefore, great care was taken to match model parameters with the general soil type observed in the field. A single homogeneous soil was used for all models and based on a classification of "silt-loam" and observations from soil pits. The unsaturated soil-water freezing and soil-water retention characteristics for this soil type were based on a recent laboratory investigation (Watanabe et al., 2011), as was the silt-loam porosity of 0.46. The soil-water freeze function (relating temperature to ice content) was simulated with a 4-section piecewise-linear function with a minimum residual unfrozen water content of 16.6% (of total porosity) at -20 °C. The soil-water retention curve was simulated with a piecewise- linear function with residual saturation at 50,000 kPa of 8%. The soil had a base permeability of $1x10^{-12}$ m^2, with a frozen minimum permeability of $1x10^{-13}$ m^2. The relatively small reduction in permeability when frozen was based on observation of water flow through frozen silt-loam, compared to other frozen soils that do not permit flow when frozen (Watanabe et al., 2011, 2013); permeabilities less than approximately $1x10^{-13}$ m^2 essentially function as confining material within the model and could have induced surface ponding, a condition for which there was no field evidence.

5.6.2 Results and Discussion

Model scenarios presented and discussed in this section include:

(1) OM-R: Open meadow base case model with seasonal recharge as specified in section 5.6.1
(2) OM-0R: Open meadow model with no seasonal recharge
(3) Sh1-R: Moderate shading effect model with 1 °C summer cooling and seasonal recharge
(4) Sh1-0R: Moderate shading effect model with 1 °C summer cooling and no seasonal recharge
(5) Sh2-R: Strong shading effect model with 2 °C summer cooling and seasonal recharge

(6) Sh2-0R: Strong shading effect model with 2 °C summer cooling and no seasonal recharge
(7) Sh2-0R-CW: Strong shading effect model with 2 °C summer cooling, no seasonal recharge, and linear climate warming trend superimposed on seasonal temperature cycle

Results from the OM-R base model show seasonal frost and temperature propagation through time (Figure 5.6.2.1). Annual frost and temperature dynamics define envelopes that encompass the range of simulated conditions with depth along the profile; for OM-R, the maximum and mean shallow soil temperatures are 12.3 and 0.6 °C, respectively. Under the expected ambient conditions of the open meadow dried lakebed, appreciable permafrost does not form. Notably, annual downward propagation of ice from the previous winter through the soil peaks near the water table in early September, yet ice content drops to zero for the rest of the annual cycle (Figure 5.6.2.1 a). This strong phase shift has important implications for field interpretations of frozen ground. The presence of low ice-content deep frost late in the summer may indicate seasonally frozen ground rather than permafrost. The simulated low year-round ice saturation (3% of porosity) at the water table in OM-R (Figures 5.6.2.1a, 5.6.2.2a) agrees with site observations from a soil pit dug in open meadow, where stiff soil and temperatures close to 0 °C were detected in a discrete band just above the water table, which supports the OM-R model.

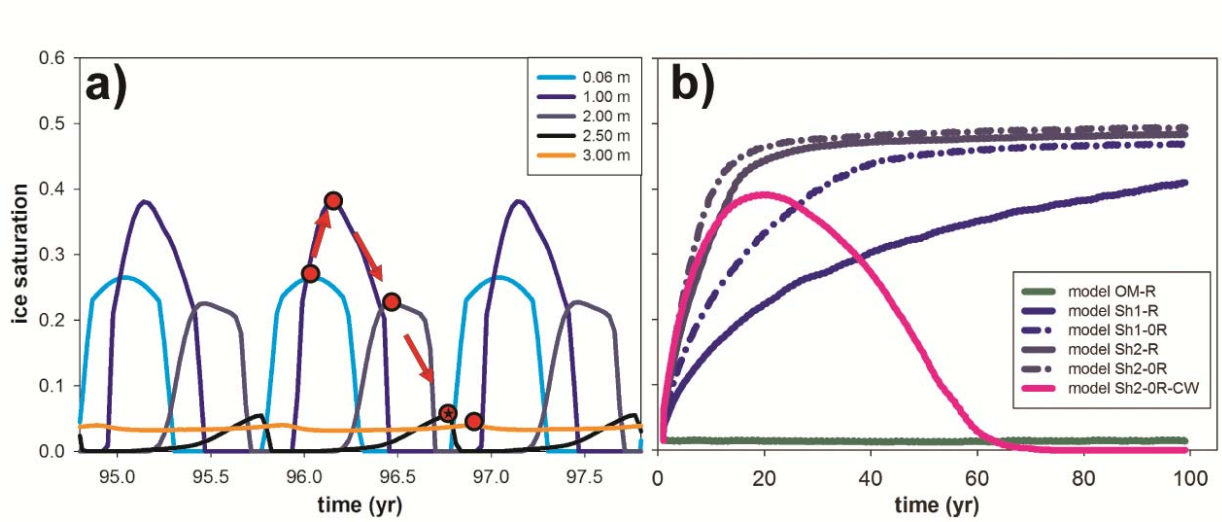

Figure 5.6.2.1 Three-year ice saturation time series for multiple depths in the open-meadow model showing that ice saturation peaks around 1-m depth, and propagates downward while shifting forward in phase with yearly peak ice content indicated by red dots; the starred dot corresponds to the time year of 2012 data collection (a). Smoothed (1 year average) time series of ice saturation at 2.5 m depth in all models, showing the accelerated frost formation caused by uptake of summer recharge and permafrost aggradation and subsequent degradation under climate change.

Simulation OM-0R indicates that willow shrub uptake of summer recharge does not result in appreciable permafrost aggradation within the Twelvemile Lake basin. When recharge is

removed from the baseline model, the original discrete band of ice-saturation at the water table interface is slightly enhanced to 7%; hence shrub-driven reduction in recharge cannot explain the thick, shallow sequence of frost observed in the field beneath shrub areas. Recharge reduction has a much stronger effect when combined with summer shading. Figure 5.6.2.1b shows how frost development at greater depth in the unsaturated zone, characterized by multiple model time-series at 2.5 m depth, is greatly accelerated in the Sh1 model when summer recharge is removed in Sh1-0R. There is muted enhancement of freezing in the stronger shading Sh2-0R model, compared to Sh2-R, indicating the importance of unsaturated zone heat advection to permafrost aggradation peaks under moderate shading conditions. Thus, the uptake of summer recharge and subsequent reduction of infiltration alone does not result in strong permafrost aggradation, but when combined with summer shading, recharge reduction does result in appreciable enhancement of freezing, particularly in the Sh1-0R model.

Thick sequences of new shallow permafrost accumulate in models Sh1-0R (5.7 m thick) and Sh2-0R (7.7 m thick), which have both shading and reduced recharge, as shown in Figure 5.6.2.2 b,c, respectively. Dynamic steady- state permafrost is 0.2 m shallower in model Sh2-0R at 1.6 m (Figure 5.6.2.2c and 5.6.2.3a); this depth is within 0.16 m of that observed near willow shrub in the field. Much of the frost accumulation takes place in the unsaturated zone in the first 25 yr, particularly with increased shading (Sh2-0R). As the unsaturated zone permafrost quasi-equilibrates, substantial freezing of the saturated zone occurs over the remainder of the simulations. The Sh1-0R and Sh2-0R models are most dissimilar in quasi-equilibration time and saturated zone freezing dynamics. Ice saturation in the shallow aquifer of both models exceeds 50% of the available porosity, thus restricting flow and the advection of heat. This result shows how critical yet subtle differences in shrub growth and subsequent shading may have pronounced impacts on shallow groundwater flow and the resultant lake water budget.

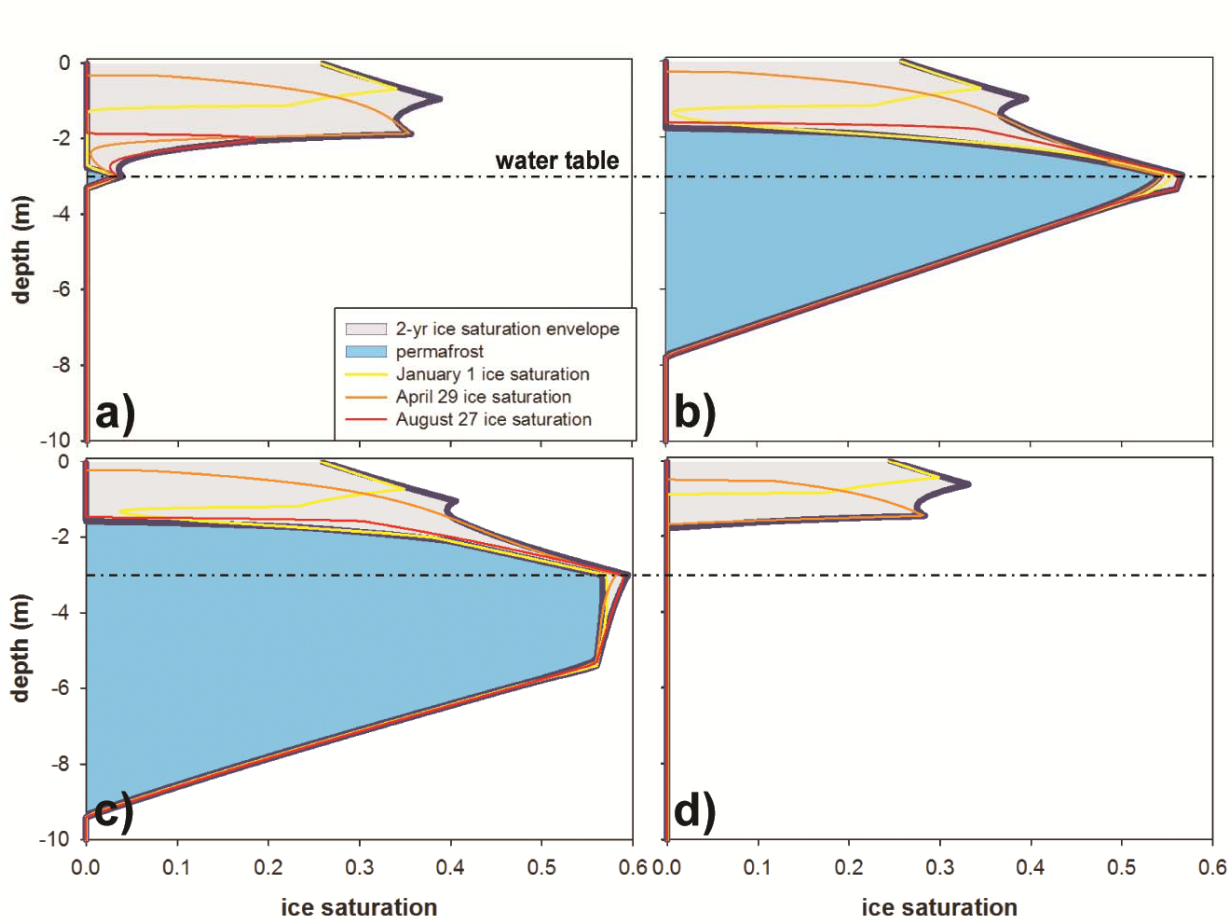

Figure 5.6.2.2 Ice saturation envelope encompassing annual frost variation (including 3 date-specific profiles) and aggraded permafrost ice saturation after 99 yr of simulation for models: open-meadow (OM-R) (a), moderate shrub effect (Sh1-0R) (b), strong shrub effect (Sh2-0R) (c), and strong shrub effect with climate change (Sh2-0R-CW) (d).

The SNAP-guided climate warming (CW) trend was imposed on the hydrologic scenario that yielded the thickest aggraded permafrost under current conditions (Sh2-0R). The Sh2-0R-CW simulation (Figure 5.6.2.3b) shows initial permafrost aggradation on the scale of several meters in thickness, similar to Sh2-0R, though after approximately 20 yr the simulations diverge and permafrost begins to degrade for Sh2-0R-CW. Ice saturation peaks at 45% with climate warming and 60% without warming. The maximum depth reached by permafrost subjected to climate warming is 6.1 m (9.3 m with no warming), and this maximum occurs at year 45, after which permafrost degrades. Under climate warming, frozen ground first thaws downwards in the unsaturated zone, vanishing by year 69 (Figure 5.6.2.1b). Along with permafrost degradation, the seasonally active freeze/thaw layer thins from a zone extending from land surface to below the water table to a zone only reaching 1.8 m depth by year 100 (Figure 5.6.2.2d). This thinning also is accompanied by a broadening in the annual temperature envelope to incorporate temperatures at depths that are warmer than observed in any other model); the envelope

converges on the geothermal gradient at several degrees above zero approximately 3 m below the water table. The effects of expected air temperature increases on near-surface soil temperatures may be countered, at least to some degree, by reductions in the thickness and duration of snowpack and particularly by the later timing of initial snow accumulation. The modeling approach presented here to represent climate change assumes such effects of potential changes in snowpack are negligible or at least overshadowed by the influence of warming air temperatures in the study region.

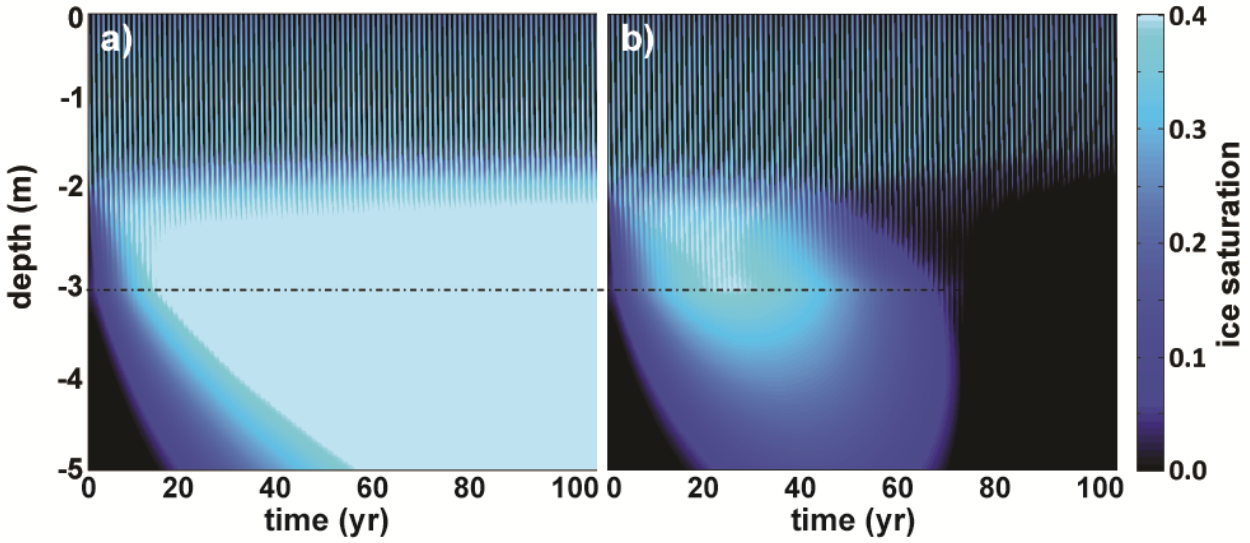

Figure 5.6.2.3 Strong shrub effect model ice saturation (Sh2-0R) (a), and shrub effect reduced by climate change model ice saturation (Sh2-0R-CW). Dashed line indicates static water table. Ice saturation is defined as fraction of pore space filled with frozen water.

Through numerical simulation, this study revealed a mechanism to explain observed permafrost aggradation under current conditions. Permafrost aggradation following lake recession and vegetation succession may be an important component in the cycle of lake or wetland contraction and expansion. Permafrost formation alters the surface-water/groundwater exchange capacity and near-surface fluxes of water and solutes. Permafrost aggradation may act to reverse the net negative water flux in a receding lake, thereby promoting the natural cycle of lake-level fluctuations observed in lake cores in the region. Should warming occur as predicted, however, simulation results point to termination of the lake-retreat/ecosystem mechanism as a driver of permafrost aggradation before the turn of the next century.

5.7 Regional Synthesis of Yukon Flats Lake Dynamics and Linkages to Permafrost Conditions

The multi-scale analyses of permafrost and hydrology interplay together with the multi-scale characterization of permafrost in the lake-rich landscape of the Yukon Flats provided a foundation for examining linkages between permafrost distribution and lake surface-area change in cold regions. Here, a large-scale examination of these linkages was made over a 5,150-km^2 area of Yukon Flats by evaluating the relationship between lake surface-area changes during 1979-2009, derived from Landsat satellite data and sublacustrine groundwater-flowpath connectivity inferred from the AEM survey of permafrost (Figure 5.7.0.1). Furthermore, insight gained from our modified SUTRA modeling analyses was used to elucidate empirical results generated by the data comparison analysis.

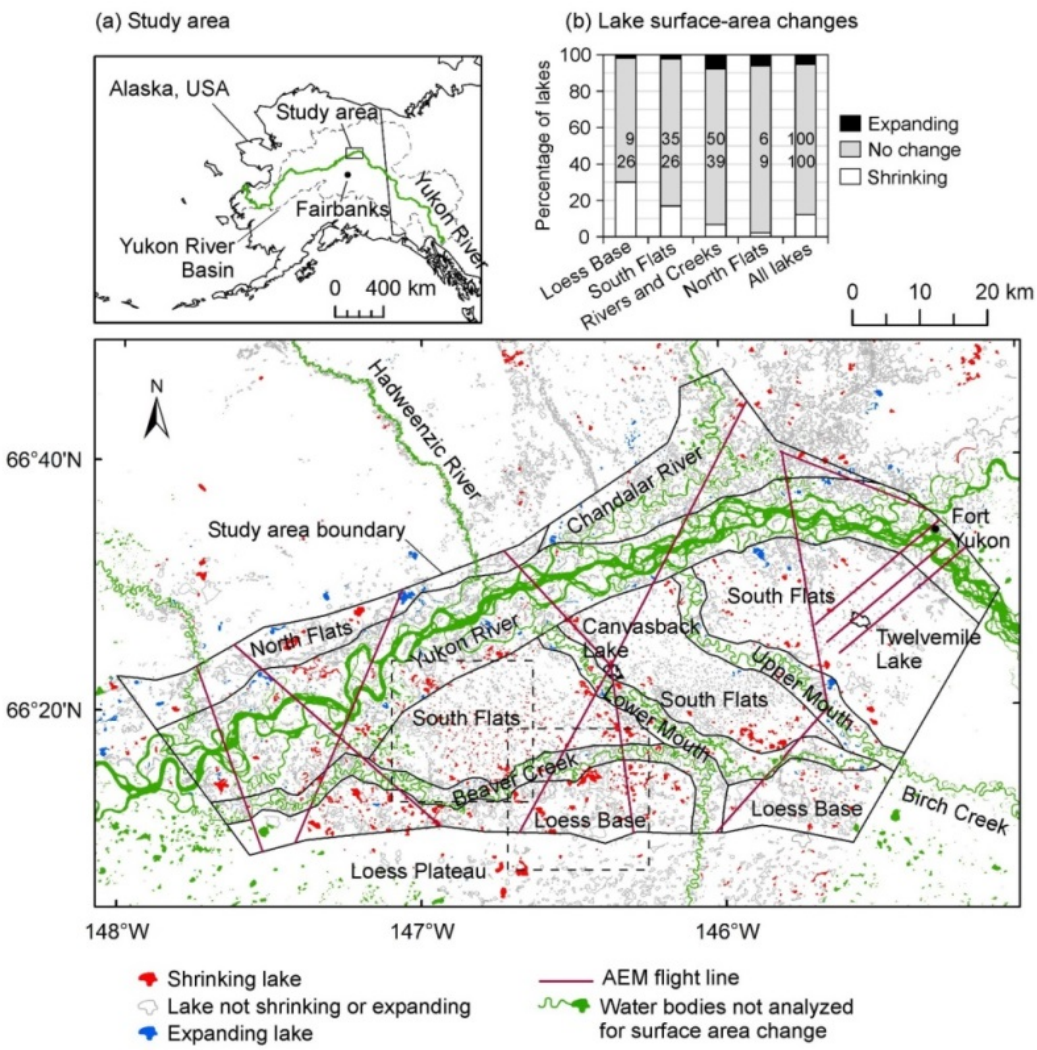

Figure 5.7.0.1 Location of study area (a, c), and lake surface-area change by physiographic unit (b). The upper and lower numbers in the bar charts of (b) are the percentages of total lakes (~8500) and total lake surface area (53.6 x 10^3 ha) in the study area.

5.7.1 Materials and Methods

Lake taliks (totaling 153) were characterized from electrical resistivity cross-sections along 392 flight-line km of the AEM survey (Figure 5.7.0.1). Interpretation of the resistivity cross-sections followed that of Minsley et al. (2012). The resistivity of geologic materials varies with both rock/soil type and thaw state (i.e., frozen versus unfrozen) (Hoekstra et al., 1975), potentially resulting in an overlap in resistivity between different materials having contrasting thaw states. To reduce this ambiguity, we incorporated knowledge about the known depositional history of the Yukon Flats (Clark et al., 2009; Williams, 1962) to develop a lithologic model and place constraints on the spatial distribution of different materials. The lithologic model consists of 2 layers: an upper layer of fluvial gravel (~15-50 m thick) and an underlying layer of lacustrine silt. The observed resistivity transition occurring at the interface between frozen gravel and frozen silt, and between frozen silt and unfrozen silt, in a deep borehole in Fort Yukon (Clark et al., 2009) (transitions illustrated along line L-L' of Figure 5.7.1.1a) were used to constrain our model relating thaw state to resistivity for each lithology (Figure 5.7.1.1, bottom). The interface between fluvial gravel and underlying lacustrine silt, given their depositional environment, is expected to be horizontal at the scale of individual lakes. Therefore, at a given depth, it is reasonable to assume that lateral resistivity transitions across lake basins are related to changes in thaw state, rather than material type. Shallow groundtruth data and a discussion about possible thaw state interpretation errors are provided as auxiliary material.

Sublacustrine silt is considered to be unfrozen if the vertical distance between the gravel-silt contact and interpreted bottom of permafrost, t_f, is less than a threshold value, set to 10 m to account for the uncertainty in interface positions (Figure 5.7.1.1). One of four possible combinations of thaw states for sublacustrine gravel and silt (Type A-D cases, Figure 5.7.1.1) are assigned to each lake. Type A cases are assumed to represent open taliks, and Type D cases are assumed to represent closed taliks with a phase boundary occurring near the gravel-silt contact. In Type B and C cases, the gravel is assumed to be completely or partially frozen.

Determination of shrinking, stable, and expanding lakes was based on the regression analysis by Rover et al. (2012) using Landsat satellite data (USGS, 2011). This analysis used decision tree classification models (average model accuracy 98.9%) to map lake surface areas, and linear regression to determine if lake surface areas have decreasing ("shrinking" lakes), no ("stable" lakes), or increasing ("expanding" lakes) trends at the 95% level of statistical significance (p-value < 0.05) for the period of 1979-2009. These surface area trends were calculated from available cloud free observations during May-September (17-20 observations per lake). Existence of a statistical association between lake surface-area trend and sublacustrine thaw state was determined using contingency tables with chi-square tests of independence (provided as auxiliary material). Lake surface-area trend was considered to be "significantly associated" with sublacustrine thaw state if the null hypothesis, postulating that area trend and thaw state are independent, was rejected at the 95% level of significance (p-value < 0.05).

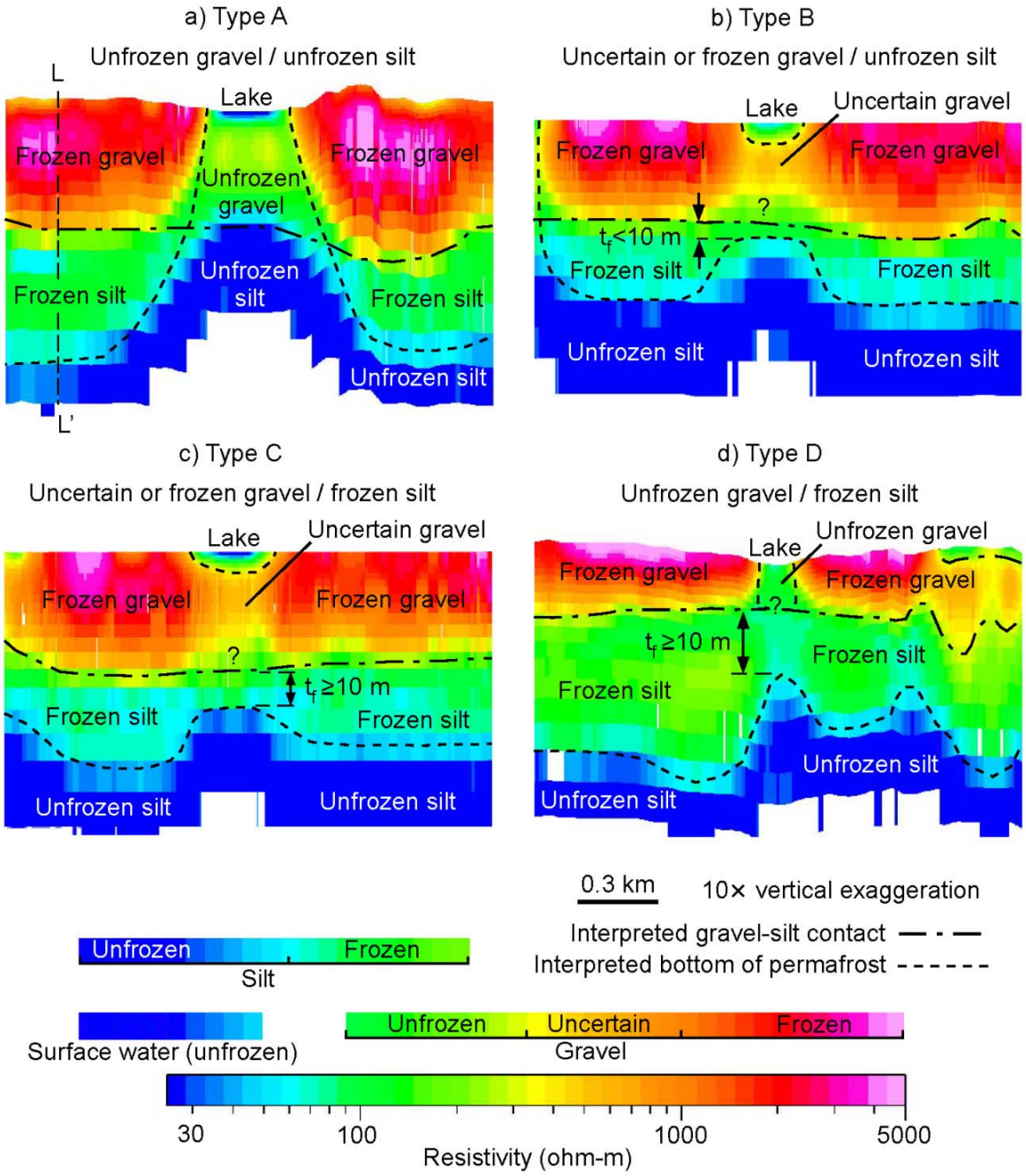

Figure 5.7.1.1 Examples of the four different gravel-silt thaw states (Types A-D) interpreted from electrical resistivity cross sections of the airborne electromagnetic survey. The vertical distance between the gravel-silt contact and the interpreted bottom of permafrost t_f, is used to determine whether silt if unfrozen (t_f < 10 m) or frozen (t_f ≥10 m).

5.7.2 Results and Discussion

The occurrence of open taliks (Type A) is not significantly associated with lake area trend (p-value = 0.37), as illustrated by the similar percentages of area trends for Type A cases and all lakes (Figure 5.7.2.1a). This suggests that the formation of open taliks is not a primary mechanism of the observed lake surface-area dynamics in the Yukon Flats. The lack of association between open taliks and lake area trends also reduces the likelihood that changes in regional groundwater flow, which influence lakewater / deep-groundwater exchange through sublacustrine open-taliks, account for the observed lake dynamics.

In contrast to open taliks, the occurrence of unfrozen sublacustrine gravel is significantly associated with lake area trend (p-value = 0.04). For example, lakes overlying unfrozen gravel are 2.5 times as likely to be shrinking as lakes not overlying unfrozen gravel (Figure 5.7.2.1b). Lakes overlying unfrozen gravel and frozen silt (Type D cases), most prevalent in the Loess Base (Figure 5.7.2.1c), are particularly susceptible to shrinkage (Figure 5.7.2.1a). These observations suggest that changes in lakewater / groundwater exchange as a potential driver of lake volume evolution result more likely from shallow (few tens of meters), rather than deeper (~50-100 m), thermal changes in permafrost. Shallow thermal changes influencing lakewater / groundwater exchange would likely need to occur in terrestrial areas of watersheds in order to provide lateral groundwater-flowpath connectivity to and from sublacustrine aquifers, possibly including deepening of the permafrost table and growth of supra- and/or intra-permafrost taliks. Such processes could allow substantial groundwater exchange between watersheds in the study area owing to the high hydraulic conductivity of unfrozen gravel. In addition, the occurrence of unfrozen gravel is more spatially variable across the landscape than deeper silt, as indicated by the greater standard deviation of unfrozen gravel than deeper unfrozen silt across physiographic units (19% in Figure 5.7.2.1d versus 13% in Figure 5.7.2.1e).

The occurrence of frozen sublacustrine silt is significantly associated with lakes that are expanding (p-value = 0.05). Lakes overlying frozen silt are 2.7 times as likely to be expanding as lakes overlying unfrozen silt (Figure 5.7.2.1f). Given the low hydraulic conductivity of frozen silt, upwelling of deep groundwater is not likely to be a significant source of recharge to many of these expanding lakes. Rather, enhanced water supply to these lakes may follow shallow flowpaths through unfrozen gravel, or overland flowpaths from adjacent water bodies. The presence of frozen silt below many of the expanding lakes may be an indication regarding their age and/or persistence of being filled with water - many of them may be too young to have formed open taliks, or may undergo cycles of filling and drainage thereby allowing their lake bottoms to freeze intermittently. The observed high occurrence of expanding lakes along rivers and creeks (Figure 5.7.0.1b), coupled with the possibility that many of these lakes are young, could be an indication of recent increases in regional groundwater discharge through taliks in low-lying river corridors (Walvoord et al., 2012).

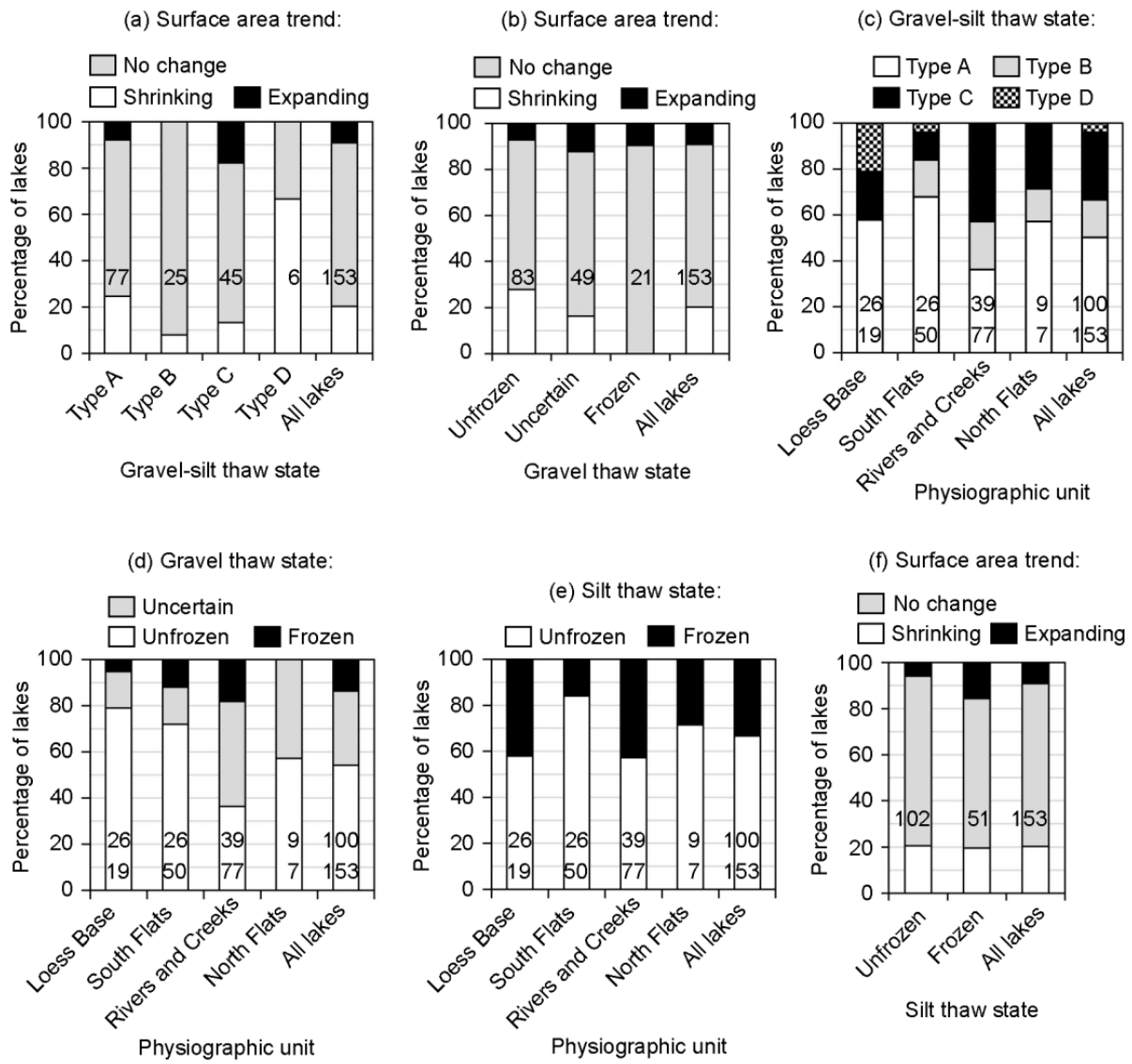

Figure 5.7.2.1 Relationships between lake surface-area trends and sublacustrine thaw states (a, b, and f) and sublacustrine thaw states and location (c-e). Thaw states in a and c are defined in Figure 5.7.1.1. Numbers in bars of a, b, and f are the number of lakes sampled by the AEM survey. In bars of the remaining panels, the upper and lower numbers are the percentages of total lake surface area from Rover et al. (2012) and the number of lakes samples by the AEM survey, respectively.

Results suggest that if increased groundwater exchange is driving the observed lake shrinkage and expansion, the process likely involves shallow thermal changes in permafrost (upper few tens of meters), such as deepening of the permafrost table and growth of supra- and intra-permafrost taliks. In the region studied, these key shallow aquifers exhibit the highest hydraulic

conductivity and greatest spatial variability in unfrozen state. The thermal and hydrological properties of these aquifers will be particularly sensitive to climate change owing to their close proximity to the atmosphere. These regional-scale results are consistent with previous studies indicating the substantial impact of shallow permafrost thaw on lakewater-groundwater exchange and hence lake water budgets. Reported thaw depths in these studies have been up to a few tens of meters, generally becoming shallower northward where permafrost becomes colder and more continuous. The integration of airborne geophysics in this study has allowed a deeper and larger-scale inspection of linkages between groundwater-flowpath connectivity and changes in lake water budgets than was available in previous ground-based studies alone.

6. Conclusions and Implications for Future Research/Implementation

The three main objectives of this multi-disciplinary study were successfully met. First, the USGS SUTRA code was modified to include new general capabilities required to simulate the hydrologic consequences of permafrost degradation and the resulting impact to military and federal infrastructure and operations. Second, geophysical investigations in an area of discontinuous permafrost of interior Alaska were performed to develop a multi-method approach for mapping ground ice to be used in any cold-region area and to provide baseline characterization of the study area. And lastly, a series of integrated numerical modeling and hydrologic analyses informed by results of the geophysical investigations elucidated the interaction between groundwater and permafrost at scales ranging from site to regional. Comparison between known cryohydrologic conditions predicted by hydrologic modeling and those inferred by geophysical forward modeling provided a means for supporting geophysical interpretations and identifying remaining measurement limitations. Collectively, the tools, methods, and insight developed here may be transferred to characterization and climate change assessments of a broad range of cold-region environments and applications. Demonstration of specific applications to the Yukon Flats study area is of particular relevance to DoD, since most of interior Alaska DoD infrastructure is located in similar low-lying regions.

6.1. Synthesis of Results and Research

Geophysical measurements consisting of electrical, seismic, radar and electromagnetic methods all have potential application for characterizing the distribution of permafrost and ground ice, with the efficacy and practicality of each depending on site conditions, the depth of the target interface (i.e., contact between frozen and unfrozen soil), and logistical issues associated with survey layout. The remoteness of some cold regions implies limited accessibility for carrying out standard hydrologic measurements. For example, much of the Yukon Flats Basin of Alaska is inaccessible by roads, and transport of equipment must occur via either river barge or airlift. In this area of Alaska, installations of typical hydrologic-studies boreholes that penetrate the thick permafrost layer are expensive and present technical challenges. Such difficulty in applying standard approaches provides strong motivation for using geophysical methods to characterize the subsurface in such regions, because such surveys can be accomplished at much lower cost. Airborne electromagnetic data are most useful for baseline characterization of subsurface properties and permafrost distribution over large areas. Repeat AEM surveys (e.g. once every 10 years) can be valuable for monitoring overall trends in permafrost distributions over large areas as they change resulting from varying climate and human impacts. Ground-based geophysical surveys provide high-resolution data sets that are highly amenable to detecting change via repeat measurement. Ground-based geophysical methods are thus useful for monitoring subtle localized changes in permafrost near specific targets of interest (such as roads, streams, lakes and buildings). Regular ground-based geophysical monitoring is valuable for informing engineering

interventions for problems caused by thawing ground ice in local target areas. Together, geophysical modeling, thermophysical hydrologic modeling, and field observations, as developed within this project, create a synergy that provides greater insight into permafrost-hydrology relations than any individual approach, and can be useful for future characterization of coupled permafrost and hydrologic processes.

Integrated hydrogeologic modeling and analysis to study permafrost/groundwater interaction has been demonstrated here in a series of studies. A groundwater flow modeling analysis of the Yukon Flats Basin elucidates the influence of permafrost on regional-scale flow magnitude and pattern. At this large scale, permafrost degradation enhances overall groundwater flow, and the component of water generated for streamflow derived from groundwater increases relative to runoff and shallow subsurface pathways. Presently, the Yukon Flats Basin is coarsely mapped as spanning the continuous-discontinuous permafrost transition that model analysis shows to be a critical hydrogeologic threshold; thus, the Yukon Flats Basin may be on the verge of major hydrologic change should the current permafrost distribution degrade. This possibility underscores the need for improved characterization of permafrost and other hydrogeologic information in the study area via geophysical techniques and ground-based observations. The regional groundwater flow model identifies the potential importance of lake taliks in enhancing groundwater circulation in the system.

Evolution of and flow through lake taliks has been explored in detail using SUTRA with new freeze/thaw capabilities that capture both rates of thaw and thaw patterns. Results confirm the importance of simulating advective heat transport in addition to conduction as an important component in accelerating thaw rates. The response of lake systems to lake area decline has been explored using both analytical and SUTRA simulation approaches. The shallow, continuous gravel layer in the Yukon Flats is particularly vulnerable to permafrost degradation, potentially resulting in large changes in watershed runoff, shallow groundwater flow, and hydrologic connectivity between lakes and stream networks. Modeling results, supported by the geophysical field investigations, indicate that permafrost aggradation in dried lake margins may offer some resilience to lake area decline, but favorable conditions for the reformation of permafrost may be countered by climate warming. Cross-scale investigations integrating characterization and dynamic cryo-hydrologic processes are needed to further constrain the fate of lake and wetland distribution in the Yukon Flats and other arctic/subarctic lowlands.

6.2 Implementation of Tools and Approaches Developed

6.2.1 SUTRA

The USGS SUTRA code, as a result of development and enhancement work done under this project, has new general capabilities that will allow scientists and practitioners worldwide to evaluate ground-ice and permafrost relations within hydrologic systems, and thereby to evaluate

impacts of climate changes on earth-surface environments. As with all USGS public hydrologic software, the new versions of the SUTRA code (both programs and executables) are made available online, free of charge, to everyone. In addition, the code documentations (i.e. user manuals) and simulation preprocessing software are made available on the same website for free download. Thus, all USGS-produced computer code and information, in the present case for SUTRA, is published online in open access format. The US public, government agencies, DoD interests, universities and private interests, as well as similar interests in other countries, regularly access the website for hydrologic information and downloading software.

As with previous new versions of the USGS-SUTRA code, the enhanced versions produced under this SERDP project will continue to be taught in USGS-led courses and workshops. Technology transfer is part and parcel of all new versions of SUTRA released by USGS. As part of this project, two workshops have already been taught that focus on the new freeze/thaw capabilities of SUTRA (at USGS in Lakewood CO and at McGill University, location of Professor J. McKenzie, one of the code developers and SERDP key performers, in Montreal, Canada). A number of presentations about the code and about results it has already given have been made during the duration of this SERDP project (domestic and foreign universities and institutes, and at USA national meetings such as AGU and GSA), and more are planned by all investigators. In 2015, Principle Investigator, C. Voss, is providing a lecture about cold-regions freeze/thaw hydrology with a focus on results of this project, particularly those obtained with the new SUTRA code, at universities and institutes throughout the USA and in some other countries. This is part of the Birdsall-Dreiss Lectureship, sponsored by the Geological Society of America (http://gsahydrogeology.org/BirdsallDreiss2015.htm) , for which Voss has been designated as the 2015 lecturer. Voss expects to present 30 to 50 lectures during 2015, a significant technology transfer effort for the hydrologic community that will make many professionals and students aware of progress made under the SERDP project.

Moreover, key factors in transitioning SUTRA to the user community have always been (1) USGS participation in and support of new projects initiated by users of SUTRA, and, (2) reliable user support based on personal contact via telephone and email of SUTRA users worldwide. In the case of SUTRA freeze/thaw capabilities, user support regarding code use and problems encountered is being provided by key performers Professor J. McKenzie (McGill University) and A. Provost and by PI C. Voss (USGS). For questions related to the simulation preprocessing and post-processing software, R. Winston (USGS) provides support. As part of code development, a beta version of SUTRA with freeze/thaw capabilities had been distributed to selected beta testers during the SERDP project period, and together with the SERDP-funded code developers at USGS, these beta testers have applied the code to study a wide variety of cold-regions settings. Results of these studies have already been published. Thus, transitioning the code to the community is a continuous process that occurred simultaneously with code development and enhancements. A small but significant user base has thus already been established for SUTRA

with freeze/thaw capabilities, with most users outside of USGS. This user base will continue to grow.

6.2.2 Geophysical Methods for Cold Regions

Our multi-scale geophysical approach is being transferred through published and planned peer-review publications, as well as direct training to cooperators in Alaska. In August 2014, project PI's delivered a 3-day training course at University of Alaska, Fairbanks, with participants from academia, federal and state agencies, and the private sector. Course materials will be made available online following USGS review and approval.

A geophysical software package for frequency-domain electromagnetic inversion (FEMIC) was developed and demonstrated under this project. The development of this software fills an important gap in geophysical analysis since commercially available software is not amenable to inversion of large, aerially distributed electromagnetic data, such as collected for this project. The FEMIC software is currently undergoing internal USGS testing prior to publication. The code and executable will be publically available, and will have a broad range of application including mapping of shallow permafrost via frequency domain electromagnetic surveys.

Understanding the hydrogeophysical responses to permafrost dynamics under different hydrologic and climatic conditions, and in different geological settings, is important for guiding the interpretation of existing geophysical datasets and also for planning future surveys. Geophysical models are inherently uncertain and ambiguous because of (1) the resolution limitations of any geophysical method and (2) the weak or non-unique relationship between hydrologic properties and geophysical properties. The general framework for coupling geophysical predictions to hydrologic simulations of permafrost evolution, including a novel physical property relationship that accounts for the electrical response to changes in lithology, temperature, and ice content, as well as a rigorous analysis of geophysical uncertainty, is readily transferrable to other cold-region studies of geophysical characterization. Although the focus here was on AEM data, other types of electrical or electromagnetic measurements could be readily simulated using the same resistivity model. For example, future efforts could focus on the simulation of other types of geophysical data (e.g. nuclear magnetic resonance or ground penetrating radar) using the same basic modeling approach.

6.2.3 Integrated Approach for Future Assessments

A comprehensive characterization of lateral and vertical distribution of permafrost may require complementary ground-based and aerial geophysics, developed as part of this project, depending on the scale of interest. Knowledge of permafrost distribution is a fundamental underpinning of effective management and possible mitigation of climate-change impacts of ground-ice changes on hydrology and land-surface environments. It is necessary to know where there is ground ice in order to predict the changes in hydrology and land surface environment that may occur should

the ground ice disappear or modify its spatial distribution. Aerial geophysics provides ground-ice distributions over distances of tens of kilometers, whereas ground-based geophysics provides more details of ground-ice distribution over distances of hundreds of meters. Linkage and correlation of geophysical characterizations with satellite remote sensing data may allow for generalization of shallow ground-ice distribution to regions not yet evaluated by geophysics, but such upscaling techniques require further development and additional ground truth information.

The new numerical simulation tool, SUTRA with groundwater freezing and thawing, allows scientific hypothesis testing to be carried out to define the most important factors that control subsurface hydrologic and thermal response to conditions on the ground surface in a particular setting. Ground surface conditions that can be considered include, insolation, vegetation and shading, vegetation loss or regrowth, air temperature, surface slope, surface hydrology (bare or surface water), organic vs mineral soil layers, fires, and human infrastructure (e.g. roads, drainage channels, structures). Elucidation of rates of change and key factors controlling the processes of concern in managing various settings in DoD lands, for example using SUTRA, must be accomplished before effective management strategies can be defined.

An example that combines the above approaches concerns the fate of a lowland lake in Alaska, studied as part of this project. A basic hydrologic question concerns the evolution of Twelvemile Lake's water level, which had been dropping steadily for 30 years. Disappearance of lakes is a widespread occurrence in interior Alaska. Airborne and ground-based geophysics allowed determination of the ground-ice and permafrost distribution, including newly developed permafrost, around the lake. Hydrologic evaluation of the lake's water budget, using basic quantitative analysis and using simulation with SUTRA, allowed identification of the candidate factors that can control lake water level. Further analysis, conducted after sudden flooding and refilling of the lake in 2013, found that the location of the permafrost table can be an important control on hydraulic connectivity between upstream lakes and Twelvemile Lake. Depending on the permafrost distribution, upstream lakes may be able to refill Twelvemile Lake during Yukon River flood events, and may subsequently control the amount of Twelvemile Lake water gain and loss on a yearly basis. This, in combination with the amount of snow that falls in the Twelvemile Lake watershed controls the rate of decrease in lake level in the years after a refilling event. Snowfall depends on climate and snow capture on the ground surface depends on the type of vegetation that exists in the watershed. Thus, this particular system is an example of how the functioning of a particular setting can be elucidated using the methods developed in this project. As an example of an intervention, consider the possibility that this watershed is a DoD concern in which it was desired that the lake level remain high, rather than drop during the years between flood events. Perhaps a re-vegetation program could be implemented after geophysical characterization that indicates the location of permafrost and after evaluation of potential intervention approaches using SUTRA simulation. The program might then consist of: (1) particular regional vegetation would be planted that captures snow, providing a greater source of spring meltwater to the lake, and, (2) the vegetation would shade the ground surface, keeping the

permafrost table shallow (this would quickly route meltwater to the lake, with less evapotranspiration losses that would occur should the permafrost table be deeper).

6.3 Ramifications for DoD Operations, Infrastructure, and Planning in Interior Alaska

The results and products derived from this study can help support decision making for DoD infrastructure and training activities in interior Alaska, particularly in areas most vulnerable to climate change and land use disturbance via permafrost degradation and resultant changes in hydrogeology. The U.S. Army is the largest DoD land user in Alaska and conducts all season training activities throughout its 1.5 million acre training areas in the Alaskan Interior (Figure 6.3.1). Most of the impact ranges used by the Air Force in Alaska are located on Army lands, and the Army and Air Force stage joint training exercises on Army lands. The main DoD sites are located between Fairbanks and Delta Junction and include Fort Wainwright and its associated training areas (Tanana Flats, Donnelly East and Donnelly West), Eielson Air Force Base, and Fort Greely.

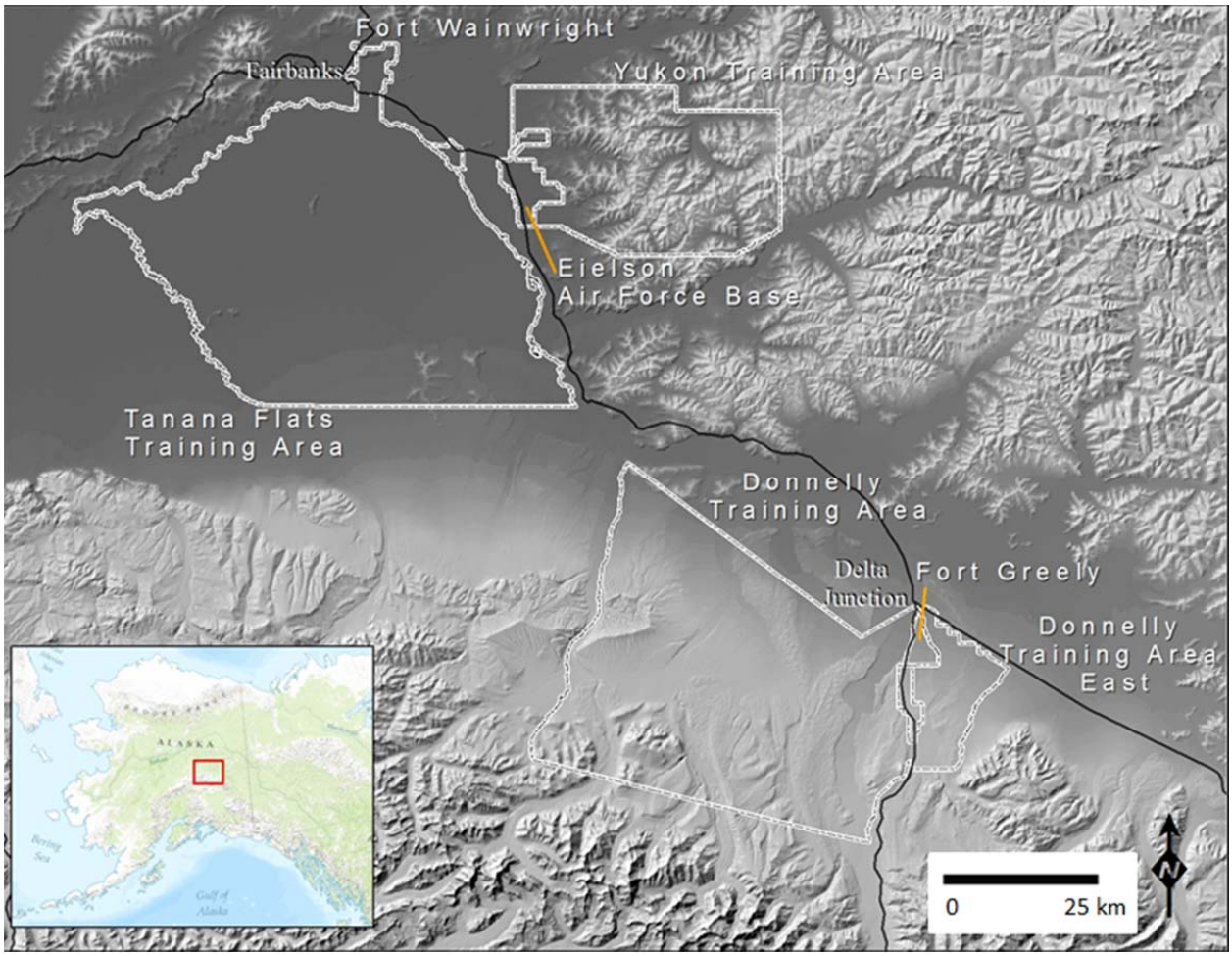

Figure 6.3.1 An elevation map of interior Alaska DoD training areas and cantonments.

The cantonments of Fort Wainwright and Eielson Air Force Base, the Tanana Flats Training Area, and most of Donnelly Training Area West and East are located on lowland landscapes underlain by discontinuous ice-rich permafrost. This complex mosaic of permafrost and permafrost-free land is predominantly low gradient (1-2 m km^{-1}) and even small changes in surface topography, vegetation, and the permafrost thermal regime can have dramatic effects on surface and shallow subsurface hydrology.

Quantitative predictive models are needed for understanding the processes occurring in the shallow subsurface in cold regions in response to infrastructure, for predicting possible future changes exacerbated by climate change, and for aiding decision making related to infrastructure. Approaches and tools developed in this study could be applied to help inform DoD decision making, particularly where numerical modeling combined with geophysical characterization could be used to evaluate the vulnerability (thaw settlement, ponding etc..) of areas to groundwater/permafrost interactions and project likely consequences. Such information is essential for accurately assessing the structural integrity of both built and proposed infrastructure. For example, the evolution of permafrost degradation affected by and affecting groundwater flow could be simulated to help guide the siting or design of roads, runways and airfields, buildings, bridges, and supportive engineering structures. Talik development and enhanced subsurface hydrologic connectivity in response to climate change and other disturbances including infrastructure development could greatly alter local hydrology, particularly near wetlands. A major challenge for road construction is in understanding how and where earthen berms will alter local and regional surface water hydrology in the low gradient terrain. Physics-based modeling, particularly using SUTRA and the enhancements made within this project, could help elucidate permafrost-controlled surface-water/groundwater interactions. The fen and bog features in lowland terrains are dynamic wetland landscapes that are also intimately related to the presence (or absence) of permafrost. They provide natural fire breaks and support numerous species of interest for natural resources planning. However, with the projected climate warming in the area (5ºC by 2100; Chapman and Walsh, 2007) many of these features could be altered.

The results from this effort and from the team representing SERDP Project RC-2110 (Addressing the impacts of Climate Change on US Army Alaska with Decision Support Tools Developed through Field Work and Modeling) could be combined to provide planning level information for DoD in interior Alaska. The measurements from fire disturbed landscapes and fens in the Tanana Flats lowlands could provide critical input to a suite of SUTRA models designed to examine current and projected hydrologic surface/subsurface connectivity and implications for surface water distribution in that region. For upland regions, like the Yukon Training Area and parts of Donnelly Training Areas East and West, SUTRA application to representative hillslopes could be used to identify the thermal and hydrologic response (and evaluate resilience) to forest fires and to provide critical information on current and projected summer season flows in watersheds in the area.

Information on the sizing of culverts and bridges and the siting of winter stream crossings could be gleaned from modeling efforts designed to address projected increased stream baseflow across discontinuous permafrost landscapes with continued climate warming. This is of particular interest for anadromous streams where a higher level of scrutiny and more robust engineering designs are required to ensure fish vitality and health. Many of the streams in Tanana Flats and Donnelly West have never been gaged and they have strong seasonal variations in flow. Some streams have glacial sources and others are predominantly spring fed. However, little is understood about the role of permafrost on stream flows in these systems. In locations where permafrost degradation contributed to enhanced groundwater flow and stream baseflow, the changes in the seasonal hydrograph and stream temperatures could be dramatic. Both factors strongly impact fish habitat.

The ground based geophysical methods used to map permafrost distribution, characterize annual ground freeze/thaw cycles, and monitor ground ice changes at our sites could be applied to a variety of settings to support the siting of buildings and could be combined with modeling efforts to help predict the likely response of permafrost to climate and anthropogenic disturbance. When coupled with airborne geophysical measurements the ground based measurement results could be more broadly applied to the remote locations in training ranges where no road access is currently available. There are instances where infrastructure in poorly characterized areas has been over-engineered, designed for thaw-unstable permafrost in an area where permafrost was thaw-stable. A carefully designed approach integrating geophysical and permafrost/hydrology techniques developed in our study could help minimize unnecessary costs and wisely allocate resources associated with proposed infrastructure projects.

6.4 Remaining Gaps in Knowledge

Geophysical characterization performed under the auspices of this project was limited in spatial extent. Large gaps in the spatial extent and depth of permafrost still exist over many areas of interior Alaska. The airborne and ground-based geophysical methods explored in this project offer a comprehensive overview of current techniques. Analysis of these methods offers guidance on the tradeoffs between resolution, depth of interrogation, and spatial coverage. Such guidance will be useful for designing future permafrost characterization campaigns to fill important baseline gaps in interior Alaska.

Recent developments in numerical models to simulate coupled heat and water transport in temperate to freezing subsurface conditions have advanced our ability to understand water movement in permafrost environments. However, several gaps exist in understanding and physically describing basic processes and property relationships associated with freeze/thaw cycles, particularly for variably saturated conditions. Accepted practices for implementing the

mechanisms of cryosuction, frost heaving, and thermokarsting (land subsidence associated with shallow permafrost thaw and soil matrix collapse) in physics-based models have not been widely established; these are areas of active research and development. Also, the responses of hydraulic, thermal, and mechanical properties of soil across the freeze/thaw transition for various soil types are not well known. Very limited attention has been given to soil freezing properties that influence the flow/impedance of water and mechanical strength of soil under variably saturated conditions in the subsurface. Additional laboratory and field investigations are needed to better constrain thermal, mechanical, and hydraulic relationships for representation in cold-region model simulations.

Understanding connections between thermally-influenced landscape processes and inland waters (rivers, streams, lakes, wetlands) in permafrost systems represents a broad area where additional research is needed. For example, hydrologic responses to land subsidence, erosion, and changes in channel geomorphology derived from permafrost thaw and climate warming are not well quantified nor are potential thermal feedbacks to these landscape processes. Improved knowledge of groundwater-surface water interaction in permafrost systems is required for predicting the trajectories of inland water bodies under a warming climate. Approaches for addressing these critical gaps will require a combination of remote sensing, geophysical and hydrologic field characterization, and coupled thermal-hydrologic modeling.

6.5 Recommendations for Long-Term Permafrost Monitoring Program

Multi-method, multi-scale approaches to characterize permafrost are needed to capture dynamic processes. Application of many geophysical methods used and developed in RC-2111 (and also distributed temperature sensor cable employment) may be used to monitor thermal and physical state of permafrost at extensive sites in different landscapes and for calibration data for airborne/satellite platforms. Several of the geophysical instruments used here, along with thermal imaging, are amenable to future deployment as payloads on unmanned aerial vehicles (unmanned aerial vehicles, i.e., drones), enabling cost-effective mapping in remote areas. Long-term shallow temperature monitoring would be useful for defining appropriate boundary conditions in SUTRA and other model applications. Extensive permafrost characterization and monitoring sites should span a spectrum of vegetation types and fire history in order to provide a comprehensive assessment. Sites could be collocated with military lands or areas of military interest to enhance DoD relevance. Monitoring equipment installed at Beaver Meadow Lake and Twelvemile Lake as part of the RC-2111 project continues to collect pressure and temperature data. Future projects could benefit from this ongoing data collection.

Monitoring of physical changes in the landscape that are reflective of permafrost thaw, such as land subsidence, thermokarst, and erosion should be included in a permafrost monitoring plan. Airborne approaches (i.e., LiDAR, interpretation of thermokarst feature using high-resolution satellite imagery and/or aerial photos, etc...) may be well suited for monitoring geomorphic

change over large scales. In addition, basic surface and subsurface hydrology data should be included in a monitoring plan to understand implications associated with permafrost change. Such data include, but are not limited to soil moisture, water table elevation, lateral and vertical hydraulic head distribution, rain and snowfall, evaporation, runoff, seasonal streamflow, and lake level. Basic surface and subsurface hydrology data should be included in permafrost monitoring to understand implications associated with permafrost change. Such data include, but are not limited to soil moisture, water table elevation, lateral and vertical hydraulic head distribution, rain and snowfall, evaporation, runoff, seasonal streamflow, and lake level.

Means to ground-truth and verify interpretations are fundamental to any long-term monitoring plan. We suggest inclusion of sentinel deep wells (for hydrologic, thermal, geochemical, and geophysical monitoring) located in areas that will provide most information on permafrost and hydrologic evolution, in sensitive ecosystems and in areas with threatened infrastructure.

Modeling studies using the approaches developed in RC-2111 can be used to guide a strategic permafrost monitoring plan in (1) identifying areas of high vulnerability, (2) constraining appropriate measurement frequency, and (3) interpreting monitoring results.

Coordination with other existing and planned monitoring programs (e.g. Department of Energy's Next-Generation Ecosystem Experiments, NASA's Arctic Boreal Vulnerability Experiment, National Science Foundation's Arctic Observing Network, USGS's Alaska Climate Science Center, and National Snow & Ice Data Center's Circumpolar Active Layer Monitoring Network) will alleviate required resources and maximize information.

7. Literature Cited

Ball, L.B., Smith, B.D., Minsley, B.J., Abraham, J.D., Voss, C.I., Astley, B.N. Deszcz-Pan, M., and Cannia, J.C. (2011) Airborne electromagnetic and magnetic geophysical survey data of the Yukon Flats and Fort Wainwright areas, central Alaska, June 2010, *U.S. Geol. Surv. Open-File Rep. 2011-1304*, 28 p.

Brewer, M.C., Carter, L.D., and Glenn, R. (1993) Sudden drainage of a thaw lake on the Alaskan Arctic coastal plain. Proceedings of the Sixth International Conference on Permafrost (Vol. 1), Beijing, China, pp. 48-53.

Briggs, M.A., Walvoord, M.A., McKenzie, J.M., Voss, C.I., Day-Lewis, F.D., and Lane, J.W. (2014) New permafrost is forming around shrinking arctic lakes, but will it last?, *Geophys. Res. Lett., 41*, 1585-1592, doi:10.1002/2014GL059251.

Brooks, R.H., and Corey, A.T. (1964) Hydraulic properties of porous media, Fort Collins, Colorado State University Hydrology Paper no. 3, 27 p.

Brown, R., Derksen, C., and Wang, L. (2010) A multi-data set analysis of variability and change in Arctic spring snow cover extent, 1967–2008, *J. Geophys Res., 115*, D16111, doi:10.1029/2010JD013975.

Burn, C.R. (2002) Tundra lakes and permafrost, Richards Island, western Arctic coast, Canada, *Can. J. Earth Sci., 39*, 1281-1298.

Burn, C.R. (2005) Lake-bottom thermal regimes, western Arctic coast, Canada, *Permafrost Periglacial Proc., 16*, 355-367.

Burt, T.P., and Williams, P.J. (1976) Hydraulic conductivity in frozen soils, *Earth Surface Proc., 9* (4), 411-416.

Carey, S.K., and Woo, M.K. (1999) Hydrology of two slopes in subarctic Yukon, Canada, *Hydrol. Proc., 13*, 2549-2562.

Chapman, W.L., Walsh, J.E. (2007) Simulations of Arctic temperature and pressure by global coupled models, *J. Climate, 20*, 609–632.

Clark, A., Barker, C.E., and Weeks, E.P. (2009) Drilling and testing the DOI-04-1A coalbed methane well, Fort Yukon, Alaska, *U.S. Geol. Surv. Open-File Rep. 2009–1064*, 69 p.

Daniels, J.J., Keller, G.V., and Jacobson, J.J. (1976) Computer-assisted interpretation of electromagnetic soundings over a permafrost section, *Geophysics, 41*, 752–765.

Day-Lewis, F. D., Singha, K. and Binley, A. M. (2005) Applying petrophysical models to radar travel time and electrical resistivity tomograms: Resolution-dependent limitations, *J. Geophys. Res. Solid Earth, 110*, B08206, doi:10.1029/2004JB003569.

Dingman, S.L. (1975) Hydrologic effects of frozen ground: Literature review and synthesis, Special Report 218, U.S. Army Corps of Engineers, Cold Regions Research and Engineering Laboratory, Hanover, N.H.

Ford, J., and Bedford, B.L. (1987) The hydrology of Alaskan wetlands, U.S.A.: a review, *Arctic Alpine Res., 19*(3), 209-229.

Foster, J.L., Robinson, D.A., Hall, D.K., and Estilow, T.W. (2008). Spring snow melt timing and changes over Arctic lands. Polar Geography, 31(3-4), 145-157.

French, H.K., Binley, A., Kharkhordin, I., Kulessa, B., and Krylov, S.S. (2006) Cold Regions Hydrogeophysics: Physical Characterisation and Monitoring, in Applied Hydrogeophysics, Chapter 7, Springer, NATO Sciences Series IV. Earth and Environmental Sciences, Vol. 71, p. 195-232.

Frey, K.E., and McClelland, J.W. (2009) Impacts of permafrost degradation on arctic river biogeochemistry, *Hydrol. Proc., 23*, 169-182, doi:10.1002/hyp.7196.

Ge S., McKenzie, J.M., Voss C.I., and Wu, Q. (2011) Exchange of groundwater and surface-water mediated by permafrost response to seasonal and long term air temperature variation, *Geophys. Res. Lett., 38,* L14402 doi:10.1029/2011GL047911.

Gesch, D.B. (2007) The National Elevation Dataset. *In* Maune, D. (ed.), Digital Elevation Model Technologies and Applications: The DEM Users Manual, 2nd Edition: Bethesda, Maryland, American Society for Photogrammetry and Remote Sensing, p. 99-118.

Granger, R.J., Gray, D.M., and Dyck, G.E. (1984) Snowmelt infiltration to frozen Prairie soils. *Can. J. Earth Sci., 21,* 669-677.

Harbaugh, A.W. (1990) A computer program for calculating subregional water budgets using results from the U.S. Geological Survey modular three-dimensional ground-water flow model, *U.S. Geol. Surv. Open-File Rep. 90-392*, 46 p.

Harbaugh, A.W. (2000) A data input program (MFI2K) for the U.S. Geological Survey modular ground-water model (MODFLOW-2000), *U.S. Geol. Surv. Open-File Rep. 02-41*.

Hastings, W. K. (1970) Monte Carlo sampling methods using Markov chains and their applications, *Biometrika, 57*(1), 97–109, doi:10.1093/biomet/57.1.97.

Hinzman, L., et al. (2005) Evidence and implications of recent climate change in Northern Alaska and other Arctic regions, *Clim. Change, 72*, 251-298.

Hoekstra, P., and McNeill, D. (1973) Electromagnetic probing of permafrost, *Proc. 2nd International Conference on Permafrost*, National Academy of Science, 517-526.

Hoekstra, P., Sellmann, P. V. and Delaney, A. (1975) Ground and airborne resistivity surveys of permafrost near Fairbanks, Alaska, *Geophysics, 40*(4), 641–656.

Horiguchi, K., and Miller, R.D. (1983) Hydraulic conductivity of frozen earth materials, in *Proceedings of the 4th International Conference on Permafrost*, pp. 504-509, Natl. Acad. Press, Washington, D.C.

Huang, H. P. and Won, I. J. (2003) Real-time resistivity sounding using a hand-held broadband electromagnetic sensor, *Geophysics, 68*(4), 1224–1231.

Ibs-von Seht, M., and Wohlenberg, J. (1999) Microtremors measurements used to map thickness of soft soil sediments, Bulletin of the Seismological Society of America, v. 89, p. 250-259.

IPCC AR4 SYR (2007) Core Writing Team; Pachauri, R.K; and Reisinger, A., ed., Climate Change 2007: Synthesis Report, Contribution of Working Groups I, II and III to the Fourth Assessment Report of the Intergovernmental Panel on Climate Change, IPCC, ISBN 92-9169-122-4.

Jepsen, S.M., Koch, J., Rose, J., Voss, C.I. and Walvoord, M.A. **(**2012) Thermal and hydrological observations near Twelvemile Lake in discontinuous permafrost, Yukon Flats, interior Alaska, September 2010 - August 2011, *U.S. Geol. Surv. Open File Rep. 2012-1121*, 25 p.

Jepsen, S.M., Voss, C.I. Walvoord, M.A., Rose, J.R. Minsley, B.J., and Smith, B.D. (2013a) Sensitivity analysis of lake mass balance in discontinuous permafrost: the example of disappearing Twelvemile Lake, Yukon Flats, Alaska (USA), *Hydrogeology J.,* DOI 10.1007/s10040-012-0896-5.

Jepsen, S.M., Voss, C.I., Walvoord, M.A., Minsley, B.J., and Rover, J. (2013b) Linkages between lake shrinkage/expansion and sublacustrine permafrost distribution determined

from remote sensing of Interior Alaska, USA, *Geophys. Res. Lett., 40* (5), 882-887, doi:10.1002/grl.50187.

Jorgenson, M.T., Yoshikawa, K., Kanevskiy, M., Shur, Y., Romanovsky, V. et al. (2008) Permafrost characteristics of Alaska (map, December update), Ninth International Conference on Permafrost (NICOP), Fairbanks, AK, June 29-July 3, 2008, downloaded 16 Sep 2011 from http://permafrost.gi.alaska.edu/content/data-and-maps.

Jorgenson, M.T., and Kreig, R.A. (1988) A Model for Mapping Permafrost Distribution Based on Landscape Component Maps and Climatic Variables, in *Proc. 5th International Conference on Permafrost*, pp. 176–182, Tapir Publishers, Trondheim, Norway.

Kane, D.L. (1980) Snowmelt infiltration into seasonally frozen soils, *Cold Regions Sci. Tech., 3*, 153-161.

Kane, D.L., and Stein, J. (1983) Water movement into seasonally frozen soils, *Water Resour. Res., 19(*6), 1547-1557.

Karlstrom, T.N.V., et al. (1964) Surficial geology of Alaska, *U.S. Geol. Surv. Misc. Geol. Invest. Series Map I-357*.

Kleinberg R.L., and Griffin D.D., (2005) NMR measurements of permafrost: unfrozen water assay, pore-scale distribution of ice, and hydraulic permeability of sediments, *Cold Regions Sci. Tech. 42*, 63-77.

Kurylyk, B.L., and Watanabe, K. (2013) Review: The mathematical representation of freezing and thawing processes in variably-saturated, non-deformable soils, *Adv. Water Resour., 60*, 160–177, doi:10.1016/j.advwatres.2013.07.016.

Kurylyk, B.L., McKenzie, J.M., MacQuarrie, K.T.B., and Voss, C.I. (2014a) Analytical solutions for benchmarking cold regions subsurface water flow and energy transport models: one-dimensional soil thaw with conduction and advection, *Adv. Water Resour.,* 70 172–184 doi:0.1016/j.advwatres.2014.05.005.

Kurylyk, B.L., MacQuarrie, K.T.B., and Voss, C.I. (2014b) Climate change impacts on the temperature and magnitude of groundwater discharge from shallow, unconfined aquifers, *Water Resources. Res. 50*(4),3253–3274 doi:10.1002/2013WR014588.

Lachenbruch, A.H., and Marshall, B.V. (1986) Changing climate: Geothermal evidence from permafrost in the Alaskan Arctic, *Science, 234*, 689-696.

Lachenbruch, A.H., Brewer, M.C., Greene, G.W., and Marshall, B.V. (1962) Temperatures in permafrost, In *Temperature: Its Measurement and Control in Science and Industry*, Vol. 3, part 1, Herzfeld, C.M. (ed.), Reinhold, New York, NY, 791-803.

Mackay, J.R. (1992) Lake instability in an ice-rich permafrost environment: examples from the western Arctic coast. In: Robarts, R.D. and M.L. Bothwell (Eds.), Aquatic Ecosystems in Semi-Arid Regions: Implications for Resource Management, N.H.R.I. Symposium Series 7, Environment Canada, Saskatoon, pp. 1-26.

Marsh, P., and Neumann, N.N. (2001) Processes controlling the rapid drainage of two ice-rich permafrost-dammed lakes in NW Canada, *Hydrol. Proc., 15*, 3433-3446.

McCauley, C.A., White, D.M., Lilly, M.R., and Nyman, D.M. (2002) A comparison of hydraulic conductivities, permeabilities, and infiltration rates in frozen and unfrozen soils, *Cold Reg. Sci. Technol., 34,* 117-125, doi:10.1016/S0165-232X(01)00064-7.

McGuire, A.D., Anderson, L.G., Christensen, T.R., Dallimore, S., Guo, L., Hayes, D.J., Heimann, M., Lorenson, T.D., Macdonald, R.W., Roulet, N. (2009) Sensitivity of the carbon cycle in the Arctic to climate change, *Ecol. Monog. 79*, 523–555.

McKenzie, J.M., Voss, C.I., Siegel, D.I. (2007) Groundwater flow with energy transport and water-ice phase change: numerical simulations, benchmarks, and application to freezing in peat bogs, *Adv. Water Resour. 30*(4):966-983.

McKenzie, J.M., and Voss, C.I. (2013) Permafrost thaw in a multiscale groundwater-flow system, *Hydrogeology J.,* doi: 10.1007/s10040-012-0942-3.

Metropolis, N., Rosenbluth, A., Rosenbluth, M., Teller, A. and Teller, E. (1953) Equation of state calculations by fast computing machines, *J. Chem. Phys., 21*(6), 1087–1092, doi:10.1063/1.1699114, 1953.

Michel, F.A., and van Everdingen, R.O. (1994) Changes in hydrogeologic regimes in permafrost regions due to climatic change, *Permafrost Periglacial Proc., 5*, 191-195.

Minsley, B.J. (2011) A trans-dimensional Bayesian Markov chain Monte Carlo algorithm for model assessment using frequency-domain electromagnetic data, *Geophys. J. Int., 187*(1), 252–272, doi:10.1111/j.1365-246X.2011.05165.x.

Minsley, B.J., Abraham, J.D., Smith, B.D., Cannia, J.C., Voss, C.I., Jorgenson, M.T., Walvoord, M.A., Wylie, B.K., Anderson, L., Ball, L.B., Deszcz-Pan, M., Wellman, T.P. and Ager, T.A. (2012) Airborne electromagnetic imaging of discontinuous permafrost, *Geophys. Res. Lett., 39,* L02503, doi:10.1029/2011GL050079.

Minsley, B.J., Wellman, T.P., Walvoord, M.A., Revil, A. (2014) Sensitivity of airborne geophysical data to sublacustrine permafrost thaw, The Cryosphere Discuss., 8, 6079-6116, doi:10.5194/tcd-8-6079-2014.

National Park Service (1999), State surficial geology map of Alaska, digital map <http://www.nps.gov/akso/gis>.

O'Donnell, J.A., Aiken, G.R., Walvoord, M.A. and Butler, K.D. (2012) Dissolved organic matter composition of winter flow in the Yukon River basin: Implications of permafrost thaw and increased groundwater discharge, *Global Biogeochem. Cycles, 26*, GB0E06, doi:10.1029/2012GB004341.

Oldenborger, G. A. and Routh, P. S. (2009) The point-spread function measure of resolution for the 3-D electrical resistivity experiment, *Geophys. J. Int., 176*(2), 405–414.

Osterkamp, T.E. (2005) The recent warming of permafrost in Alaska, *Global Planetary Change, 49*, 187-202.

Osterkamp, T.E., and Romanovsky, V.E. (1999) Evidence for warming and thawing of discontinuous permafrost in Alaska, *Permafrost and Periglac. Process., 10*(1), 17–37.

Parolai, S., Bormann, P., and Milkert, C. (2002) New relationships between Vs, thickness of sediments, and resonance frequency calculated by the H/V ratio of seismic noise for Cologne Area (Germany), Bulletin of the Seismological Society of America, v. 92, p. 2521-2527.

Pollock, D.W. (1994) User's Guide for MODPATH/MODPATH-PLOT, Version 3: A particle tracking post-processing package for MODFLOW, the U.S. Geological Survey finite-difference ground-water flow model, *U.S. Geol. Surv. Open-File Rep. 94-464*, 6 ch.

Polubarinova-Kochina, P. (1962) Theory of ground water movement, Princeton, N.J., Princeton Univ. Press.

Provost, A.M., and Voss, C.I. (2014, USGS-approved and in final production) SUTRA, a Model for Saturated-Unsaturated, Variable-Density Groundwater Flow with Solute or Energy Transport – Documentation of Generalized Boundary Conditions, a Modified Implementation of Specified Pressures and Concentrations or Temperatures.

Revil, A. (2012) Spectral induced polarization of shaly sands: Influence of the electrical double layer, *Water Resour. Res., 48*(2), doi:10.1029/2011WR011260.

Riordan, B., Verbyla, D., and McGuire, D. (2006) Shrinking ponds in subarctic Alaska based on 1950–2002 remotely sensed images, *J. Geophys. Res. 111,* G04002, doi:10.1029/2005JG000150.

Rover, J., Ji, L., Wylie, B.K., and Tieszen, L.L. (2012) Establishing water body areal extent trends in interior Alaska from multi-temporal Landsat data, *Remote Sens. Lett., 3(*7), 595-604.

Serreze M.C., et al. (2000) Observational evidence of recent change in the northern high-latitude environment, *Clim. Change, 46*, 159-207.

Shur, Y., Hinkel, K.M., and Nelson, F.E. (2005) The transient layer: Implications for geocryology and climate-change science, *Permafrost Periglacial Proc., 16*(1), 5-17.

Smith, M.W. (1975) Microclimatic Influences on Ground Temperatures and Permafrost Distribution, Mackenzie Delta, Northwest Territories, *Can. J. Earth Sci., 12*, 1421–1438.

Smith, L.C., Pavelsky, T.M., MacDonald, G.M., Shiklomanov, A.I., and Lammers, R.B. (2007) Rising minimum daily flows in northern Eurasian rivers: A growing influence of groundwater in the high-latitude hydrologic cycle, *J. Geophys. Res., 112*, G04S47, doi:10.1029/2006JG000327.

St. Jacques, J-M., and Sauchyn, D.J. (2009) Increasing winter baseflow and mean annual streamflow from possible permafrost thawing in the Northwest Territories, Canada, *Geophys. Res. Lett., 26*, L04104, doi: 10.1029/2008GL035822.

Striegl, R.G., Aiken, G.R., Dornblaser, M.M., Raymond, P.A., and Wickland, K.P. (2005) A decrease in discharge-normalized DOC export by the Yukon River during summer through autumn, *Geophys. Res. Lett., 32,* L21413.

Sturm, M., Taras, B., Liston, G.E., Derksen, C., Jonas, T., and Lea, J. (2010) Estimating snow water equivalent using snow depth data and climate classes, *J. Hydromet., 11,* doi: 10.1175/2010JHM1202.1, 1380-1394.

Sturm, M., Hiemstra, C., Gelvin, A., and Saari S. (2011) Preliminary report on the snow cover of the Yukon Flats, March 2011, U.S. Army Cold Regions Research and Engineering Laboratory-Alaska (CRREL), special report to the U.S. Fish and Wildlife Service, Yukon Flats National Wildlife Refuge.

Suzuki, K., Kubota, J., Ohata, T., and Vuglinsky, V. (2006) Influence of snow ablation and frozen ground on spring runoff generation in the Mogot Experimental Watershed, southern mountainous taiga of eastern Siberia, *Nordic Hydrology, 37*(1), 21-29.

Tóth, J. (1963) A theoretical analysis of groundwater flow in small drainage basins, *J. Geophys. Res., 68*(16), 4795-4812.

van Genuchten, M.Th. (1980) A closed-form equation for predicting the hydraulic conductivity of unsaturated soils, *Soil Sci. Soc. Amer. J., 44*, 892-898.

Voss, C.I., and Provost, A.M. (2002) SUTRA: A model for saturated-unsaturated variable-density ground-water flow with solute or energy transport. *Water-Resour Invest Rep 02-4231*, Reston, VA.

Voss, C.I., McKenzie, J.M., Provost, A.M. and Kurylyk, B.L. (in final preparation) SUTRA, a Model for Saturated-Unsaturated, Variable-Density Groundwater Flow with Solute or Energy Transport – Documentation of the Freezing Capability, Unsaturated-Flow and

Ice-Saturation Functions, and Spatially Varying Properties, USGS Techniques and Methods publication.

Walsh, J.E., Chapman, W.L., Romanovsky, V., Christensen, J.H., and Stendel, M. (2008) Global climate model performance over Alaska and Greenland, *J. Climate 21* (23), 6156–6174.

Walvoord, M.A., and Striegl, R.G. (2007) Increased groundwater to stream discharge from permafrost thawing in the Yukon River basin: Potential impacts on lateral export of carbon and nitrogen, *Geophys. Res. Lett., 34,* L12402, doi:10.1029/2007GL030216.

Walvoord, M.A., Voss, C.I., and Wellman, T.P. (2012) Influence of permafrost distribution on groundwater flow in the context of climate-driven permafrost thaw: Example from Yukon Flats Basin, Alaska, USA, *Water Resour. Res., 48, 7,* doi:10.1029/2011WR011595.

Ward, S.H. and Hohmann, G. W. (1988) Electromagnetic theory for geophysical applications, in Electromagnetic methods in applied geophysics: Volume 1, theory, edited by M. N. Nabighian, Society of Exploration Geophysicists, Tulsa.

Watanabe, K., Kito, T., Wake, T., and Sakai, M. (2011) Freezing experiments on unsaturated sand, loam and silt loam, *Ann. Glaciol., 52*(58), 37–43, doi:10.3189/172756411797252220.

Watanabe, K., Kito, T., Dun, S., Wu, J.Q., Greer, R.C., and Flury, M. (2013) Water infiltration into a frozen soil with simultaneous melting of the frozen layer, *Vadose Zone J., 12*(1), doi:10.2136/vzj2011.0188.

Wellman, T.P., Voss, C.I., and Walvoord, M.A. (2013) Impacts of climate, lake size, and supra- and sub-permafrost groundwater flow on lake talik evolution, Yukon Flats, Alaska (USA), *Hydrogeology J.,* doi:10.1007/s10040-012-0941-4.

Williams, J.R. (1962) Geologic reconnaissance of the Yukon Flats district, Alaska. Geological Survey Bulletin 1111-H. United States Government Printing Office, Washington, D.C.

Williams, J.R. (1970) Ground water in the permafrost regions of Alaska, U.S. Geological Professional Paper 696, 83 p.

Woo, M.K. (1980) Hydrology of a small lake in the Canadian high arctic, *Arctic, Alpine Res,, 12*(2), 227-235.

Woo, M.K., and Mielko, C. (2007) An integrated framework of lake-stream connectivity for a semi-arid, subarctic environment, *Hydrol. Proc., 21*, 2668-2674.

Woo, M.K. and Steer, P. (1983) Slope hydrology as influenced by thawing of the active layer, Resolute, N.W.T. *Can. J. Earth Sci., 20*, 978-986.

Yoshikawa, K., and Hinzman, L.D. (2003) Shrinking thermokarst ponds and groundwater dynamics in discontinuous permafrost near Council, Alaska, *Permafrost Periglacial Proc., 14,* 151-160.

Zimov, S.A., Schuur, E.A.G., and Chapin III, F.S. (2006) Permafrost and the global carbon budget, *Science, 312*, 1612–1613.

APPENDIX A. LIST OF SCIENTIFIC/TECHNICAL PUBLICATIONS

A-1. Articles in Peer-Reviewed Journals

Briggs, M.A., Walvoord, M.A., McKenzie, J.M., Voss, C.I., Day-Lewis, F.D., and Lane, J.W. (2014) New permafrost is forming around shrinking arctic lakes, but will it last?, *Geophys. Res. Lett., 41*, 1585-1592, doi:10.1002/2014GL059251.

Minsley, B.J., Wellman, T.P., Walvoord, M.A., Revil, A. (2014) Sensitivity of airborne geophysical data to sublacustrine permafrost thaw, The Cryosphere Discuss., 8, 6079-6116, doi:10.5194/tcd-8-6079-2014.

Jepsen, S.M., Voss, C.I., Walvoord, M.A., Rose, J.R., Smith, B.D., and Minsley, B.J. (2013) Sensitivity analysis of lake mass balance in discontinuous permafrost: the example of disappearing Twelvemile Lake, Yukon Flats, Interior Alaska (USA), *Hydrogeology J., 21,* 185-200, doi: 10.1007/s10040-012-896-5.

Jepsen, S.M., Voss, C.I., Walvoord, M.A., Minsley, B.J., and Rover, J. (2013) Linkages between lake shrinkage/expansion and sublacustrine permafrost distribution determined from remote sensing of Interior Alaska, USA, *Geophys. Res. Lett., 40* (5), 882-887, doi:10.1002/grl.50187.

McKenzie, J.M., and Voss, C.I. (2013) Permafrost thaw in a nested groundwater-flow system, *Hydrogeol. J., 21,* doi: 10.1007/s10040-012-0942-3.

Walvoord, M.A., Voss, C.I., and Wellman, T.P. (2012) Influence of permafrost distribution on groundwater flow in the context of climate-driven permafrost thaw: Example from Yukon Flats Basin, Alaska, USA, *Water Resour. Res., 48*, 7, doi:10.1029/2011WR011595.

Wellman, T.P., Voss, C.I., and Walvoord, M.A. (2013) Impacts of climate, lake size, and supra- and sub-permafrost groundwater flow on lake talik evolution, Yukon Flats, Alaska (USA), *Hydrogeol. J.,* doi:10.1007/s10040-012-0941-4.

A-2. Technical Reports

Jepsen, S.M., Koch, J., Rose, J., Voss, C.I., and Walvoord, M.A. (2012) Thermal and hydrological observations near Twelvemile Lake in discontinuous permafrost, Yukon Flats, interior Alaska, September 2010 - August 2011, U.S. Geol. Surv. Open File Rep. 2012-1121. http://pubs.usgs.gov/of/2012/1121/

Provost, A.M., and Voss, C.I. (2014, USGS-approved and in final production) SUTRA, a Model for Saturated-Unsaturated, Variable-Density Groundwater Flow with Solute or Energy Transport – Documentation of Generalized Boundary Conditions, a Modified

Implementation of Specified Pressures and Concentrations or Temperatures, and the Lake Capability, USGS Techniques and Methods publication.

Voss, C.I., McKenzie, J.M., Provost, A.M., and Kurylyk, B.L. (in final preparation) SUTRA, a Model for Saturated-Unsaturated, Variable-Density Groundwater Flow with Solute or Energy Transport – Documentation of the Freezing Capability, Unsaturated-Flow and Ice-Saturation Functions, and Spatially Varying Properties, USGS Techniques and Methods publication.

A-3. Conference Proceedings

Minsley, B.M., Wellman, T.P., Walvoord, M.A., Revil, A. (2014) Modeling the hydrogeophysical response of lake talik evolution, *SEG Technical Program Expanded Abstracts 2014*, pp. 4528-4533, doi: 10.1190/segam2014-0311.1.

Provost, A.M., McKenzie, J.M., and Voss, C.I. (2011) Enhancement of SUTRA to allow simulation of freezing of groundwater and exchange of groundwater and solute or energy with lakes, in *Proceedings of MODFLOW and More 2011 Integrated Hydrologic Modeling*, International Groundwater Modeling Center (IGWMC) at Colorado School of Mines, Golden, CO, June 5-8, 2011, p. 133.

A-4. Conference Abstracts

Briggs, M., Walvoord, M. McKenzie, J., Voss, C., Day-Lewis, F., Lane, J., Shrinking arctic lakes are forming new local permafrost, but for how long?, EOS Transactions, AGU Fall Meeting Suppl., Abstract C53A-0547, San Francisco, CA, Dec 9-13, 2013.

Briggs, M.A., McKenzie, J.M., Walvoord, M.A., Voss, C.I., Day-Lewis, F.D., Lane, J.W., New local permafrost is forming on the margins of shrinking arctic lakes, but for how long?, Canadian Geophysical Union, Banff, CANADA, May 4-7, 2014.

Campbell, S.W., Saari, S., Douglas, T.A., Day-Lewis, F.D., Walvoord, M.A., and Nolan, J.T., Shallow geology and permafrost characterization using ground-penetrating radar to infer hydrological controls and landscape evolution in interior Alaska, EOS Transactions, AGU Fall Meeting Suppl., San Francisco, CA, Dec 3-7, 2012 .

Jepsen, S.M., Voss, C.I., Walvoord, M.A., Minsley, B.J., Rose, J., Smith, B.D., Disappearing Twelvemile Lake in Alaska's Discontinuous Permafrost: Scoping Analysis of Water Budget, Eos Transactions AGU, Fall Meet. Suppl., Abstract C21B-0469, Dec 5-9, 2011.

Jepsen, S.M., Voss, C.I., Walvoord, M.A., Minsley, B.J., Rose, J.R., and Smith, B.D., Water budget analysis of a lake in discontinuous permafrost, Yukon Flats, Interior Alaska, USGS National Groundwater Workshop, Denver, CO, Aug 5-9, 2012.

Jepsen, S., Walvoord, M.A., Voss, C.I., Minsley, B.J., Rover, J., Linkages between changes in lake surface area and the distribution of permafrost, Yukon Flats basin, interior Alaska, USA, Proceedings of the 39th International Association of Hydrogeologists Congress, Niagara Falls, Canada, Sep 16-21, 2012.

McKenzie, J.M., Voss, C.I., The importance of groundwater flow in thawing permafrost systems, Eos Transactions AGU, Fall Meet. Suppl., Abstract C41B-0386, Dec 5-9, 2011.

McKenzie, J., Voss, C.I., Groundwater flow in thawing permafrost systems, Proceedings of the 39th International Association of Hydrogeologists Congress, Niagara Falls, Canada, Sep 16-21, 2012.

Minsley, B.J., Abraham, J.D., Smith, B.D., Ball, L., Anderson, L., Walvoord, M.A., Cannia, J.C., Voss, C.I., and Wylie, B.K., Airborne electromagnetic mapping of the 3-D distribution of permafrost in the Yukon Basin, Alaska, Tenth International Conference on Permafrost, Salekhard, Russia, Jun 25-29, 2012.

Minsley, B., Wellman, T., Cox, L., Walvoord, M., Abraham, J., Hydrogeophysical modeling for improved understanding of permafrost distributions in the Yukon Flats, Alaska, SEG-AGU Hydrogeophysics Workshop Proceedings, Boise, ID, Jul 8-11, 2012.

Minsley, B.J., Abraham, J.D., Smith, B.D., Walvoord, M.A., Wellman, T.P., Informing permafrost/groundwater models using airborne electromagnetic data – background and example from the Yukon Flats Basin, Alaska, USGS National Groundwater Workshop, Denver, CO, Aug 5-9, 2012.

Minsley, B., Wellman, T., Walvoord, M., Voss, C., Revil, A., Predicting the geophysical response to changes in permafrost associated with lake talik evolution, EOS Transactions, Fall Meeting Suppl., Abstract C52A-08, San Francisco, CA, Dec 9-13, 2013.

Minsley, B.M., Wellman, T.P., Walvoord, M.A., Revil, A., Modeling the hydrogeophysical response of lake talik evolution, Proceedings of the Society of Exploration Geophysicists, Denver, CO, Oct 26-31, 2014.

Minsley, B.J., Ball, L., Bloss, B., Kass, A., Pastick, N., Smith, B.D., Walsh, D., Walvoord, M.A., Wylie, B., Voss, C.I., Mapping permafrost with airborne electromagnetics, EOS Transactions, AGU Fall Meeting Suppl., Abstract NS34A-01, San Francisco, CA, Dec. 15-19, 2014.

Smith, B.D., Walvoord, M.A., Wylie, B.K., Voss, C.I., Pastick, N., Minsley, B.J., Jepsen, S.M., Jorgenson, T., Cannia, J.C., Abraham, J.D., Anderson, L., New Perspectives of Permafrost Distribution and its Influence on Groundwater Flow and Ecosystem Performance for the Yukon Flats Area, Northern Alaska, Eos Transactions, AGU Fall Meet. Suppl., Abstract C41B-0389, Dec 5-9, 2011.

Striegl, R.G., Walvoord, M.A., Hydrological and biogeochemical trajectories change in response to permafrost thaw in arctic and subarctic regions, EOS Transactions, AGU Fall Meeting Suppl., San Francisco, CA, Dec 3-7, 2012.

Voss, C.I, Abraham, J.D., Day-Lewis, F.D., Jepsen, S.M., McKenzie, J.M., Minsley, B.J., Nolan, J., Rover, J., Smith, B.D., Walvoord, M.A., Wellman, T.P., Wylie, B.K., Geophysical permafrost mapping and permafrost-hydrology interaction - US Geological Survey studies in Yukon Flats, Alaska, Amer. Water Resour. Assoc. Meeting, Juneau, AK, Mar 5-7, 2012.

Voss, C.I., Abraham, J.D., Day-Lewis, F.D., Jepsen, S.M., McKenzie, J.M., Minsley, B.J., Nolan, J., Rover, J., Smith, B.D., Walvoord, M.A., Wellman, T.P., Wylie, B.K., Geophysical permafrost mapping and permafrost-hydrology interaction – USGS studies in Yukon Flats, Alaska, Proceedings of the 39th International Association of Hydrogeologists Congress, Niagara Falls, Canada, Sep 16-21, 2012.

Walvoord, M., Voss, C., Wellman, T., Impact of permafrost distribution on groundwater flow in the Yukon Flats Basin, Alaska, in Proceedings of MODFLOW and More 2011 Integrated Hydrologic Modeling, International Groundwater Modeling Center (IGWMC) at Colorado School of Mines, Golden, CO, June 5-8, 2011.

Walvoord, M.A., Astley, B.N., Best, H.R., Day-Lewis, F.D., Lane, J.W., Nolan, J., Impact of permafrost distribution on groundwater flow in the Yukon Flats Basin, Alaska, in Proceedings of the Fourth Interagency Conference on Research in the Watersheds, Fairbanks, AK, Sept. 26-29, 2011.

Walvoord, M.A., Voss, C.I., Wellman, T.P., Influence of permafrost distribution on regional groundwater flow in the Yukon Flats Basin, Alaska, Eos Transactions, AGU Fall Meet. Suppl., Abstract C41B-0388, Dec 5-9, 2011.

Walvoord, M., Day-Lewis, F., Campbell, S., Lane, J., Nolan, J., Voss, C., Wellman, T., Improving understanding of permafrost/groundwater interactions using an integrated and iterative approach of hydrogeophysical imaging and hydrologic modeling – an example from the Yukon Flats Basin, Alaska, USGS National Groundwater Workshop, Denver, CO, Aug 5-9, 2012.

Walvoord, M., Jepsen, S., Voss, C., Minsley, B., Rover, J. Linkages between changes in lake extent and the distribution of permafrost, Yukon Flats Basin, Interior Alaska, USA, EOS Transactions, AGU Fall Meeting Suppl., Abstract C43A-0660, San Francisco, CA, Dec 9-13, 2013.

Walvoord, M.A., Briggs, M.A., Day-Lewis, F.D., Jepsen, S.M., Lane, J.W. Jr., McKenzie, J.M., Minsley, B.J., Striegl, R.G., Voss, C.I., Wellman, T.P., Permafrost dynamics and

changing hydrogeology in a lake-rich landscape, Abstracts with Programs Geol. Soc. Amer., Vol. 46, Paper 102-2, Vancouver, British Columbia, CANADA, Oct. 19-22, 2014.

Walvoord, M.A., Striegl, R.G., Identifying hydrologic vulnerabilities to permafrost change and the effects on carbon transport to aquatic systems, EOS Transactions, Fall Meeting Suppl., Abstract B34B-03, Dec. 15-19, 2014.

Walvoord, M.A., Briggs, M.A., Day-Lewis, F.D., Jepsen, S.M., Lane, J.W. Jr., McKenzine, J.M., Minsley, B.J., Striegl, R.G., Voss, C.I., Wellman, T.P., Hydrogeologic controls on water dynamics in a discontinuous permafrost, lake-rich landscape, EOS Transactions, AGU Fall Meeting Suppl., Abstract C14A-03 , San Francisco, CA, Dec. 15-19, 2014.

Wellman, T., Voss, C., Provost, A., Walvoord, M., Integration of coupled groundwater and heat transport modeling and geophysical imaging to examine lake dynamics and talik evolution in Yukon Flats, Alaska, in Proceedings of MODFLOW and More 2011 Integrated Hydrologic Modeling, International Groundwater Modeling Center (IGWMC) at Colorado School of Mines, Golden, CO, June 5-8, 2011.

Wellman, T., Voss, C., Provost, A., Walvoord, M., Integration of coupled groundwater and heat transport modeling and geophysical imaging to examine lake dynamics and talik evolution in Yukon Flats, Alaska, in Proceedings of the Fourth Interagency Conference on Research in the Watersheds, Fairbanks, AK, Sept. 26-29, 2011.

Wellman, T., Voss, C., Walvoord, M., Minsley, B., Understanding response times and groundwater flow dynamics of lake talik evolution through permafrost in the Yukon Flats, Alaska, USGS National Groundwater Workshop, Denver, CO, Aug 5-9, 2012.

Wellman, T., Minsley, B., Voss, C., Walvoord, M., Understanding response times and groundwater flow dynamics of thaw zone (talik) evolution below lakes in the Yukon Flats, Alaska, USA, EOS Transactions, Fall Meeting Suppl., Abstract C53A-0534, San Francisco, CA, Dec 9-13, 2013.